Search for supersymmetry in proton-proton collisions at 13 TeV in final states with jets and missing transverse momentum

The CMS collaboration

2019-10-25

The CMS Collaboration , Eerola , P , Kirschenmann , H , Voutilainen , M , Havukainen , J , Heikkila , J K , Jarvinen , T , Karimaki , V , Kinnunen , R , Lampen , T , Lassila-Perini , K , Laurila , S , Lehti , S , Linden , T , Luukka , P , Maenpaa , T , Siikonen , H , Tuominen , E , Tuominiemi , J , Tuuva , T , Forthomme , L , Österberg , K , Garcia , F & Sirunyan , A M 2019 , ' Search for supersymmetry in proton-proton collisions at 13 TeV in final states with jets and missing transverse momentum ' , Journal of High Energy Physics , no. 10 , 244 . https://doi.org/10.1007/JHE

http://hdl.handle.net/10138/307943
https://doi.org/10.1007/JHEP10(2019)244

Published for SISSA by Springer

Received: *August 13, 2019*
Accepted: *October 9, 2019*
Published: *October 25, 2019*

Search for supersymmetry in proton-proton collisions at 13 TeV in final states with jets and missing transverse momentum

The CMS collaboration

E-mail: cms-publication-committee-chair@cern.ch

Abstract: Results are reported from a search for supersymmetric particles in the final state with multiple jets and large missing transverse momentum. The search uses a sample of proton-proton collisions at $\sqrt{s} = 13\,\text{TeV}$ collected with the CMS detector in 2016–2018, corresponding to an integrated luminosity of $137\,\text{fb}^{-1}$, representing essentially the full LHC Run 2 data sample. The analysis is performed in a four-dimensional search region defined in terms of the number of jets, the number of tagged bottom quark jets, the scalar sum of jet transverse momenta, and the magnitude of the vector sum of jet transverse momenta. No significant excess in the event yield is observed relative to the expected background contributions from standard model processes. Limits on the pair production of gluinos and squarks are obtained in the framework of simplified models for supersymmetric particle production and decay processes. Assuming the lightest supersymmetric particle to be a neutralino, lower limits on the gluino mass as large as 2000 to 2310 GeV are obtained at 95% confidence level, while lower limits on the squark mass as large as 1190 to 1630 GeV are obtained, depending on the production scenario.

Keywords: Hadron-Hadron scattering (experiments), Supersymmetry

ArXiv ePrint: 1908.04722

https://doi.org/10.1007/JHEP10(2019)244

Contents

1 Introduction

The search for particles and interactions beyond the standard model (SM) is a major goal of experiments at the CERN LHC. The search described here focuses on experimental signatures in which a proton-proton (pp) collision produces at least two jets (collimated sprays of particles), in conjunction with large unbalanced ("missing") momentum in the direction transverse to the beam axis. The jets result from the production and hadronization of energetic quarks or gluons that could be generated in the decay chains of new heavy

JHEP10(2019)244

particles. The jets are classified according to whether their properties are consistent with a jet initiated by the production of a bottom quark (b jet), a key experimental signature in many models of new-particle production. The large missing transverse momentum is typically associated with the production of a stable, weakly interacting particle that is not detected by the apparatus. In this analysis, this quantity is inferred from the total momentum of the observed jets in the transverse plane, which should sum to approximately zero if there are no unobserved particles. Signatures of this type have been studied extensively by both the ATLAS and CMS Collaborations [1–8]. This signature arises frequently in theoretical models based on supersymmetry (SUSY) [9–18] as well as in a broad range of other theories [19–24] extending the SM.

The analysis uses a sample of pp collision events at $\sqrt{s} = 13\,\text{TeV}$ recorded with the CMS detector in 2016–2018, corresponding to an integrated luminosity of $137\,\text{fb}^{-1}$. This represents essentially the complete CMS Run 2 data sample and is about four times larger than the 2016 data sample alone, which was used in the previous analysis based on this methodology [8].

The motivation for searches for new physics in the final state with jets and large missing transverse momentum arises from several considerations. Astrophysical observations provide compelling evidence for the existence of dark matter, known empirically to be the dominant component of matter in the universe. A weakly interacting massive particle (WIMP) is one class of candidates for dark matter. However, the SM does not contain such a particle. Within the SM, the Higgs boson presents special theoretical challenges. Assuming that the Higgs boson is a fundamental particle, its spin-0 nature implies that the physical mass of the Higgs boson, as a quantity in the SM, is unstable against corrections from quantum-loop processes. In the absence of extreme fine tuning [25–28] that would precisely cancel these effects, the Higgs boson mass is generically driven to the cutoff scale of validity of the theory, which could be as high as the Planck scale of quantum gravity. The instability of the Higgs boson mass, and with it, that of the entire electroweak scale (including the W and Z boson masses), is known as the gauge hierarchy problem. This problem has been a major challenge confronting theoretical particle physics for several decades. The discovery by ATLAS and CMS of a Higgs boson with a mass around 125 GeV has strongly highlighted this puzzle. The concept of "naturalness," [26–28], which refers to the degree of fine tuning of parameters, has been discussed extensively as an important, yet difficult to quantify, consideration in assessing theoretical scenarios.

Theories postulating physics beyond the SM, such as SUSY, can potentially address these problems. Supersymmetry relates each SM bosonic field degree of freedom to a corresponding fermionic superpartner field, and vice versa. Each spin $J = 1/2$ particle in the SM (the quarks and leptons) therefore has a spin $J = 0$ superpartner, so the SUSY spectrum contains a large number of scalar quarks (squarks, $\widetilde{\text{q}}$) and scalar leptons (sleptons, $\widetilde{\text{l}}$). The SUSY partners of the SM gauge bosons ($J = 1$) are referred to as gauginos ($J = 1/2$). For example, the superpartner of the gluon is a gluino ($\widetilde{\text{g}}$). The minimal supersymmetric SM (MSSM) [16–18] contains five Higgs bosons ($J = 0$) plus the usual four electroweak gauge bosons ($J = 1$) of the SM. In the MSSM, the partners of the Higgs and gauge bosons map onto a set of four $J = 1/2$ higgsinos and four electroweak gauginos. Because

JHEP10(2019)244

of possible mixing among these particles, these superpartners are generically referred to as electroweakinos, four of which are electrically neutral (neutralinos, $\widetilde{\chi}_i^0$, $i = 1, \ldots, 4$) and four of which are charged (charginos, $\widetilde{\chi}_j^{\pm}$, $j = 1, 2$). Supersymmetry provides a dark matter candidate if the lightest supersymmetric particle (LSP) is stable and has no electric or color charge. Stability of the LSP is guaranteed if the model conserves R parity [15, 29], which also implies that SUSY particles are produced in pairs. In this scenario, which is assumed in this paper, the lightest neutralino $\widetilde{\chi}_1^0$ is the LSP and could be a WIMP dark matter candidate.

Because gluinos and squarks carry color charges, like their SM partners, they can be produced via the strong interaction: they therefore have the highest production cross sections among SUSY particles for a given mass. The absence of signals for these particles has so far led to lower limits on their masses of roughly $m_{\widetilde{\mathrm{g}}} \approx 2\,\mathrm{TeV}$ for gluinos and $m_{\widetilde{\mathrm{q}}} \approx 1\,\mathrm{TeV}$ for light-flavored squarks [1, 4–8, 30], although these results are model dependent. The present search focuses on processes involving the production of colored SUSY particles, either gluinos or squarks. Once the SUSY particles are produced, they typically decay via a sequence of processes that generates jets, leptons, and large missing transverse momentum ($p_{\mathrm{T}}^{\mathrm{miss}}$), where $p_{\mathrm{T}}^{\mathrm{miss}}$ is the vector p_{T} sum of the particles in an event. Large $p_{\mathrm{T}}^{\mathrm{miss}}$ is a feature of models in which the masses involved in the decay chains allow the LSP to carry substantial transverse momentum (p_{T}). So that this study is orthogonal to ones explicitly requiring leptons, and to help enable a well-structured and independent set of SUSY searches in CMS, the present search vetoes events in which leptons (electrons or muons) are detected above a certain threshold in p_{T}.

2 Analysis methodology

The basic approach of the analysis involves defining search regions in a four-dimensional space specified by key event variables that characterize the topology and kinematics of the events: the total number of jets (N_{jet}), the number of tagged b jets ($N_{\text{b-jet}}$), the scalar sum of jet p_{T} (H_{T}), and the magnitude of the vector p_{T} sum of the jets ($H_{\mathrm{T}}^{\mathrm{miss}}$). The $H_{\mathrm{T}}^{\mathrm{miss}}$ variable is used to estimate the missing transverse momentum in the event. For all-hadronic events, $H_{\mathrm{T}}^{\mathrm{miss}}$ is similar to $p_{\mathrm{T}}^{\mathrm{miss}}$, but $H_{\mathrm{T}}^{\mathrm{miss}}$ is less susceptible to uncertainties in the modeling of soft energy deposits.

In total, there are 174 exclusive analysis bins in the four-dimensional search region, which together provide sensitivity to a wide range of SUSY scenarios. In each of the 174 analysis bins, the background from SM processes is evaluated using event yields measured in corresponding control samples in the data, in conjunction with correction factors obtained from Monte Carlo (MC) simulated event samples. The principal sources of background arise from several SM processes: production of a top quark, either through top quark-antiquark ($\mathrm{t\bar{t}}$) pair production or, less often, a single top quark; production of an on- or off-mass-shell W or Z boson (W+jets and Z+jets events, respectively); and production of multijet events through quantum chromodynamics (QCD) processes. Both top quark and W+jets events can exhibit significant $H_{\mathrm{T}}^{\mathrm{miss}}$ and thus contribute to the background if a W boson decays to a neutrino and an undetected or out-of-acceptance charged lepton, including

JHEP10(2019)244

a τ lepton with either a leptonic or hadronic decay. These backgrounds are determined using a single-lepton control sample. Similarly, Z+jets events can exhibit significant $H_{\mathrm{T}}^{\mathrm{miss}}$ if the Z boson decays to two neutrinos. This background is determined using a control sample of γ+jets events, in conjunction with a control sample in which a Z boson decays into an $\mathrm{e}^{+}\mathrm{e}^{-}$ or $\mu^{+}\mu^{-}$ pair. Significant $H_{\mathrm{T}}^{\mathrm{miss}}$ in QCD multijet events can arise if the p_{T} of a jet is mismeasured, if a jet falls outside the acceptance of the jet selection, or from b jets that produce one or more neutrinos. The QCD background contribution is evaluated using specially defined control samples together with the "rebalance and smear" technique [8, 31, 32].

The search is performed using methodologies similar to those presented in ref. [8]. The search regions, however, have been optimized for the larger amount of data, and refinements to the background estimation procedures have been implemented. The main difference with respect to ref. [8] is that for the evaluation of background from top quark and W+jets events, we now implement a transfer factor method rather than construct event-by-event background predictions separately for events with a hadronic tau lepton decay and for events with an electron or a muon. Also, the larger data set of the current analysis allows us to evaluate the background from $\mathrm{Z}(\to \nu\overline{\nu})$+jets events, in the cases with $N_{\text{b-jet}} > 0$, using extrapolation factors based entirely on data, rather than relying on simulation for these extrapolations when $N_{\text{jet}} \geq 9$.

The interpretation of the results is performed using a set of representative SUSY models, each of which is characterized by a small number of mass parameters. For this purpose, we use so-called simplified models [33–36]. For gluino pair production, the T1tttt, T1bbbb, T1qqqq, and T5qqqqVV [37] simplified models are considered (figure 1). In the T1tttt model, each gluino undergoes a three-body decay $\widetilde{\mathrm{g}} \to \mathrm{t}\overline{\mathrm{t}}\widetilde{\chi}_1^0$, where $\widetilde{\chi}_1^0$ is the LSP. The T1bbbb and T1qqqq models are the same as the T1tttt model, except the $\mathrm{t}\overline{\mathrm{t}}$ system is replaced by bottom quark-antiquark ($\mathrm{b}\overline{\mathrm{b}}$) or light-flavored (u, d, s, c) quark-antiquark ($\mathrm{q}\overline{\mathrm{q}}$) pairs, respectively. In the T5qqqqVV scenario, each gluino decays to a light-flavored $\mathrm{q}\overline{\mathrm{q}}$ pair and either to the next-to-lightest neutralino $\widetilde{\chi}_2^0$ or to the lightest chargino $\widetilde{\chi}_1^{\pm}$. The probability for the decay to proceed via the $\widetilde{\chi}_2^0$, $\widetilde{\chi}_1^{+}$, or $\widetilde{\chi}_1^{-}$ is 1/3 for each channel. The $\widetilde{\chi}_2^0$ ($\widetilde{\chi}_1^{\pm}$) subsequently decays to the $\widetilde{\chi}_1^0$ and to an on- or off-mass-shell Z ($\mathrm{W}^{\pm}$) boson. In this model, we assign $m_{\widetilde{\chi}_1^{\pm}} = m_{\widetilde{\chi}_2^0} = 0.5(m_{\widetilde{\chi}_1^0} + m_{\widetilde{\mathrm{g}}})$.

For squark-antisquark production, three simplified models are considered, denoted T2tt, T2bb, and T2qq (figure 2). In the T2tt model, top squark-antisquark production is followed by the decay of the (anti)squark to a top (anti)quark and the $\widetilde{\chi}_1^0$. The T2bb and T2qq models are the same as T2tt except with bottom squarks and quarks, or light-flavored squarks and quarks, respectively, in place of the top squarks and quarks.

3 Detector and trigger

A detailed description of the CMS detector, along with a definition of the coordinate system and pertinent kinematic variables, is given in ref. [38]. Briefly, a cylindrical superconducting solenoid with an inner diameter of 6 m provides a 3.8 T axial magnetic field. Within the cylindrical volume are a silicon pixel and strip tracker, a lead tungstate crystal elec-

JHEP10(2019)244

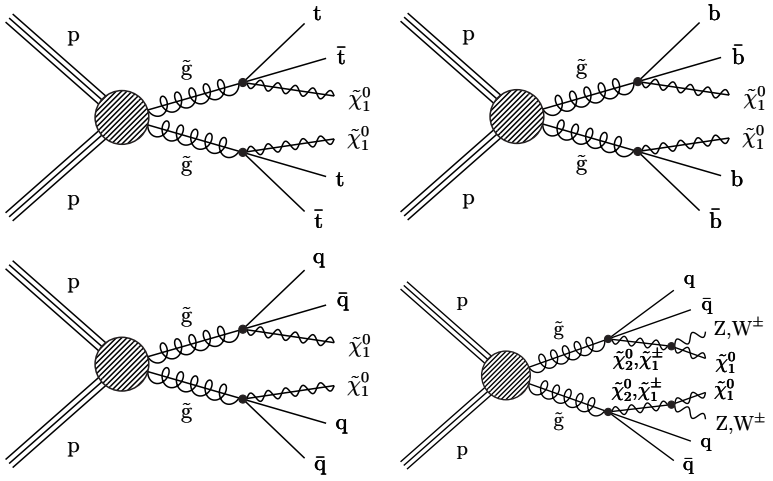

Figure 1. Diagrams for the simplified models with direct gluino pair production considered in this study: (upper left) T1tttt, (upper right) T1bbbb, (lower left) T1qqqq, and (lower right) T5qqqqVV.

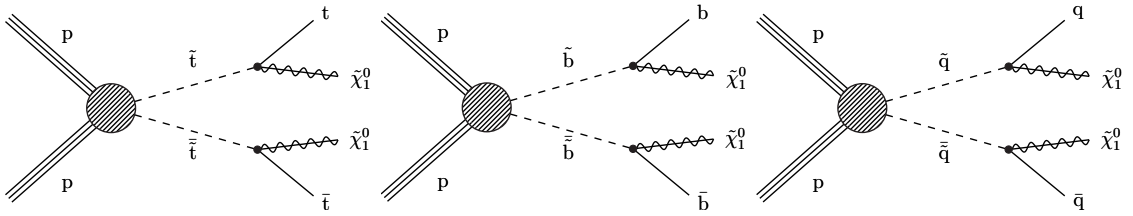

Figure 2. Diagrams for the simplified models with direct squark pair production considered in this study: (left) T2tt, (middle) T2bb, and (right) T2qq.

tromagnetic calorimeter (ECAL), and a brass and scintillator hadron calorimeter (HCAL). The tracking detectors cover the range $|\eta| < 2.5$, where η is the pseudorapidity. The ECAL and HCAL, each composed of a barrel and two endcap sections, cover $|\eta| < 3.0$. Forward calorimeters extend the coverage to $3.0 < |\eta| < 5.2$. Muons are measured within $|\eta| < 2.4$ by gas-ionization detectors embedded in the steel flux-return yoke outside the solenoid. The detector is nearly hermetic, permitting accurate measurements of $H_{\mathrm{T}}^{\mathrm{miss}}$.

The CMS trigger is described in ref. [39]. For this analysis, signal event candidates were recorded by requiring $H_{\mathrm{T}}^{\mathrm{miss}}$ at the trigger level to exceed a threshold that varied between 100 and 120 GeV, depending on the LHC instantaneous luminosity. The efficiency of this trigger is measured in data and is found to exceed 97% for events satisfying the event selection criteria described below. Additional triggers requiring the presence of charged leptons, photons, or minimum values of H_{T} are used to select control samples for the evaluation of backgrounds, as described below.

4 Event reconstruction

Individual particles are reconstructed with the CMS particle-flow (PF) algorithm [40], which identifies them as photons, charged hadrons, neutral hadrons, electrons, or muons. To improve the quality of the photon and electron reconstruction, additional criteria are

JHEP10(2019)244

imposed on the $\sigma_{\eta\eta}$ variable [41], which is a measure of the width of the ECAL shower shape with respect to the η coordinate, and on the ratio of energies associated with the photon or electron candidate in the HCAL and ECAL [41, 42]. For muon candidates [43], more stringent requirements are imposed on the matching between silicon tracker and muon detector track segments. Photon and electron candidates are restricted to $|\eta| < 2.5$ and muon candidates to $|\eta| < 2.4$.

The reconstructed vertex with the largest value of summed physics-object p_{T}^2 is taken to be the primary pp interaction vertex, where the physics objects are the jets, clustered using the jet finding algorithm [44, 45] with the charged particle tracks assigned to the vertex as inputs, and the associated missing transverse momentum, taken as the negative vector sum of the p_{T} of those jets. Charged particle tracks associated with vertices other than the primary vertex are removed from further consideration. The primary vertex is required to lie within 24 cm of the center of the detector in the direction along the beam axis and within 2 cm in the plane transverse to that axis.

To suppress jets erroneously identified as leptons and genuine leptons from hadron decays, electron and muon candidates are subjected to an isolation requirement. The isolation criterion is based on the variable I, which is the scalar p_{T} sum of charged hadron, neutral hadron, and photon PF candidates within a cone of radius $\Delta R = \sqrt{(\Delta\phi)^2 + (\Delta\eta)^2}$ around the lepton direction, divided by the lepton p_{T}, where ϕ is the azimuthal angle. The expected contributions of neutral particles from extraneous pp interactions (pileup) are subtracted [46]. The radius of the cone is 0.2 for lepton $p_{\mathrm{T}} < 50$ GeV, $10\,\mathrm{GeV}/p_{\mathrm{T}}$ for $50 \leq p_{\mathrm{T}} \leq 200$ GeV, and 0.05 for $p_{\mathrm{T}} > 200$ GeV. The decrease in cone size with increasing lepton p_{T} accounts for the increased collimation of the decay products from the lepton's parent particle as the Lorentz boost of the parent particle increases [47]. The isolation requirement is $I < 0.1$ (0.2) for electrons (muons).

To further suppress leptons from hadron decays and also single-prong hadronic τ lepton decays, charged particle tracks not identified as an isolated electron or muon, including PF electrons and muons, are subjected to a track isolation requirement. (Note that PF electrons and muons that do not satisfy the isolation requirements of the previous paragraph are not considered to be electron and muon candidates in this analysis.) To be identified as an isolated track, the scalar p_{T} sum of all other charged particle tracks within a cone of radius 0.3 around the track direction, divided by the track p_{T}, must be less than 0.2 if the track is identified as a PF electron or muon and less than 0.1 otherwise. Isolated tracks are required to satisfy $|\eta| < 2.4$.

Similarly, we require photon candidates to be isolated. The photon isolation requirement is based on the individual sums of energy from charged hadrons, neutral hadrons, and electromagnetic particles, excluding the photon candidate itself, within a cone of radius $\Delta R = 0.3$ around the photon candidate's direction, corrected for pileup [41]. Each of the three individual sums is required to lie below a (different) threshold that depends on whether the photon appears in the barrel or endcap calorimeter.

Jets are defined by clustering PF candidates using the anti-k_{T} jet algorithm [44, 45] with a distance parameter of 0.4. Jet quality criteria [48, 49] are imposed to eliminate

JHEP10(2019)244

jets from spurious sources such as electronics noise. The jet energies are corrected for the nonlinear response of the detector [50] and to account for the expected contributions of neutral particles from pileup [46]. Jets are required to have $p_{\mathrm{T}} > 30\,\mathrm{GeV}$.

The identification of b jets (b jet tagging) is performed by applying, to the selected jet sample, a version of the combined secondary vertex algorithm based on deep neural networks (DeepCSV) [51]. The medium working point of this algorithm is used. The tagging efficiency for b jets with $p_{\mathrm{T}} \approx 30\,\mathrm{GeV}$ is 65%. The corresponding misidentification probability for gluon and up, down, and strange quark jets is 1.6% while that for charm quark jets is 13%.

5 Event selection and search regions

Events considered as signal candidates are required to satisfy:

- $N_{\mathrm{jet}} \geq 2$, where jets must appear within $|\eta| < 2.4$;
- $H_{\mathrm{T}} > 300\,\mathrm{GeV}$, where H_{T} is the scalar p_{T} sum of jets with $|\eta| < 2.4$;
- $H_{\mathrm{T}}^{\mathrm{miss}} > 300\,\mathrm{GeV}$, where $H_{\mathrm{T}}^{\mathrm{miss}}$ is the magnitude of $\vec{H}_{\mathrm{T}}^{\mathrm{miss}}$, the negative of the vector p_{T} sum of jets with $|\eta| < 5$; an extended η range is used to calculate $H_{\mathrm{T}}^{\mathrm{miss}}$ so that it better represents the total missing momentum in an event;
- $H_{\mathrm{T}}^{\mathrm{miss}} < H_{\mathrm{T}}$, because events with $H_{\mathrm{T}}^{\mathrm{miss}} > H_{\mathrm{T}}$ are likely to arise from mismeasurement;
- no identified isolated electron or muon candidate with $p_{\mathrm{T}} > 10\,\mathrm{GeV}$;
- no isolated track with $m_{\mathrm{T}} < 100\,\mathrm{GeV}$ and $p_{\mathrm{T}} > 10\,\mathrm{GeV}$ ($p_{\mathrm{T}} > 5\,\mathrm{GeV}$ if the track is identified as a PF electron or muon), where m_{T} is the transverse mass [52] formed from $\vec{p}_{\mathrm{T}}^{\,\mathrm{miss}}$ and the isolated-track p_{T} vector, with $\vec{p}_{\mathrm{T}}^{\,\mathrm{miss}}$ the negative of the vector p_{T} sum of all PF objects with appropriate calibration applied as explained in ref. [53]; the m_{T} requirement restricts the veto to situations consistent with a W boson decay;
- no identified, isolated photon candidate with $p_{\mathrm{T}} > 100\,\mathrm{GeV}$; this requirement has a minimal impact on signal efficiency and is implemented to make the analysis orthogonal to SUSY searches based on events with photons and missing transverse energy, which typically require photon $p_{\mathrm{T}} \gtrsim 100\,\mathrm{GeV}$ (e.g., ref. [54]);
- $\Delta\phi_{H_{\mathrm{T}}^{\mathrm{miss}},\mathrm{j_i}} > 0.5$ for the two highest p_{T} jets $\mathrm{j_1}$ and $\mathrm{j_2}$, with $\Delta\phi_{H_{\mathrm{T}}^{\mathrm{miss}},\mathrm{j_i}}$ the azimuthal angle between $\vec{H}_{\mathrm{T}}^{\mathrm{miss}}$ and the p_{T} vector of jet $\mathrm{j_i}$; if $N_{\mathrm{jet}} \geq 3$, then, in addition, $\Delta\phi_{H_{\mathrm{T}}^{\mathrm{miss}},\mathrm{j_3}} > 0.3$ for the third-highest p_{T} jet $\mathrm{j_3}$; if $N_{\mathrm{jet}} \geq 4$, then, yet in addition, $\Delta\phi_{H_{\mathrm{T}}^{\mathrm{miss}},\mathrm{j_4}} > 0.3$ for the fourth-highest p_{T} jet $\mathrm{j_4}$; all considered jets must have $|\eta| < 2.4$; these requirements suppress background from QCD events, for which $\vec{H}_{\mathrm{T}}^{\mathrm{miss}}$ is usually aligned along a jet direction.

JHEP10(2019)244

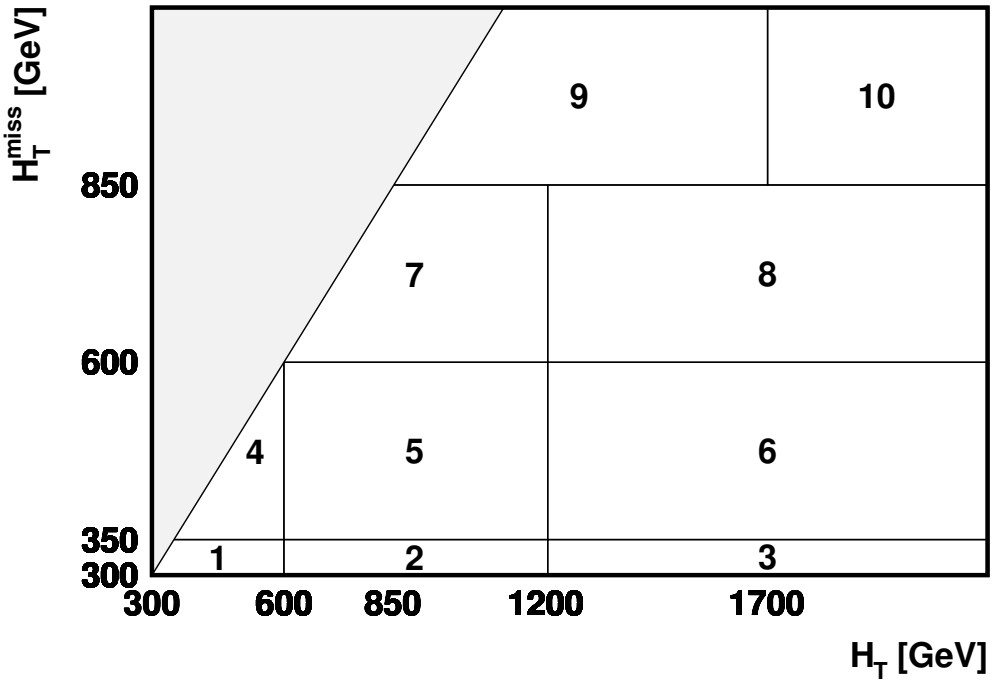

Figure 3. Schematic illustration of the 10 kinematic search intervals in the $H_{\mathrm{T}}^{\mathrm{miss}}$ versus H_{T} plane. The diagonal line delineating the leftmost edge of regions 1, 4, 7, and 9 corresponds to the restriction $H_{\mathrm{T}}^{\mathrm{miss}} < H_{\mathrm{T}}$. Regions 1 and 4 are excluded for $N_{\mathrm{jet}} \geq 8$. The rightmost and topmost bins are unbounded, extending to $H_{\mathrm{T}} = \infty$ and $H_{\mathrm{T}}^{\mathrm{miss}} = \infty$, respectively.

In addition, anomalous events with reconstruction failures or that arise from noise or beam halo interactions are removed [53].

The search is performed in a four-dimensional region defined by exclusive intervals in N_{jet}, $N_{\text{b-jet}}$, H_{T}, and $H_{\mathrm{T}}^{\mathrm{miss}}$. The search intervals in N_{jet} and $N_{\text{b-jet}}$ are:

- N_{jet}: 2–3, 4–5, 6–7, 8–9, $\geq$10;
- $N_{\text{b-jet}}$: either 0, 1, 2, $\geq$3 (for intervals with $N_{\mathrm{jet}} \geq 4$), or 0, 1, $\geq$2 (for the $N_{\mathrm{jet}} = 2$–3 interval).

For H_{T} and $H_{\mathrm{T}}^{\mathrm{miss}}$, 10 kinematic intervals are defined, as indicated in table 1 and figure 3. For $N_{\mathrm{jet}} \geq 8$, the kinematic intervals labeled 1 and 4 are discarded because of the small numbers of events. The total number of search bins in the four-dimensional space is 174.

6 Simulated event samples

The evaluation of background (section 7) is primarily based on data control regions. Samples of MC simulated SM events are used to evaluate multiplicative transfer factors that account for kinematic or other selection criteria differences between the data control and signal regions and to validate the analysis procedures.

JHEP10(2019)244

Interval	H_T^{miss} [GeV]	H_T [GeV]
1	300–350	300–600
2	300–350	600–1200
3	300–350	>1200
4	350–600	350–600
5	350–600	600–1200
6	350–600	>1200
7	600–850	600–1200
8	600–850	>1200
9	>850	850–1700
10	>850	>1700

Table 1. Definition of the search intervals in the H_T^{miss} and H_T variables. Intervals 1 and 4 are discarded for $N_{jet} \geq 8$. In addition, regions with $H_T^{miss} > H_T$ are excluded as illustrated in figure 3.

The SM production of $t\bar{t}$, W+jets, Z+jets, γ+jets, and QCD events is simulated using the MadGraph5_aMC@NLO 2.2.2 [55, 56] event generator with leading order (LO) precision. The $t\bar{t}$ events are generated with up to three additional partons in the matrix element calculations. The W+jets, Z+jets, and γ+jets events are generated with up to four additional partons. Single top quark events produced through the s channel, diboson events such as those originating from WW, ZZ, or ZH production (with H a Higgs boson), and rare events such as those from $t\bar{t}W$, $t\bar{t}Z$, and WWZ production, are generated with MadGraph5_aMC@NLO 2.2.2 at next-to-leading order (NLO) [57], except that WW events in which both W bosons decay leptonically are generated using the POWHEG v2.0 [58–62] program at NLO. This same POWHEG generator is used to describe single top quark events produced through the t and tW channels. The detector response is modeled with the Geant4 [63] suite of programs. Normalization of the simulated background samples is performed using the most accurate cross section calculations available [55, 61, 62, 64–72], which generally correspond to NLO or next-to-NLO (NNLO) precision.

Samples of simulated signal events are generated at LO using MadGraph5_aMC@NLO 2.2.2, with up to two additional partons included in the matrix element calculations. The production cross sections are determined with approximate NNLO plus next-to-next-to-leading logarithmic (NNLL) accuracy [73–84]. Events with gluino (squark) pair production are generated for a range of gluino $m_{\tilde{g}}$ (squark $m_{\tilde{q}}$) and LSP $m_{\tilde{\chi}_1^0}$ mass values, with $m_{\tilde{\chi}_1^0} < m_{\tilde{g}}$ ($m_{\tilde{\chi}_1^0} < m_{\tilde{q}}$). The ranges of mass considered vary according to the model, but are generally from around 600–2500 GeV for $m_{\tilde{g}}$, 200–1700 GeV for $m_{\tilde{q}}$, and 0–1500 GeV for $m_{\tilde{\chi}_1^0}$ (see section 9). For the T5qqqqVV model, the masses of the intermediate $\tilde{\chi}_2^0$ and $\tilde{\chi}_1^\pm$ are given by the mean of $m_{\tilde{\chi}_1^0}$ and $m_{\tilde{g}}$, as was already stated in the introduction. The gluinos and squarks decay according to the phase space model [85]. To render the computational requirements manageable, the detector response is described using the CMS fast simulation program [86, 87], which yields results that are generally consistent with the Geant4-based simulation. To improve

JHEP10(2019)244

the consistency of the fast simulation description with respect to that based on GEANT4, we apply a correction of 1% to account for differences in the efficiency of the jet quality requirements [48, 49], corrections of 5–12% to account for differences in the b jet tagging efficiency, and corrections of 0–14% to account for differences in the modeling of H_T and H_T^{miss}.

All simulated samples make use of the PYTHIA 8.205 [85] program to describe parton showering and hadronization. The CUETP8M1 [88] (CP5 [89]) PYTHIA 8.205 tune was used to produce the SM background samples for the analysis of the 2016 (2017 and 2018) data, with signal samples based on the CUETP8M1 tune for 2016 and on the CP2 tune [89] for 2017 and 2018. Simulated samples generated at LO (NLO) with the CUETP8M1 tune use the NNPDF2.3LO (NNPDF2.3NLO) [90] parton distribution function (PDF), while those using the CP2 or CP5 tune use the NNPDF3.1LO (NNPDF3.1NNLO) [91] PDF. The simulated events are generated with a distribution of pp interactions per bunch crossing that is adjusted to match the corresponding pileup distribution measured in data.

To improve the description of initial-state radiation (ISR), the MADGRAPH5_aMC@NLO prediction is compared to data in a control region enriched in $t\bar{t}$ events: two leptons (ee, $\mu\mu$, or $e\mu$) and two tagged b jets are required. The number of all remaining jets in the event is denoted N_{jet}^{ISR}. A correction factor is applied to simulated $t\bar{t}$ and signal events so that the N_{jet}^{ISR} distribution agrees with that in data. The correction is found to be unnecessary for $t\bar{t}$ samples that are generated with the CP5 tune, so it is not applied to those samples. The central value of the correction ranges from 0.92 for $N_{jet}^{ISR} = 1$ to 0.51 for $N_{jet}^{ISR} \geq 6$. From studies with a single-lepton data control sample, dominated by $t\bar{t}$ events, the associated systematic uncertainty is taken to be 20% of the correction for $t\bar{t}$ events and 50% of the correction for signal events, where the larger uncertainty in the latter case accounts for possible differences between signal and $t\bar{t}$ event production.

7 Background evaluation

The evaluation of the SM backgrounds is primarily based on data control regions (CRs). Signal events, if present, could populate the CRs, an effect known as signal contamination. The impact of signal contamination is accounted for in the interpretation of the results (section 9). Signal contamination is negligible for all CRs except for the single-lepton CR described in section 7.1. Similarly, it is negligible for all signal models except those that can produce an isolated track or lepton. With respect to the models examined here, signal contamination is relevant only for the T1tttt, T5qqqqVV, and T2tt models.

7.1 Background from top quark and W+jets events: "lost leptons"

The background from the SM production of $t\bar{t}$, single top quark, and W+jets events originates from W bosons that decay leptonically to yield a neutrino and a charged lepton. The charged lepton can be an electron, a muon, or a τ lepton. The τ lepton can decay leptonically to produce an electron or a muon or it can decay hadronically, in each case yielding at least one additional neutrino. For W boson decays that produce electrons or muons, top quark and W+jets events can enter as background to the signal region if there

JHEP10(2019)244

is large $H_{\mathrm{T}}^{\mathrm{miss}}$ from the neutrino(s) and if the electron or muon lies outside the analysis acceptance, is not reconstructed, or is not isolated. For W boson decays that produce a hadronically decaying τ lepton, top quark and W+jets events can enter as background if there is large $H_{\mathrm{T}}^{\mathrm{miss}}$ from the neutrinos. Collectively, the background from events with top quark and W+jets production is referred to in this paper as the "lost-lepton" background.

To evaluate the lost-lepton background, a single-lepton (e, μ) CR is selected using the same trigger and event selection criteria used for signal events, except the electron and muon vetoes are inverted and the isolated-track veto is not applied. Exactly one isolated electron or muon is required to be present. The single-electron and single-muon samples are combined to form a single CR. The transverse mass m_{T} formed from $\vec{p}_{\mathrm{T}}^{\,\mathrm{miss}}$ and the lepton p_{T} vector is required to satisfy $m_{\mathrm{T}} < 100\,\mathrm{GeV}$. This requirement has a high efficiency for SM events while reducing potential contamination from signal events with large $p_{\mathrm{T}}^{\mathrm{miss}}$.

The signal contamination in the resulting CR is generally small, with a typical value of 7, 3, and 1% for the T1tttt, T5qqqqVV, and T2tt model, respectively. The contamination tends to be larger in search regions with large values of N_{jet}, $N_{\text{b-jet}}$, H_{T}, and/or $H_{\mathrm{T}}^{\mathrm{miss}}$, while it is usually negligible in search regions with small H_{T} and $H_{\mathrm{T}}^{\mathrm{miss}}$. For certain values of $m_{\tilde{\mathrm{g}}}$ or $m_{\tilde{\mathrm{t}}}$ and $m_{\tilde{\chi}_1^0}$, the contamination can be as large as 30–50, 4–12, and 20–50% for the respective model. In a narrow diagonal range in the $m_{\tilde{\chi}_1^0}$ versus $m_{\tilde{\mathrm{t}}}$ plane, for which $m_{\tilde{\mathrm{t}}} - m_{\tilde{\chi}_1^0} \approx m_{\mathrm{t}}$, the signal contamination for the T2tt model can even be as large as around 90% at small $m_{\tilde{\chi}_1^0}$. Because of this large contamination, this diagonal region is excluded from the analysis as explained in section 9 (see figure 14 (upper left)).

The lost-lepton background is evaluated by applying an MC-derived multiplicative transfer factor to the observed single-lepton CR yields, with a separate transfer factor determined for each of the 174 search bins. The transfer factor is defined by the ratio, in simulation, of the number of lost-lepton events in a search bin to the number of events in the corresponding bin of the single-lepton CR, following normalization to the same integrated luminosity. The simulated events are corrected to account for differences with respect to data in the lepton, isolated track, and b jet tagging efficiencies.

The upper panel of figure 4 shows the simulated results, as a function of N_{jet} and $N_{\text{b-jet}}$, for the number of lost-lepton events. The corresponding results from simulation for the number of events in the single-lepton CR are shown in the middle panel of figure 4. The ratio of the results in the upper to the middle panels, equivalent to the transfer factor integrated over H_{T} and $H_{\mathrm{T}}^{\mathrm{miss}}$, is shown in the lower panel. At lower values of N_{jet}, the distributions are enhanced in W+jets events, for which a larger fraction of leptons lie outside the kinematic acceptance of the analysis compared to $\mathrm{t\bar{t}}$ events. This reduces the event acceptance in the single-lepton CR, increasing the value of the integrated transfer factors above unity as seen in the lower panel of figure 4 for $2 \leq N_{\mathrm{jet}} \leq 3$. As $N_{\text{b-jet}}$ increases, the probability for a lepton to fail the isolation requirement increases, leading to a larger rate of lost-lepton events and to an increase in the integrated transfer factors. This latter effect is especially visible for $2 \leq N_{\mathrm{jet}} \leq 3$ in figure 4 (lower).

The dominant uncertainty in the lost-lepton background prediction is statistical, arising from the limited number of events in the CR. Other uncertainties are evaluated to

JHEP10(2019)244

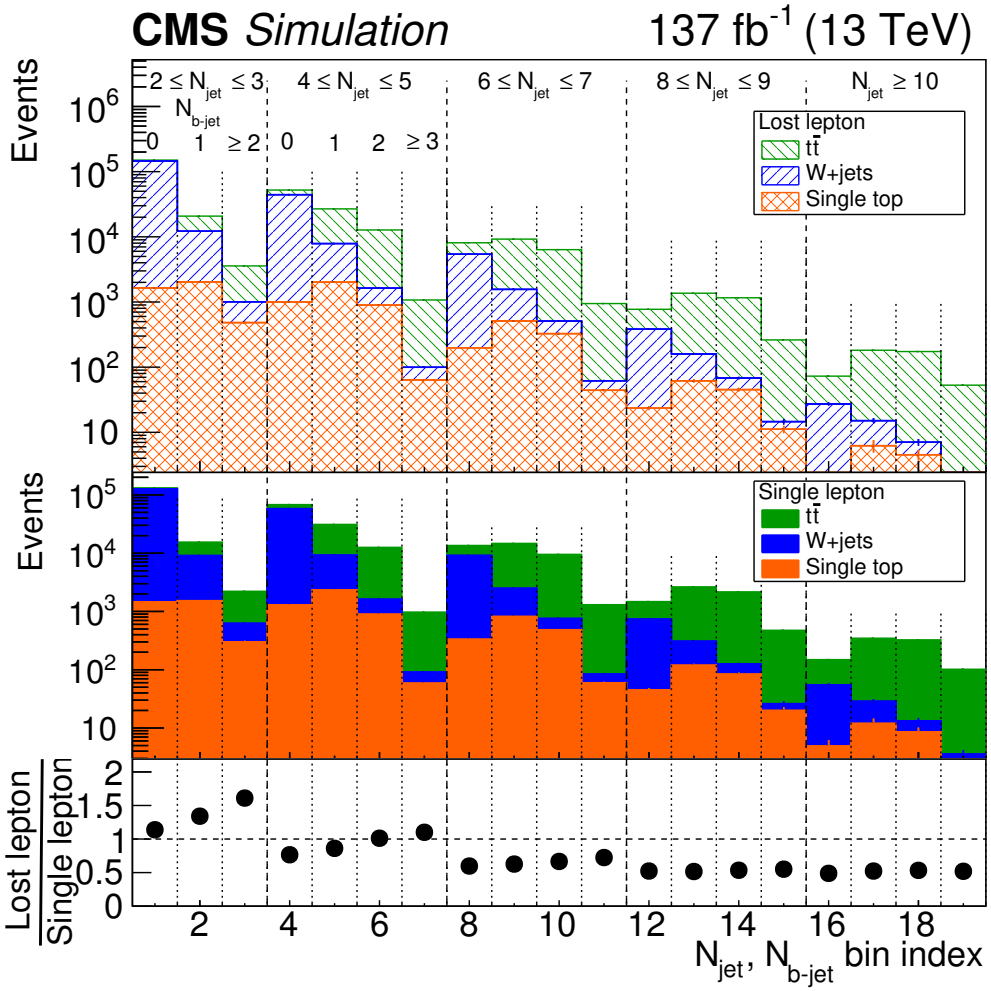

Figure 4. (Upper) The number of lost-lepton events in simulation, integrated over H_T and H_T^{miss}, as a function of N_{jet} and $N_{b\text{-}jet}$. (middle) Corresponding results from simulation for the number of events in the single-lepton control region. (lower) The ratio of the simulated lost-lepton to the single-lepton results, with statistical uncertainties (too small to be visible). These ratios are equivalent to the transfer factors used in the evaluation of the lost-lepton background, except integrated over H_T and H_T^{miss}.

account for the lepton and b jet tagging scale factors, the m_T selection requirement, the PDFs, the renormalization and factorization scales [92], and the jet energy corrections. These uncertainties are summed in quadrature to obtain the total uncertainty in the lost-lepton background prediction.

7.2 Background from Z($\to \nu\bar{\nu}$)+jets events

The background from Z+jets events with $Z \to \nu\bar{\nu}$ decay is evaluated using a CR with a single photon (γ+jets CR), in conjunction with a Z($\to \ell^+\ell^-$)+jets CR in which the Z boson decays to an e^+e^- or $\mu^+\mu^-$ pair. The method relies on the kinematic similarity between the production of Z bosons and photons. The Z($\to \nu\bar{\nu}$)+jets background in search bins with $N_{b\text{-}jet} = 0$ is determined by applying multiplicative transfer factors from simulation

JHEP10(2019)244

to the observed rate of γ+jets events, analogous to the method described in section 7.1 for the evaluation of the lost-lepton background. A correction is made to the normalization based on the observed rate of $Z(\to \ell^+\ell^-)$+jets CR events. An extrapolation to the search bins with $N_{\text{b-jet}} \geq 1$ is then made based on factors constructed from the $Z(\to \ell^+\ell^-)$+jets data. We follow this procedure in order to take advantage of both the higher statistical precision of the γ+jets CR and the more direct transfer factors of the $Z \to \ell^+\ell^-$ CR, while preserving the $N_{\text{b-jet}}$–N_{jet} correlation observed in the latter.

7.2.1 The γ+jets events

Events in the γ+jets CR were collected using a single-photon trigger, with an online threshold that varied between 180 and 190 GeV, depending on the data collection period. In the offline analysis, events are required to contain exactly one photon with $p_{\text{T}} > 200$ GeV. In each CR event, the photon serves as a proxy for a Z boson and is removed to emulate the undetected Z boson in $Z \to \nu\overline{\nu}$ decays. To ensure that the kinematics of the γ+jets events match those expected for $Z(\to \nu\overline{\nu})$+jets events, jets are reclustered after removing the photon and all event-level variables are recomputed. The same event selection criteria used to select signal events are then applied except, in addition, we require $N_{\text{b-jet}} = 0$.

The γ+jets CR contains nonnegligible contributions from photons produced in neutral meson decays. These photons are referred to as "nonprompt." The contamination of the CR from nonprompt photons, and thus the purity of signal photons in the sample, is evaluated using a binned maximum likelihood fit to the distribution of the photon candidate's charged hadron isolation variable. The fit is based on templates for nonprompt and signal photons. For signal photons, the template is taken from simulation, using the nominal photon selection criteria. For nonprompt photons, three different versions of the template are made: i) from simulation using the nominal criteria; ii) from simulation in a high-$\sigma_{\eta\eta}$ sideband (defined by inverting the $\sigma_{\eta\eta}$ selection criterion), where nonprompt photon production is expected to dominate; and iii) from data in this same high-$\sigma_{\eta\eta}$ sideband. The arithmetic mean of the three nonprompt templates is used in the fit, with the variation in the results obtained using the three templates individually defining a systematic uncertainty. The purity is determined as a function of $H_{\text{T}}^{\text{miss}}$ and typically exceeds 90%.

In the generation of simulated γ+jets events, photons that are approximately collinear with a parton ($\Delta R < 0.4$) are removed to improve the fraction of events with well-isolated photons and thus the statistical precision of the sample. A correction denoted $\mathcal{F}_{\text{dir}}$ is evaluated to account for a bias from this requirement, using simulated events with a looser restriction on the angular separation between the generator-level photons and partons. The corrections are typically less than 10%. A systematic uncertainty in the correction given by $0.30(1 - \mathcal{F}_{\text{dir}})$ is determined by evaluating the level of agreement between simulation and data in the distribution of the angular separation between a photon and the nearest jet, and the effect of changing the definition of collinear photons in the simulation.

7.2.2 The $Z(\to \ell^+\ell^-)$+jets events

The $Z(\to \ell^+\ell^-)$+jets CR, collected using single-lepton triggers, is selected by requiring two oppositely charged electrons or muons with a dilepton invariant mass $m_{\ell\ell}$ within 15 GeV

JHEP10(2019)244

of the Z boson mass. The selection requirements for electrons and muons are the same as those described in section 4, including the isolation requirements. To suppress $\mathrm{t\bar{t}}$ events, the p_{T} of the dilepton system is required to exceed 200 GeV. Similar to the γ+jets CR, the lepton pair in each $\mathrm{Z}(\to \ell^+\ell^-)$+jets event is removed to emulate the undetected Z boson in $\mathrm{Z}(\to \nu\bar{\nu})$+jets events, following which jets are reclustered and the event-level quantities recalculated.

Top quark pair production typically constitutes <5% of the observed dilepton event yield, except for events with $N_{\text{b-jet}} \geq 2$ where it can comprise up to ≈15% of the sample. Using fits to the observed $m_{\ell\ell}$ distribution, the purity $\beta_{\ell\ell}^{\text{data}}$ of the $\mathrm{Z}(\to \ell^+\ell^-)$+jets sample is evaluated for each individual N_{jet} and $N_{\text{b-jet}}$ region.

7.2.3 The $\mathrm{Z}(\to \nu\bar{\nu})$+jets background prediction

For each of the 46 search bins with $N_{\text{b-jet}} = 0$, the $\mathrm{Z}(\to \nu\bar{\nu})$+jets background is evaluated according to:

$$N^{\text{pred}}_{\mathrm{Z}\to\nu\bar{\nu}}\Big|_{N_{\text{b-jet}}=0} = \langle\rho\rangle \mathcal{R}^{\text{sim}}_{\mathrm{Z}\to\nu\bar{\nu}/\gamma} \mathcal{F}_{\text{dir}} \beta_\gamma N^{\text{data}}_\gamma \,/\, \mathcal{C}^{\gamma}_{\text{data/sim}}, \tag{7.1}$$

where N^{data}_γ is the number of observed events in the γ+jets CR, $\mathcal{R}^{\text{sim}}_{\mathrm{Z}\to\nu\bar{\nu}/\gamma}$ is the transfer factor, $\mathcal{C}^{\gamma}_{\text{data/sim}}$ accounts for the trigger efficiency and for differences between data and simulation in the photon reconstruction efficiency [41], and β_γ is the photon purity. The transfer factors, which account for known differences between photon and Z boson production, are given by the ratio from simulation of the rates of $\mathrm{Z}(\to \nu\bar{\nu})$+jets events to γ+jets events in the 46 bins. For the photon selection criteria used in this analysis, the transfer factor has a value of around 0.5, with a relatively mild dependence on the signal region kinematics. The distribution of N^{data}_γ, along with the simulated results for signal and nonprompt γ+jets events, is shown in figure 5 (upper). Figure 5 (lower) shows the transfer factors $\mathcal{R}^{\text{sim}}_{\mathrm{Z}\to\nu\bar{\nu}/\gamma}$.

The term denoted $\langle\rho\rangle$ in eq. (7.1) accounts for possible residual mismodeling of $\mathcal{R}^{\text{sim}}_{\mathrm{Z}\to\nu\bar{\nu}/\gamma}$. The value of $\langle\rho\rangle$ is expected to be close to unity, with possible deviations due to differences in missing higher-order terms between the γ+jets and Z+jets simulation. It is the average over all search bins with $N_{\text{b-jet}} = 0$ of the double ratio

$$\rho = \frac{\mathcal{R}^{\text{data}}_{\mathrm{Z}\to\ell^+\ell^-/\gamma}}{\mathcal{R}^{\text{sim}}_{\mathrm{Z}\to\ell^+\ell^-/\gamma}} = \frac{N^{\text{data}}_{\mathrm{Z}\to\ell^+\ell^-}}{N^{\text{sim}}_{\mathrm{Z}\to\ell^+\ell^-}} \frac{N^{\text{sim}}_\gamma}{N^{\text{data}}_\gamma} \frac{\beta^{\text{data}}_{\ell\ell}}{\mathcal{C}^{\ell\ell}_{\text{data/sim}}} \frac{\mathcal{C}^{\gamma}_{\text{data/sim}}}{\mathcal{F}_{\text{dir}}\beta_\gamma}, \tag{7.2}$$

where $N^{\text{data}}_{\mathrm{Z}\to\ell^+\ell^-}$ and $N^{\text{sim}}_{\mathrm{Z}\to\ell^+\ell^-}$ represent the number of events in the observed and simulated $\mathrm{Z} \to \ell^+\ell^-$ CR, respectively, N^{sim}_γ is the number of events in the simulated γ+jets CR, and $\mathcal{C}^{\ell\ell}_{\text{data/sim}}$ accounts for the trigger efficiency and for differences between data and simulation in the lepton reconstruction efficiencies in $\mathrm{Z}(\to \ell^+\ell^-)$+jets events [42, 43]. The event yields in the $\mathrm{Z}(\to \ell^+\ell^-)$+jets CR are too small to allow a meaningful determination of ρ in all search bins and thus we calculate the average $\langle\rho\rangle$ and apply it to all bins.

From studies of the variation of ρ with H_{T}, $H_{\mathrm{T}}^{\text{miss}}$, and N_{jet}, we observe a mild trend in ρ with respect to H_{T}. This trend is parameterized as $\rho(H_{\mathrm{T}}) = 0.86 + (2.0 \times 10^{-4})\min(H_{\mathrm{T}}, 900\,\text{GeV})$. Using this parameterization, an event-by-event weight is applied

JHEP10(2019)244

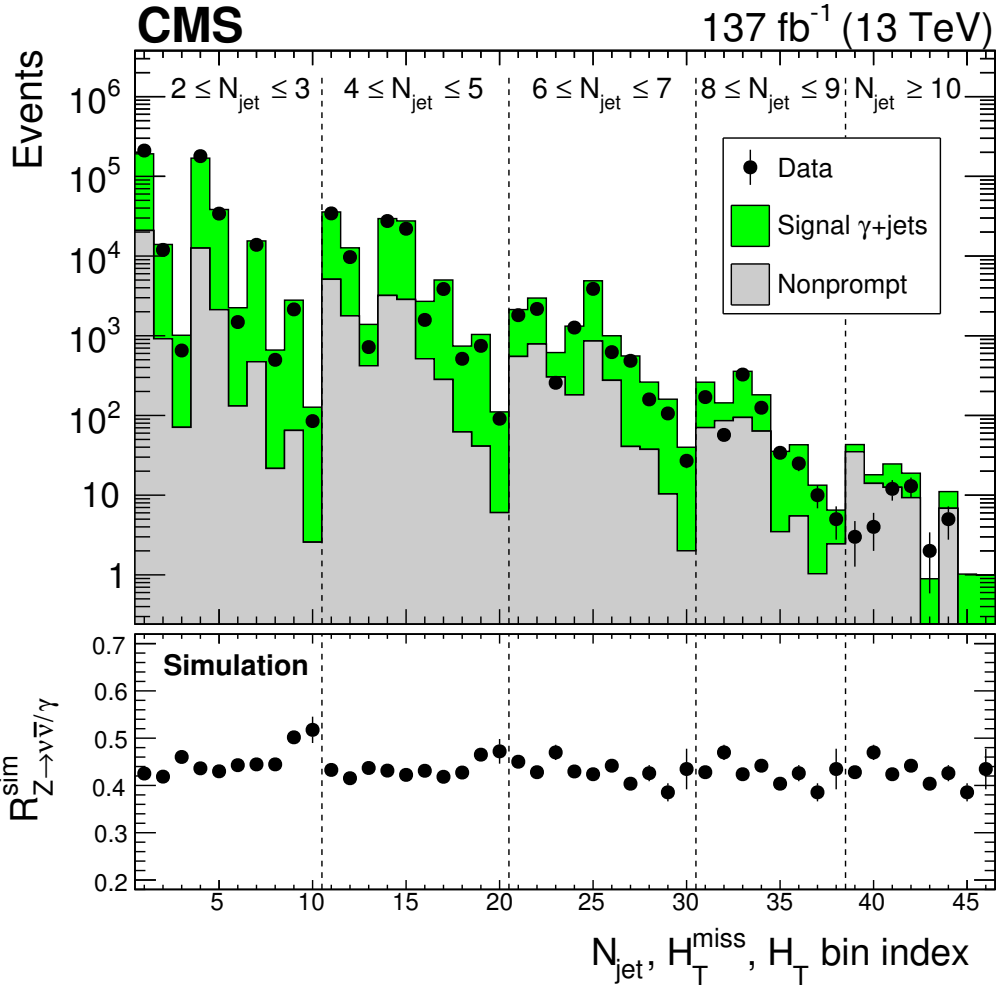

Figure 5. (Upper) The number of events in the γ+jets control region for data and simulation. (lower) The transfer factors $\mathcal{R}^{\text{sim}}_{\text{Z}\to\nu\bar{\nu}/\gamma}$ from simulation. The respective results are shown for the 46 search bins with $N_{\text{b-jet}} = 0$. The 10 results (8 for $N_{\text{jet}} \geq 8$) within each region delineated by vertical dashed lines correspond sequentially to the 10 (8) kinematic intervals in H_{T} and $H_{\text{T}}^{\text{miss}}$ listed in table 1 and figure 3. The uncertainties are statistical only. For the upper plot, the simulated results show the stacked event rates for the γ+jets and nonprompt MC event samples, where "nonprompt" refers to SM MC events other than γ+jets. The simulated nonprompt results are dominated by events from the QCD sample. Because of limited statistical precision in the simulated event samples at large N_{jet}, the transfer factors determined for the $8 \leq N_{\text{jet}} \leq 9$ region are also used for the $N_{\text{jet}} > 10$ region.

to each simulated γ+jets CR event before it enters eq. (7.1). Prior to this event weighting, we find $\langle\rho\rangle = 0.95$. Following the event weighting, $\langle\rho\rangle = 1.00$. It is this latter value of $\langle\rho\rangle$, along with its uncertainty, that enters eq. (7.1). In each bin, the residual deviation of ρ from unity as a function of H_{T} is added in quadrature with the associated statistical uncertainty, and analogously but separately for $H_{\text{T}}^{\text{miss}}$ and N_{jet}, and the largest of the three resulting terms is taken as the corresponding systematic uncertainty in the background prediction. The values of this bin-dependent uncertainty range from 1 to 13%.

JHEP10(2019)244

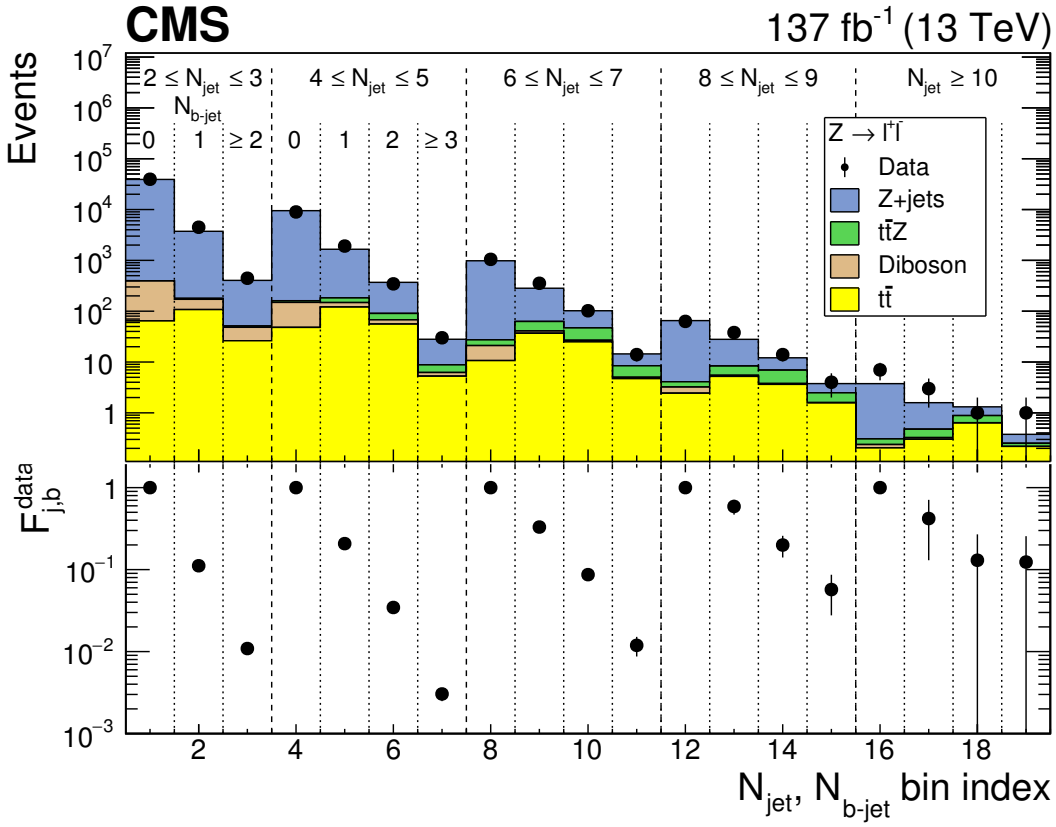

Figure 6. (Upper) The observed event yield in the $\mathrm{Z}(\to \ell^+\ell^-)$+jets control region, integrated over H_T and $H_\mathrm{T}^\mathrm{miss}$, as a function of N_jet and $N_\text{b-jet}$. The uncertainties are statistical only. The stacked histograms show the corresponding results from simulation. (lower) The extrapolation factors $\mathcal{F}_\mathrm{j,b}^\mathrm{data}$ with their statistical uncertainties.

To evaluate the $\mathrm{Z}(\to \nu\bar{\nu})$+jets background for search bins with $N_\text{b-jet} \geq 1$, we assume that the relative population of $\mathrm{Z}(\to \nu\bar{\nu})$+jets events in the H_T–$H_\mathrm{T}^\mathrm{miss}$ plane is independent of $N_\text{b-jet}$ for fixed N_jet. A systematic uncertainty deduced from a closure test (described below) is assigned to account for this assumption, where "closure test" refers to a check of the ability of the method, applied to simulated event samples, to correctly predict the genuine number of background events in simulation. We extend the result from eq. (7.1) using extrapolation factors $\mathcal{F}_\mathrm{j,b}^\mathrm{data}$ from $\mathrm{Z}(\to \ell^+\ell^-)$+jets data, as follows:

$$\left(N_{\mathrm{Z}\to\nu\bar{\nu}}^\mathrm{pred}\right)_{j,b,k} = \left(N_{\mathrm{Z}\to\nu\bar{\nu}}^\mathrm{pred}\right)_{j,0,k} \mathcal{F}_\mathrm{j,b}^\mathrm{data} \equiv \left(N_{\mathrm{Z}\to\nu\bar{\nu}}^\mathrm{pred}\right)_{j,0,k} \frac{\left(N_{\mathrm{Z}\to\ell^+\ell^-}^\mathrm{data}\,\beta_{\ell\ell}^\mathrm{data}\right)_{j,b}}{\left(N_{\mathrm{Z}\to\ell^+\ell^-}^\mathrm{data}\,\beta_{\ell\ell}^\mathrm{data}\right)_{j,0}}, \tag{7.3}$$

where j corresponds to the five N_jet regions, b to the four $N_\text{b-jet}$ regions (three for $N_\mathrm{jet} \leq 3$), and k to the 10 kinematic regions of H_T and $H_\mathrm{T}^\mathrm{miss}$ (table 1). The data used and the resulting extrapolation factors $\mathcal{F}_\mathrm{j,b}^\mathrm{data}$ are shown in figure 6.

The rare process $\mathrm{t\bar{t}Z}$ and the even more rare processes ZZ, WWZ, WZZ, and ZZZ can also contribute to the background. Those processes with a counterpart when the Z boson

JHEP10(2019)244

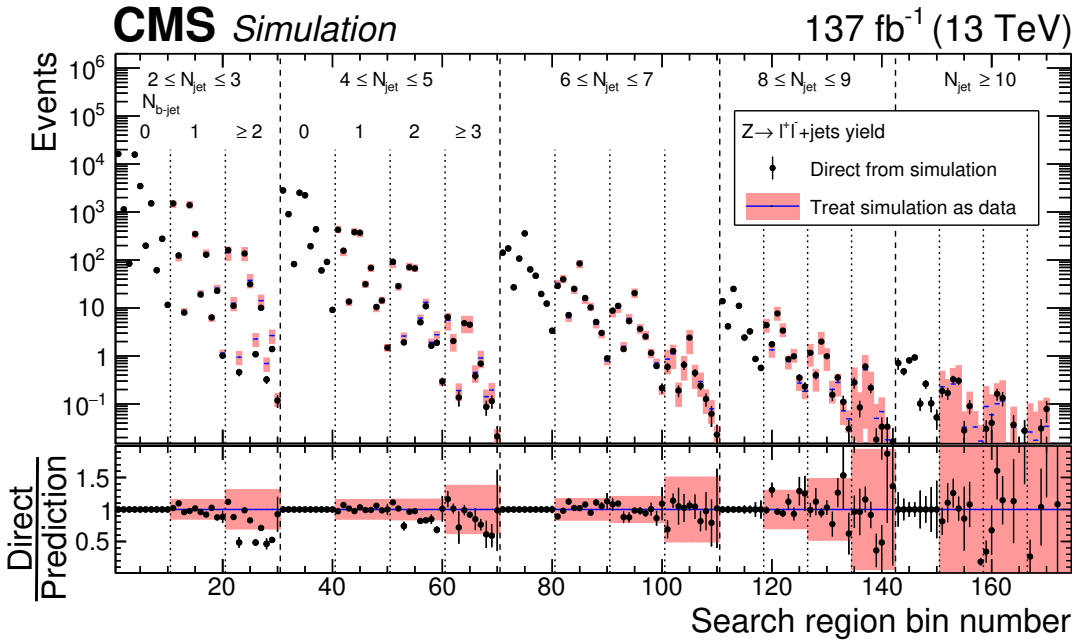

Figure 7. Prediction from simulation for the $\mathrm{Z}(\to \ell^+\ell^-)$+jets event yields in the 174 search bins as determined by computing the $\mathcal{F}_{\mathrm{j,b}}^{\mathrm{data}}$ factors (eq. (7.3)) and the $N_{\text{b-jet}} = 0$ event yields in the same manner as for data, in comparison to the corresponding direct $\mathrm{Z}(\to \ell^+\ell^-)$+jets prediction from simulation. The 10 results (8 for $N_{\mathrm{jet}} \geq 8$) within each region delineated by vertical dashed lines correspond sequentially to the 10 (8) kinematic intervals in H_{T} and $H_{\mathrm{T}}^{\mathrm{miss}}$ listed in table 1 and figure 3. For bins with $N_{\mathrm{jet}} \geq 10$, some points do not appear in the upper panel because they lie below the minimum of the displayed range. In the case that the direct expected yield is zero, there is no result in the lower, ratio panel. The pink bands show the statistical uncertainties in the prediction, scaled to correspond to the integrated luminosity of the data, combined with the systematic uncertainty attributable to the kinematic (H_{T} and $H_{\mathrm{T}}^{\mathrm{miss}}$) dependence. The black error bars show the statistical uncertainties in the simulation. For bins corresponding to $N_{\text{b-jet}} = 0$, the agreement is exact by construction.

is replaced with a photon are already accounted for in $N_{\gamma}^{\mathrm{data}}$ and thus are automatically included in the background estimate. We assume that the ratio of the rate of the rare process to its counterpart with a photon, e.g., the ratio of $\mathrm{t\bar{t}Z}$ (with $\mathrm{Z} \to \nu\bar{\nu}$) to $\mathrm{t\bar{t}}\gamma$ events, equals $\mathcal{R}_{\mathrm{Z}\to\nu\bar{\nu}/\gamma}^{\mathrm{sim}}$.

A closure test of the procedure is performed by treating event yields from the $\mathrm{Z}(\to \ell^+\ell^-)$+jets simulation as data, as shown in figure 7. Based on this study, the following systematic uncertainties are assigned. For $N_{\mathrm{jet}} = 2$–3, a systematic uncertainty of 15 and 30% is assigned to the $N_{\text{b-jet}} = 1$ and ≥ 2 regions, respectively. For $N_{\mathrm{jet}} \geq 4$, a systematic uncertainty of 15 and 30% is assigned to the $N_{\text{b-jet}} = 1$–2 and ≥ 3 regions. These uncertainties account for correlations between $N_{\text{b-jet}}$ and the H_{T} and/or $H_{\mathrm{T}}^{\mathrm{miss}}$ variables in the shape of the $\mathrm{Z} \to \nu\bar{\nu}$ prediction.

JHEP10(2019)244

7.3 Background from QCD events

The QCD background comprises only a small fraction (<5%) of the total background but, because it typically arises from the mismeasurement of jet p_{T}, is difficult to evaluate with simulation. We use data to model this background, exploiting knowledge of the jet energy resolution. Briefly, the method employs a set of CR events collected using triggers requiring H_{T} to exceed various thresholds between 200 and 1050 GeV, with no condition on $H_{\mathrm{T}}^{\mathrm{miss}}$. Corresponding prescale factors ranging from around 10 000 to 1 are applied, where a prescale factor reduces the recorded event rate relative to the raw trigger rate in order to maintain a manageable data flow. The jet momenta in each CR event are adjusted so that the event has well-balanced jet p_{T}, consistent with the kinematics of a generator-level (i.e., ideally measured) QCD event. This step is called rebalancing. The rebalancing step removes the intrinsic $p_{\mathrm{T}}^{\mathrm{miss}}$ from the event, thus effectively eliminating the contributions of events like W+jets and Z+jets events that can have genuine $p_{\mathrm{T}}^{\mathrm{miss}}$ [31]. The jet momenta are then smeared according to the known detector jet p_{T} resolution in order to determine the probability that a given event will populate a given search bin. This latter step is the smear stage. The so-called rebalance and smear (R&S) method was introduced in refs. [31, 32] and was further developed in ref. [4].

To rebalance an event, a Bayesian inference procedure is used, in which the p_{T} of each jet in a CR event is varied within its uncertainty to maximize the probability:

$$\mathcal{P}(\vec{\mathcal{J}}_{\mathrm{true}}|\vec{\mathcal{J}}_{\mathrm{meas}}) \sim \mathcal{P}(\vec{\mathcal{J}}_{\mathrm{meas}}|\vec{\mathcal{J}}_{\mathrm{true}})\, \pi(\vec{H}_{\mathrm{T,true}}^{\mathrm{miss}}, \Delta\phi_{\mathrm{j}_{1(\mathrm{b})},\mathrm{true}}), \tag{7.4}$$

where $\mathcal{P}(\vec{\mathcal{J}}_{\mathrm{true}}|\vec{\mathcal{J}}_{\mathrm{meas}})$ is the posterior probability density for a given configuration of jets with true (or ideal) momentum assignments $\vec{\mathcal{J}}_{\mathrm{true}}$, given a configuration of measured jet momenta $\vec{\mathcal{J}}_{\mathrm{meas}}$. The $\mathcal{P}(\vec{\mathcal{J}}_{\mathrm{meas}}|\vec{\mathcal{J}}_{\mathrm{true}})$ term, taken to be the product of the individual jet response functions of all jets in an event, is the likelihood to observe a configuration of measured jet momenta given a configuration of jets with a particular set of true momenta. The jet response functions are constructed from the distributions in simulation of the ratio of the reconstructed jet p_{T} to the p_{T} of well-matched generator-level jets. The response functions are derived as a function of jet p_{T} and η and are corrected to account for differences in the jet response shape between data and simulation. The $\pi(\vec{H}_{\mathrm{T,true}}^{\mathrm{miss}}, \Delta\phi_{\mathrm{j}_{1(\mathrm{b})},\mathrm{true}})$ term is the prior distribution, determined as a function of the true (i.e., generator level) $\vec{H}_{\mathrm{T}}^{\mathrm{miss}}$ and $\Delta\phi_{\mathrm{j}_{1(\mathrm{b})}}$, where $\Delta\phi_{\mathrm{j}_{1(\mathrm{b})}}$ is the azimuthal angle between $\vec{H}_{\mathrm{T}}^{\mathrm{miss}}$ and either the highest p_{T} jet in the event (for $N_{\text{b-jet}} = 0$), or the highest p_{T} tagged b jet (for $N_{\text{b-jet}} \geq 1$). This prior represents the distribution of the magnitude and direction of the genuine $H_{\mathrm{T}}^{\mathrm{miss}}$ expected in QCD events.

After the transverse momenta of the individual jets have been adjusted according to the posterior probability density in eq. (7.4), the jet p_{T} values are smeared by rescaling them using factors sampled randomly from the jet response functions. This sampling is performed numerous times for each rebalanced event. Each event is then weighted by the inverse of the number of times it is smeared. Events are smeared in up to 1000 independent trials, with a final target event weight of 0.05, equal to the prescale value of the trigger

JHEP10(2019)244

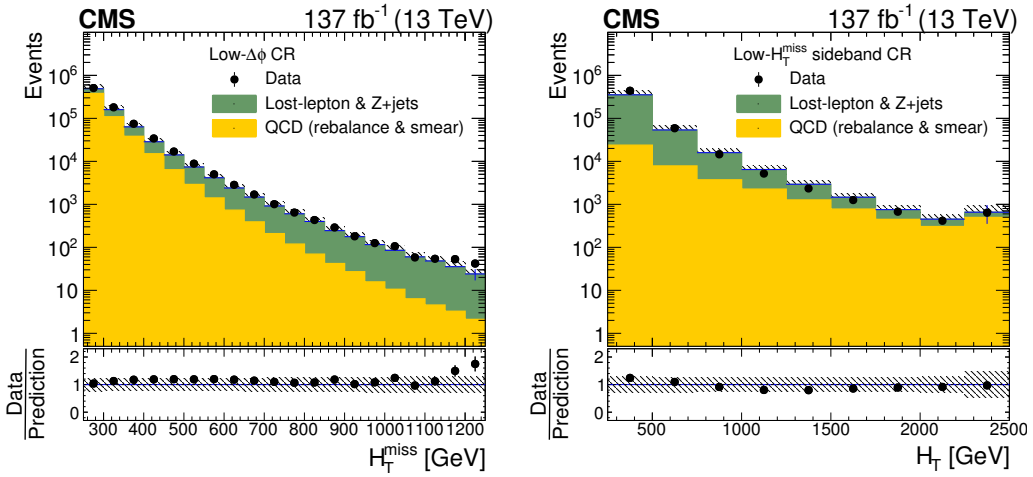

Figure 8. The observed and predicted distributions of (left) $H_{\mathrm{T}}^{\mathrm{miss}}$ in the inverted-$\Delta\phi$ control region and (right) H_{T} in the low-$H_{\mathrm{T}}^{\mathrm{miss}}$ sideband. The uncertainties are statistical only. The lower panels show the ratios of the observed to the predicted distributions, with their statistical uncertainties. The hatched regions indicate the total uncertainties in the predictions, with statistical and systematic uncertainties combined in quadrature.

that collected the seed event divided by the number of times the event was reused in the smearing step.

The R&S procedure produces a sample of events that closely resembles the original sample of CR events, except with the contributions of the electroweak backgrounds effectively removed. The resulting events are subjected to the signal event selection criteria of section 5 to obtain the QCD background prediction in each search bin. The overall normalization is adjusted based on a scaling factor derived from a QCD-dominated CR selected by inverting the $\Delta\phi$ selection criteria and requiring $N_{\text{b-jet}} = 0$ and $250 < H_{\mathrm{T}}^{\mathrm{miss}} < 300\,\mathrm{GeV}$. The $\Delta\phi$ selection criteria are inverted by requiring at least one of the two (for $N_{\mathrm{jet}} = 2$), three (for $N_{\mathrm{jet}} = 3$), or four (for $N_{\mathrm{jet}} \geq 4$) highest p_{T} jets in an event to fail at least one of the corresponding $\Delta\phi_{H_{\mathrm{T}}^{\mathrm{miss}},\mathrm{j_i}}$ requirements given in section 5. The normalization scale factors typically have values around 1.4.

Comparisons between the predicted QCD background yields and observations are examined as a function of $H_{\mathrm{T}}^{\mathrm{miss}}$, H_{T}, N_{jet}, and $N_{\text{b-jet}}$, both in a CR defined by inverting the $\Delta\phi$ requirements and in a low-$H_{\mathrm{T}}^{\mathrm{miss}}$ sideband defined by $250 < H_{\mathrm{T}}^{\mathrm{miss}} < 300\,\mathrm{GeV}$. As examples, figure 8 shows the distribution of $H_{\mathrm{T}}^{\mathrm{miss}}$ in the inverted-$\Delta\phi$ CR and the distribution of H_{T} in the low-$H_{\mathrm{T}}^{\mathrm{miss}}$ sideband.

Figure 9 shows the observed and predicted event yields in 174 analysis control bins defined using the same criteria as for the search bins except with the inverted-$\Delta\phi$ requirement. For all these validation tests, contributions from QCD events are evaluated using the R&S method, contributions from top quarks and W+jets events are evaluated using the lost-lepton method described in section 7.1, and contributions from $\mathrm{Z}(\to \nu\overline{\nu})$+jets events are taken from simulation.

The principal uncertainty in the R&S QCD background prediction is systematic, associated with the uncertainty in the shape of the jet response functions. This uncertainty is

JHEP10(2019)244

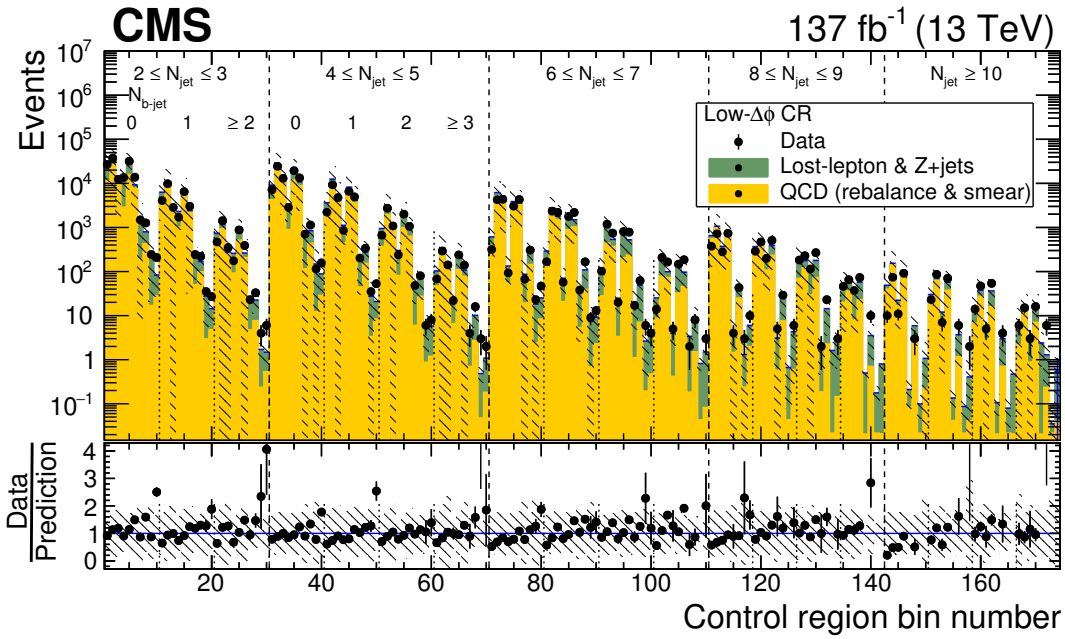

Figure 9. Distribution of observed and predicted event yields in the inverted-$\Delta\phi$ control region analysis bins. The uncertainties are statistical only. The labeling of the bin numbers is the same as in figure 7. The lower panel shows the ratio of the observed to the predicted event yields, with their statistical uncertainties. The hatched region indicates the total uncertainty in the prediction, with statistical and systematic uncertainties combined in quadrature.

evaluated by varying the jet energy resolution scale factors within their uncertainties, resulting in uncertainties in the prediction that range from 30–70%, depending on the search bin. Smaller uncertainties related to the trigger and the finite size of the seed sample are evaluated, as well as a nonclosure uncertainty that accounts for inaccuracies identified from simulation-based studies.

8 Signal systematic uncertainties

Systematic uncertainties in the signal event yield are listed in table 2. To evaluate the uncertainty associated with the renormalization (μ_R) and factorization (μ_F) scales, each scale is varied independently by a factor of 2.0 and 0.5 [92–94]. The uncertainties associated with μ_R, μ_F, and ISR, integrated over all search bins, typically lie below 0.1%. Nonetheless, they can be as large as the maximum values noted in table 2 if $\Delta m \approx 0$, where Δm is the difference between the gluino or squark mass and the sum of the masses of the particles into which the gluino or squark decays. For example, for the T1tttt model, $\Delta m = m_{\tilde{g}} - (m_{\tilde{\chi}_1^0} + 2m_t)$, with m_t the top quark mass. The uncertainties associated with the jet energy scale and jet energy resolution are evaluated as functions of jet p_T and η. To evaluate the uncertainty associated with the pileup reweighting, the value of the total inelastic cross section is varied by 5% [95]. The isolated-lepton and isolated-track vetoes have a minimal impact on the T1bbbb, T1qqqq, T2bb, and T2qq models because

JHEP10(2019)244

Item	Relative uncertainty (%)
Renormalization and factorization scales μ_R & μ_F	0.0–5.7
Initial-state radiation	0.0–14
Jet energy scale	0.0–14
Jet energy resolution	0.0–10
Pileup modeling	0.0–2.4
Isolated-lepton & isolated-track vetoes (T1tttt, T5qqqqVV, and T2tt models)	2.0
Integrated luminosity	2.3–2.5
Trigger efficiency (statistical)	0.2–2.6
Trigger efficiency (systematic)	2.0
Statistical uncertainty in simulated samples	1.2–31
H_T and H_T^{miss} modeling	0.0–11
Jet quality requirements	1.0
Total	4.0–33

Table 2. Systematic uncertainties in the yield of signal events, averaged over all search bins. The variations correspond to different signal models and choices for the SUSY particle masses. Results reported as 0.0 correspond to values less than 0.05%.

events in these models rarely contain an isolated lepton. Thus, the associated uncertainty is negligible ($\lesssim$0.1%). The systematic uncertainty in the determination of the integrated luminosity varies between 2.3 and 2.5% [96–98], depending on the year of data collection.

Systematic uncertainties in the signal predictions associated with the b jet tagging and misidentification efficiencies are also evaluated. These uncertainties do not affect the signal yield but can potentially alter the shape of signal distributions. The systematic uncertainties associated with μ_R, μ_F, ISR, jet energy scale, jet energy resolution, the trigger, statistical precision in the event samples, and H_T^{miss} modeling can also affect the shapes of the signal distributions. We account for these potential changes in shape, i.e., migration of events among search bins, in the limit setting procedure described in section 9.

9 Results

Figure 10 presents the observed numbers of events in the 174 search bins. The data are shown in comparison to the stacked pre-fit predictions for the SM backgrounds, where "pre-fit" refers to the predictions determined as described in section 7, before constraints from the fitting procedure have been applied. Numerical values are given in appendix A. The uncertainties in the background predictions are mainly from systematic uncertainties in the transfer factors, statistical uncertainties in control sample yields, and systematic uncertainties in the modeling of the search variables. Appendix A lists the overall statistical and systematic uncertainties for the individual background components and for their sum. In addition to the finely segmented search bins of figure 10, we determine the results for 12 aggregate search bins, each representing a potentially interesting signal topology. These results are presented in appendix B.

JHEP10(2019)244

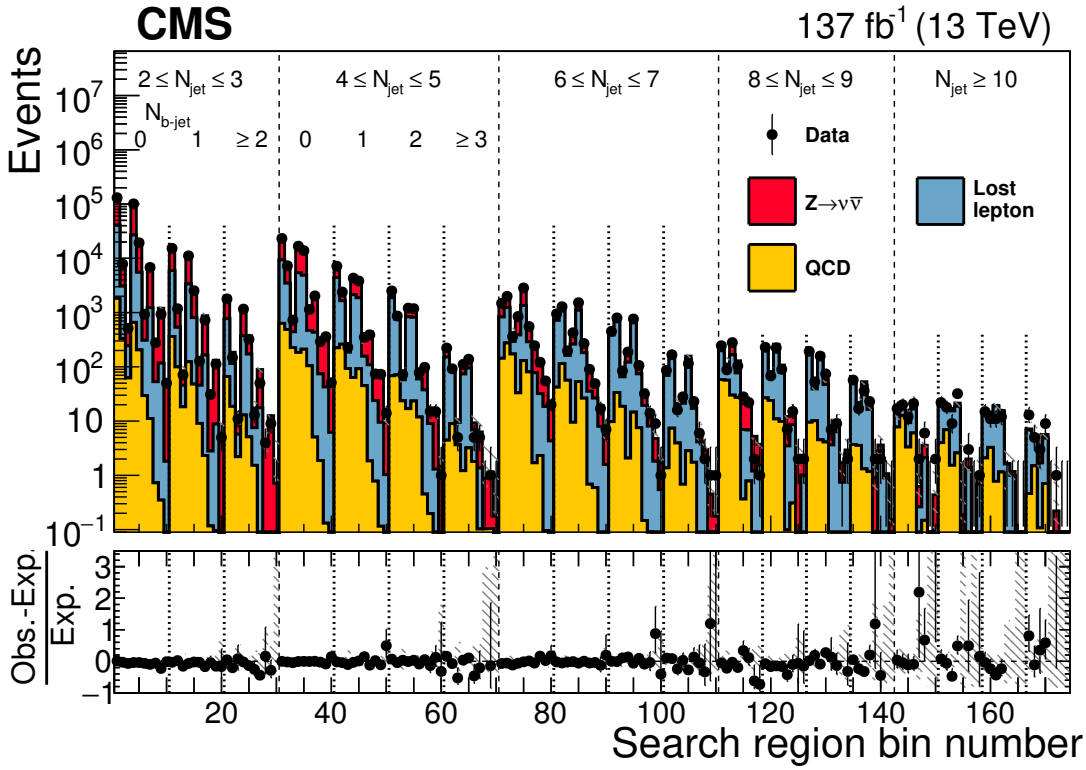

Figure 10. The observed numbers of events and pre-fit SM background predictions in the 174 search bins of the analysis, where "pre-fit" means there is no constraint from the likelihood fit. The labeling of the bin numbers is the same as in figure 7. Numerical values are given in appendix A. The hatching indicates the total uncertainty in the background predictions. The lower panel displays the fractional differences between the data and SM predictions.

The observed event counts are consistent with the predicted backgrounds. Thus we do not obtain evidence for supersymmetry.

Figure 11 presents one-dimensional projections of the data and SM predictions in $H_{\mathrm{T}}^{\mathrm{miss}}$, N_{jet}, and $N_{\mathrm{b\text{-}jet}}$. Additional projections are shown in figure 12. For these latter results, criteria have been imposed, as indicated in the legends, to enhance the sensitivity for a particular signal process. For both figures 11 and 12, two example signal distributions are shown: one with $\Delta m \gg 0$ and one with $\Delta m \approx 0$, where both example scenarios lie well within the parameter space excluded by the present study. The notation $\Delta m \gg 0$ means that the mass difference Δm is large compared to the sum of the masses of the particles into which the gluino or squark decays.

Upper limits are evaluated for the production cross sections of the signal scenarios using a likelihood fit. The SUSY signal strength μ, defined by the ratio of cross sections $\mu \equiv \sigma_{\mathrm{SUSY}}/\sigma_{\mathrm{SM}}$, the signal uncertainties described in section 8, the predicted SM background contributions shown in figure 10, the uncertainties in these backgrounds listed in appendix A, and the control sample yields are all inputs to the fit. The background uncertainties, uncertainties in the signal shape and normalization, and control sample statistical uncertainties are assigned as nuisance parameters, which are constrained in the fit.

JHEP10(2019)244

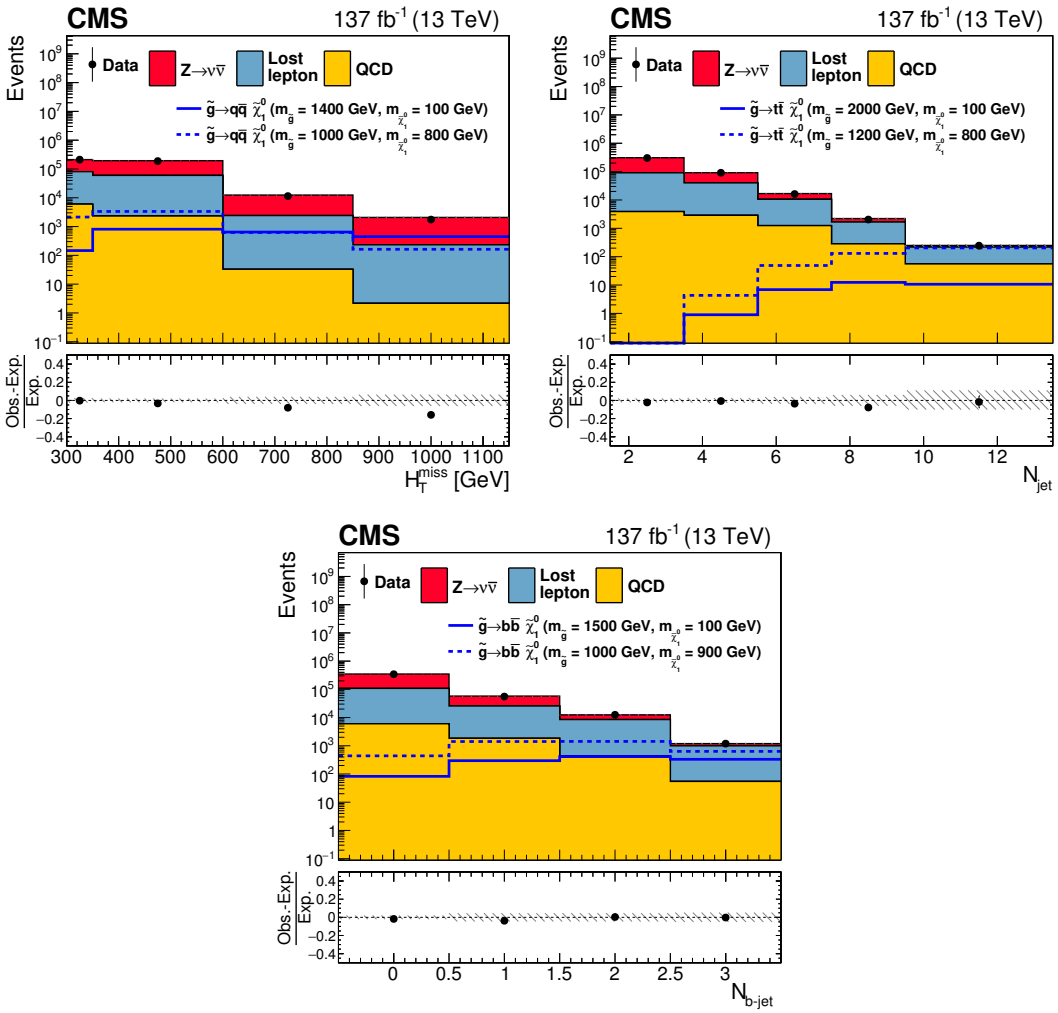

Figure 11. One-dimensional projections of the data and pre-fit SM predictions in $H_{\mathrm{T}}^{\mathrm{miss}}$, N_{jet}, and $N_{\text{b-jet}}$. The hatched regions indicate the total uncertainties in the background predictions. The (unstacked) results for two example signal scenarios are shown in each instance, one with $\Delta m \gg 0$ and the other with $\Delta m \approx 0$, where Δm is the difference between the gluino or squark mass and the sum of the masses of the particles into which it decays.

For the models of gluino (squark) pair production, the limits are derived as a function of $m_{\tilde{\mathrm{g}}}$ ($m_{\tilde{\mathrm{q}}}$) and $m_{\tilde{\chi}_1^0}$. All 174 search bins are used for each choice of the SUSY particle masses. The likelihood function is given by a product of probability density functions, one for each search bin. Each of these is a product of Poisson functions for the CR yields and log-normal constraint functions for the nuisance parameters. Correlations among bins are taken into account. The signal yield uncertainties associated with the renormalization and factorization scales, ISR, jet energy scale, b jet tagging, pileup, and statistical fluctuations are evaluated as a function of $m_{\tilde{\mathrm{g}}}$ and $m_{\tilde{\chi}_1^0}$, or $m_{\tilde{\mathrm{q}}}$ and $m_{\tilde{\chi}_1^0}$. The test statistic is $q_\mu = -2\ln(\mathcal{L}_\mu/\mathcal{L}_{\max})$, where $\mathcal{L}_{\max}$ is the maximum likelihood determined by allowing all parameters including the SUSY signal strength μ to vary, and $\mathcal{L}_\mu$ is the maximum likeli-

JHEP10(2019)244

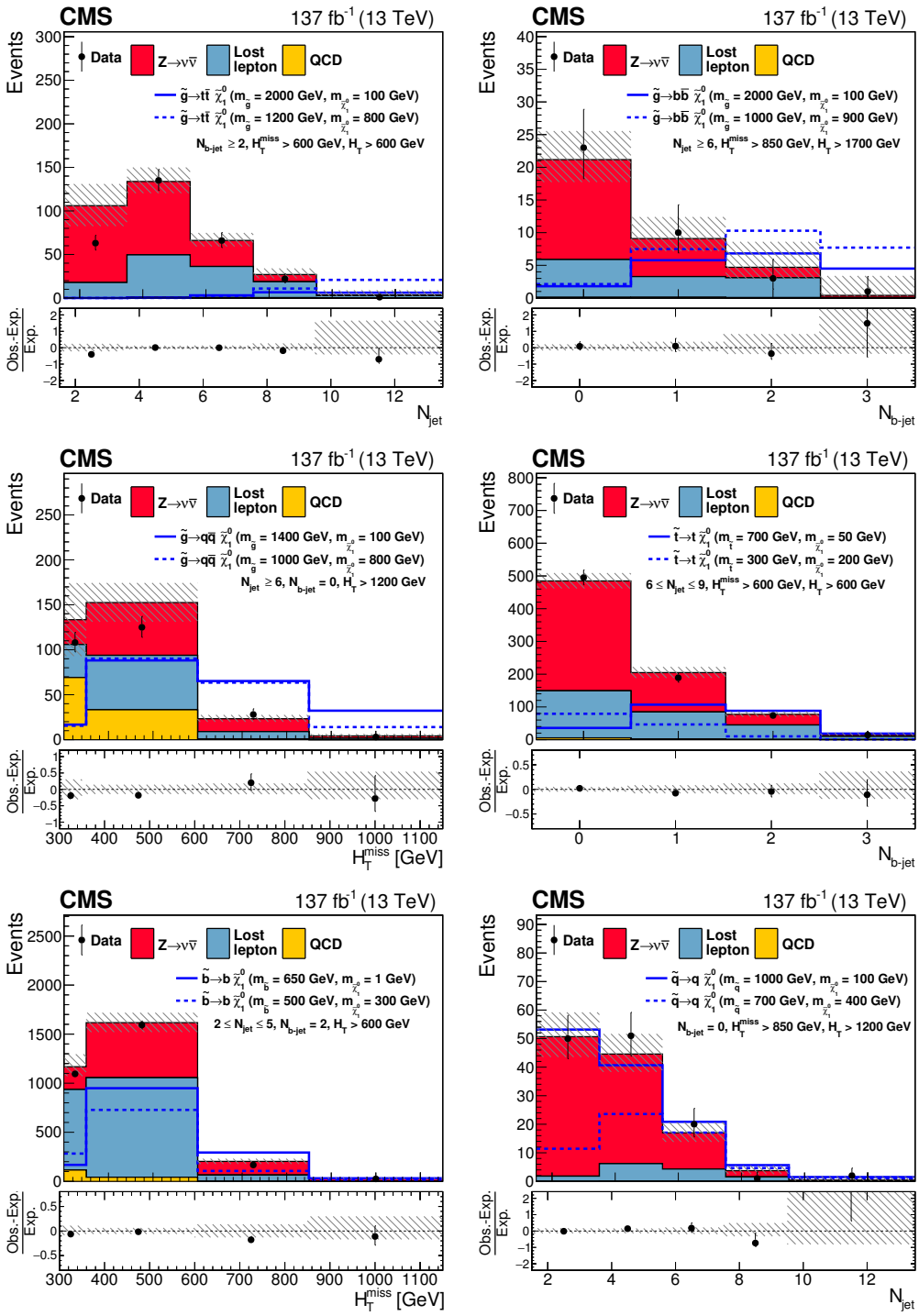

Figure 12. One-dimensional projections of the data and pre-fit SM predictions in either $H_{\mathrm{T}}^{\mathrm{miss}}$, N_{jet}, or $N_{\text{b-jet}}$ after applying additional selection criteria, given in the figure legends, to enhance the sensitivity to the (upper left) T1tttt, (upper right) T1bbbb, (middle left) T1qqqq, (middle right) T2tt, (lower left) T2bb, and (lower right) T2qq signal processes. The (unstacked) results for two example signal scenarios are shown in each instance, one with $\Delta m \gg 0$ and the other with $\Delta m \approx 0$, where Δm is the difference between the gluino or squark mass and the sum of the masses of the particles into which it decays.

JHEP10(2019)244

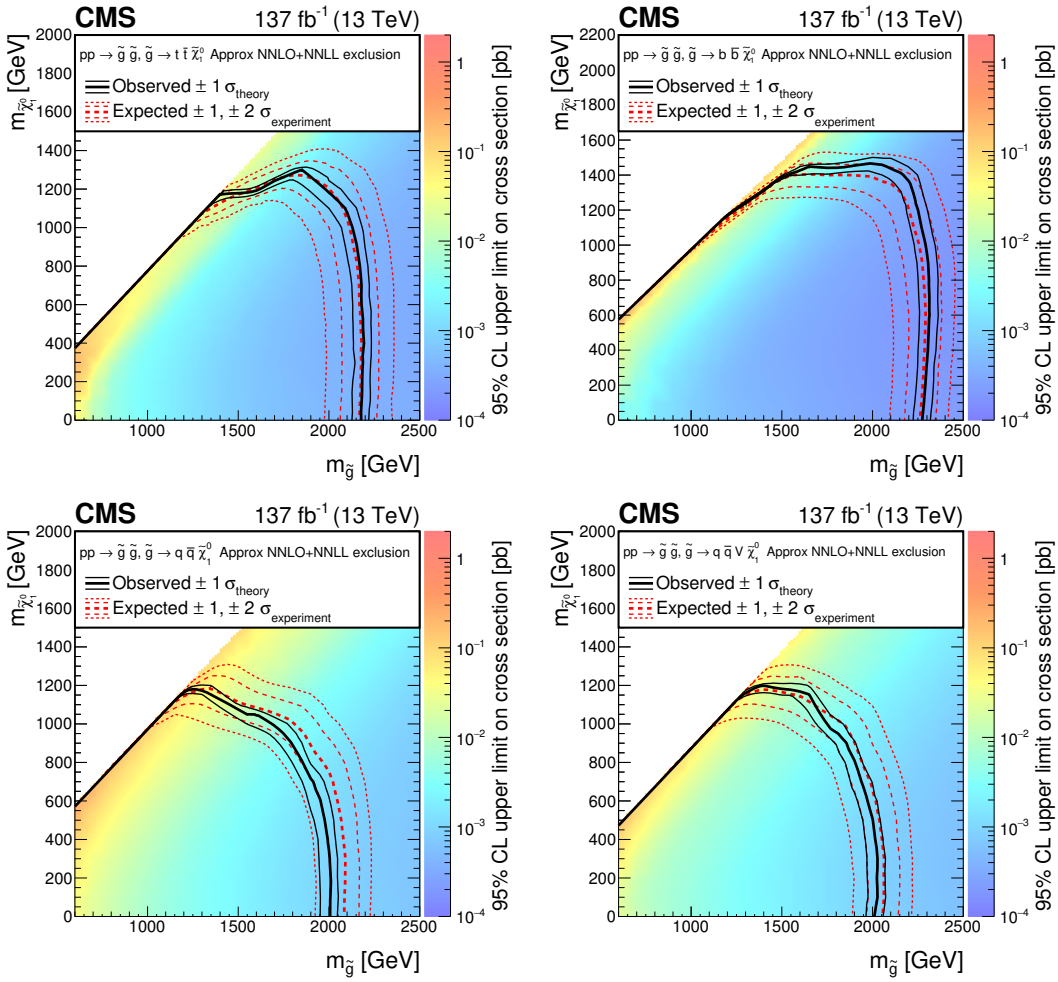

Figure 13. The 95% CL upper limits on the production cross sections of the (upper left) T1tttt, (upper right) T1bbbb, (lower left) T1qqqq, and (lower right) T5qqqqVV signal models as a function of the gluino and LSP masses $m_{\tilde{g}}$ and $m_{\tilde{\chi}_1^0}$. The thick solid (black) curves show the observed exclusion limits assuming the approximate-NNLO+NNLL cross sections [73–84]. The thin solid (black) curves show the changes in these limits as the signal cross sections are varied by their theoretical uncertainties [102]. The thick dashed (red) curves present the expected limits under the background-only hypothesis, while the two sets of thin dotted (red) curves indicate the region containing 68 and 95% of the distribution of limits expected under this hypothesis.

hood for a fixed signal strength. Limits are set under the asymptotic approximation [99], with q_μ approximated with an Asimov data set and used in conjunction with the CL_s criterion described in refs. [100, 101].

We evaluate 95% confidence level (CL) upper limits on the signal cross sections. The approximate NNLO+NNLL cross section is used to determine corresponding exclusion curves. Before computing these limits, the signal yields are corrected to account for the predicted signal contamination in the CRs from the signal model under consideration. Beyond the observed exclusion limits, we derive expected exclusion limits by evaluating the test statistic using the predicted numbers of background events with their expected Poisson fluctuations.

JHEP10(2019)244

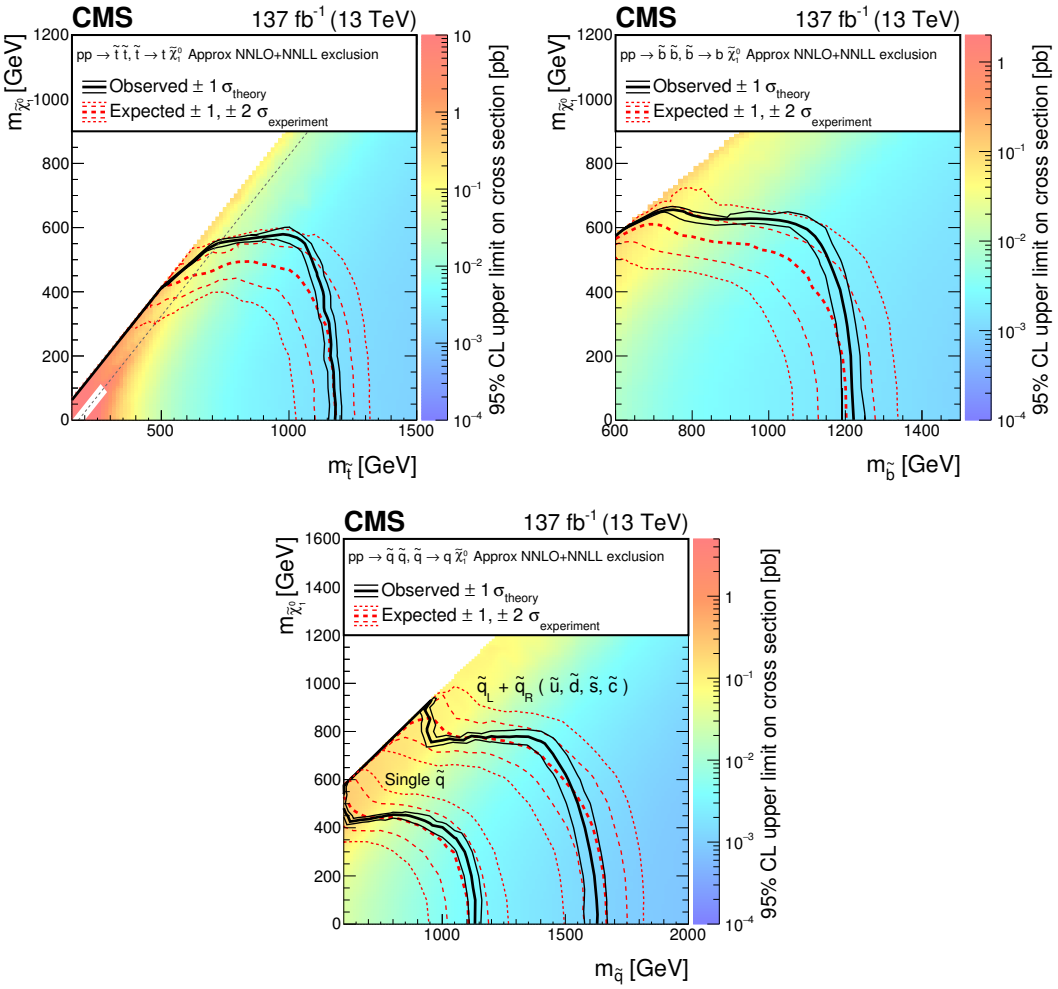

Figure 14. The 95% CL upper limits on the production cross sections of the (upper left) T2tt, (upper right) T2bb, and (lower) T2qq signal models as a function of the squark and LSP masses $m_{\tilde{q}}$ and $m_{\tilde{\chi}_1^0}$. The meaning of the curves is described in the figure 13 caption. For the T2tt model, we do not present cross section upper limits in the unshaded diagonal region at low $m_{\tilde{\chi}_1^0}$ for the reason discussed in the text. The diagonal dotted line shown for this model corresponds to $m_{\tilde{t}} - m_{\tilde{\chi}_1^0} = m_t$.

The results for the T1tttt, T1bbbb, T1qqqq, and T5qqqqVV models are shown in figure 13. Depending on the value of $m_{\tilde{\chi}_1^0}$, gluinos with masses as large as 2180, 2310, 2000, and 2030 GeV, respectively, are excluded. These results significantly extend those of our previous study [8], for which the corresponding limits are 1960, 1950, 1825, and 1800 GeV.

Figure 14 shows the corresponding results for the T2tt, T2bb, and T2qq models. Squarks with masses up to 1190, 1220, and 1630 GeV, respectively, are excluded, compared to 960, 990, and 1390 GeV in our previous study [8]. Note that for the T2tt model we do not present cross section upper limits at small values of $m_{\tilde{\chi}_1^0}$ if $m_{\tilde{t}} - m_{\tilde{\chi}_1^0} \approx m_t$, corresponding to the unshaded diagonal region at low $m_{\tilde{\chi}_1^0}$ in figure 14 (upper left), because signal events

JHEP10(2019)244

are essentially indistinguishable from SM $\mathrm{t\bar{t}}$ events in this region, resulting in large signal contamination of the CRs and rendering the signal event acceptance difficult to model.

In addition to the main T2qq model, with four mass-degenerate squark flavors (up, down, strange, and charm), each arising from two different quark spin states, figure 14 (lower) shows the results should only one of these eight states ("Single $\widetilde{\mathrm{q}}$") be accessible at the LHC. In this case, the upper limit on the squark mass is reduced to 1130 GeV.

10 Summary

Using essentially the full CMS Run 2 data sample of proton-proton collisions at $\sqrt{s} = 13\,\mathrm{TeV}$, corresponding to an integrated luminosity of $137\,\mathrm{fb}^{-1}$ collected in 2016–2018, a search for supersymmetry has been performed based on events containing multiple jets and large missing transverse momentum. The event yields are measured in 174 nonoverlapping search bins defined in a four-dimensional space of missing transverse momentum ($H_\mathrm{T}^\mathrm{miss}$), the scalar sum of jet transverse momenta (H_T), the number of jets, and the number of tagged bottom quark jets. The events are required to satisfy $H_\mathrm{T}^\mathrm{miss} > 300\,\mathrm{GeV}$, $H_\mathrm{T} > 300\,\mathrm{GeV}$, and to have at least two jets with transverse momentum $p_\mathrm{T} > 30\,\mathrm{GeV}$. Events with isolated high p_T leptons or photons are vetoed.

The results are compared to the expected number of background events from standard model (SM) processes. The principal backgrounds arise from events with neutrino production or jet mismeasurement. The SM background is evaluated using control regions in data supplemented by information from Monte Carlo event simulation. The observed event yields are found to be consistent with the SM background and no evidence for supersymmetry is obtained.

The results are interpreted in the context of simplified models for gluino and squark pair production. For the gluino models, each of the produced gluinos decays either to a $\mathrm{t\bar{t}}$ pair and an undetected, stable, lightest supersymmetric particle, assumed to be the $\widetilde{\chi}_1^0$ neutralino (T1tttt model); to a $\mathrm{b\bar{b}}$ pair and the $\widetilde{\chi}_1^0$ (T1bbbb model); to a light-flavored (u, d, s, c) $\mathrm{q\bar{q}}$ pair and the $\widetilde{\chi}_1^0$ (T1qqqq model); or to a light-flavored quark and antiquark and either the second-lightest neutralino $\widetilde{\chi}_2^0$ or the lightest chargino $\widetilde{\chi}_1^\pm$, followed by decay of the $\widetilde{\chi}_2^0$ ($\widetilde{\chi}_1^\pm$) to the $\widetilde{\chi}_1^0$ and an on- or off-mass-shell Z ($\mathrm{W}^\pm$) boson (T5qqqqVV model). For the squark models, each of the produced squarks decays either to a top quark and the $\widetilde{\chi}_1^0$ (T2tt model), to a bottom quark and the $\widetilde{\chi}_1^0$ (T2bb model), or to a light-flavored quark and the $\widetilde{\chi}_1^0$ (T2qq model).

Using the predicted cross sections with next-to-leading order plus approximate next-to-leading logarithm accuracy as a reference, gluinos with masses as large as from 2000 to 2310 GeV are excluded at 95% confidence level, depending on the signal model. The corresponding limits on the masses of directly produced squarks range from 1190 for top squarks to 1630 GeV for light-flavored squarks. The results presented here supersede those of ref. [8], extending the mass limits of this previous study by, typically, 200 GeV or more.

Acknowledgments

We congratulate our colleagues in the CERN accelerator departments for the excellent performance of the LHC and thank the technical and administrative staffs at CERN and at

JHEP10(2019)244

other CMS institutes for their contributions to the success of the CMS effort. In addition, we gratefully acknowledge the computing centers and personnel of the Worldwide LHC Computing Grid for delivering so effectively the computing infrastructure essential to our analyses. Finally, we acknowledge the enduring support for the construction and operation of the LHC and the CMS detector provided by the following funding agencies: BMBWF and FWF (Austria); FNRS and FWO (Belgium); CNPq, CAPES, FAPERJ, FAPERGS, and FAPESP (Brazil); MES (Bulgaria); CERN; CAS, MoST, and NSFC (China); COLCIENCIAS (Colombia); MSES and CSF (Croatia); RPF (Cyprus); SENESCYT (Ecuador); MoER, ERC IUT, PUT and ERDF (Estonia); Academy of Finland, MEC, and HIP (Finland); CEA and CNRS/IN2P3 (France); BMBF, DFG, and HGF (Germany); GSRT (Greece); NKFIA (Hungary); DAE and DST (India); IPM (Iran); SFI (Ireland); INFN (Italy); MSIP and NRF (Republic of Korea); MES (Latvia); LAS (Lithuania); MOE and UM (Malaysia); BUAP, CINVESTAV, CONACYT, LNS, SEP, and UASLP-FAI (Mexico); MOS (Montenegro); MBIE (New Zealand); PAEC (Pakistan); MSHE and NSC (Poland); FCT (Portugal); JINR (Dubna); MON, RosAtom, RAS, RFBR, and NRC KI (Russia); MESTD (Serbia); SEIDI, CPAN, PCTI, and FEDER (Spain); MOSTR (Sri Lanka); Swiss Funding Agencies (Switzerland); MST (Taipei); ThEPCenter, IPST, STAR, and NSTDA (Thailand); TUBITAK and TAEK (Turkey); NASU and SFFR (Ukraine); STFC (United Kingdom); DOE and NSF (U.S.A.).

Individuals have received support from the Marie-Curie program and the European Research Council and Horizon 2020 Grant, contract Nos. 675440, 752730, and 765710 (European Union); the Leventis Foundation; the A.P. Sloan Foundation; the Alexander von Humboldt Foundation; the Belgian Federal Science Policy Office; the Fonds pour la Formation à la Recherche dans l'Industrie et dans l'Agriculture (FRIA-Belgium); the Agentschap voor Innovatie door Wetenschap en Technologie (IWT-Belgium); the F.R.S.-FNRS and FWO (Belgium) under the "Excellence of Science — EOS" — be.h project n. 30820817; the Beijing Municipal Science & Technology Commission, No. Z181100004218003; the Ministry of Education, Youth and Sports (MEYS) of the Czech Republic; the Lendület ("Momentum") Program and the János Bolyai Research Scholarship of the Hungarian Academy of Sciences, the New National Excellence Program ÚNKP, the NKFIA research grants 123842, 123959, 124845, 124850, 125105, 128713, 128786, and 129058 (Hungary); the Council of Science and Industrial Research, India; the HOMING PLUS program of the Foundation for Polish Science, cofinanced from European Union, Regional Development Fund, the Mobility Plus program of the Ministry of Science and Higher Education, the National Science Center (Poland), contracts Harmonia 2014/14/M/ST2/00428, Opus 2014/13/B/ST2/02543, 2014/15/B/ST2/03998, and 2015/19/B/ST2/02861, Sonatabis 2012/07/E/ST2/01406; the National Priorities Research Program by Qatar National Research Fund; the Ministry of Science and Education, grant no. 3.2989.2017 (Russia); the Programa Estatal de Fomento de la Investigación Científica y Técnica de Excelencia María de Maeztu, grant MDM-2015-0509 and the Programa Severo Ochoa del Principado de Asturias; the Thalis and Aristeia programs cofinanced by EU-ESF and the Greek NSRF; the Rachadapisek Sompot Fund for Postdoctoral Fellowship, Chulalongkorn University and the Chulalongkorn Academic into Its 2nd Century Project Advancement Project (Thailand); the Welch Foundation, contract C-1845; and the Weston Havens Foundation (U.S.A.).

JHEP10(2019)244

A Numerical results for the full set of search bins

In this appendix, we present numerical values for the results in the 174 search bins shown in figure 10.

Bin	H_T^{miss} [GeV]	H_T [GeV]	N_{jet}	$N_{b\text{-jet}}$	Lost-lepton background	$Z \to \nu\bar{\nu}$ background	QCD background	Total background	Observed
1	300–350	300–600	2–3	0	$38\,870 \pm 320 \pm 580$	$89\,100 \pm 200 \pm 2600$	$1800 \pm 1000^{+1200}_{-800}$	$129\,800 \pm 1100 \pm 2800$	130 718
2	300–350	600–1200	2–3	0	$2760 \pm 61 \pm 39$	$4970 \pm 50 \pm 150$	$330 \pm 180 \pm 160$	$8060 \pm 200 \pm 220$	7820
3	300–350	≥1200	2–3	0	$181 \pm 17 \pm 3$	$308 \pm 12 \pm 18$	$62 \pm 34 \pm 27$	$552 \pm 40 \pm 32$	514
4	350–600	350–600	2–3	0	$26\,230 \pm 240 \pm 540$	$78\,000 \pm 200 \pm 2200$	$660 \pm 360 \pm 300$	$104\,900 \pm 500 \pm 2300$	100 828
5	350–600	600–1200	2–3	0	$5319 \pm 81 \pm 78$	$14\,570 \pm 80 \pm 430$	$210 \pm 110 \pm 100$	$20\,100 \pm 160 \pm 450$	19 319
6	350–600	≥1200	2–3	0	$279 \pm 21 \pm 6$	$689 \pm 17^{+41}_{-36}$	$29 \pm 16 \pm 13$	$997 \pm 32 \pm 40$	933
7	600–850	600–1200	2–3	0	$1220 \pm 43 \pm 25$	$6290 \pm 50 \pm 370$	$11.1 \pm 6.0^{+5.4}_{-5.1}$	$7520 \pm 70 \pm 360$	6786
8	600–850	≥1200	2–3	0	$52 \pm 9 \pm 2$	$240 \pm 11 \pm 15$	$0.73 \pm 0.65^{+0.31}_{-0.07}$	$293 \pm 14 \pm 16$	277
9	≥850	850–1700	2–3	0	$116 \pm 14 \pm 3$	$1088 \pm 23 \pm 98$	$0.35 \pm 0.21 \pm 0.15$	$1205 \pm 28 \pm 98$	933
10	≥850	≥1700	2–3	0	$1.8^{+4.1}_{-1.5} \pm 0.1$	$48.9^{+5.3}_{-4.8} \pm 0.5$	$0.02 \pm 0.02^{+0.01}_{-0.00}$	$50.7^{+6.7}_{-5.0} \pm 5.1$	50
11	300–350	300–600	2–3	1	$5590 \pm 100 \pm 100$	$9800 \pm 20 \pm 1500$	$360 \pm 200^{+330}_{-160}$	$15\,800 \pm 200 \pm 1500$	15 272
12	300–350	600–1200	2–3	1	$436 \pm 25 \pm 6$	$616 \pm 6 \pm 95$	$99 \pm 54^{+79}_{-45}$	$1150 \pm 60 \pm 110$	1177
13	300–350	≥1200	2–3	1	$27.4^{+7.9}_{-6.3} \pm 0.4$	$38.4 \pm 1.5 \pm 6.1$	$18 \pm 10^{+14}_{-8}$	$84 \pm 13^{+15}_{-10}$	71
14	350–600	350–600	2–3	1	$3237 \pm 75 \pm 99$	$8600 \pm 20 \pm 1300$	$124 \pm 67^{+96}_{-57}$	$11\,900 \pm 100 \pm 1300$	11 121
15	350–600	600–1200	2–3	1	$757 \pm 32 \pm 14$	$1780 \pm 10 \pm 270$	$48 \pm 27^{+38}_{-21}$	$2590 \pm 40 \pm 270$	2530
16	350–600	≥1200	2–3	1	$36.7^{+8.9}_{-7.3} \pm 0.5$	$86 \pm 2 \pm 14$	$9.1 \pm 5.0^{+6.9}_{-4.1}$	$132 \pm 10 \pm 15$	127
17	600–850	600–1200	2–3	1	$162 \pm 17 \pm 4$	$710 \pm 10 \pm 120$	$2.3 \pm 1.3^{+1.8}_{-1.0}$	$880 \pm 20 \pm 110$	728
18	600–850	≥1200	2–3	1	$2.7^{+3.5}_{-1.7} \pm 0.1$	$29.5 \pm 1.3 \pm 4.8$	$0.12 \pm 0.10^{+0.09}_{-0.02}$	$32.3^{+3.8}_{-2.1} \pm 4.8$	31
19	≥850	850–1700	2–3	1	$8.7^{+5.2}_{-3.5} \pm 0.2$	$124 \pm 3 \pm 22$	$0.10 \pm 0.07^{+0.07}_{-0.02}$	$133 \pm 5 \pm 22$	112
20	≥850	≥1700	2–3	1	$0.0^{+3.6}_{-0.0} \pm 0.0$	$6.0 \pm 0.7 \pm 1.1$	$0.03^{+0.04+0.02}_{-0.03-0.00}$	$6.0^{+3.6}_{-0.6} \pm 1.1$	5
21	300–350	300–600	2–3	≥2	$706 \pm 37 \pm 13$	$940 \pm 2 \pm 290$	66^{+68+72}_{-66-0}	$1710 \pm 80 \pm 290$	1787
22	300–350	600–1200	2–3	≥2	$96 \pm 13 \pm 1$	$71 \pm 1 \pm 22$	$19 \pm 11^{+19}_{-8}$	$186 \pm 18^{+29}_{-23}$	148
23	300–350	≥1200	2–3	≥2	$3.5^{+4.7}_{-2.3} \pm 0.1$	$4.4 \pm 0.2 \pm 1.4$	$2.2 \pm 1.3^{+2.1}_{-0.9}$	$10.2^{+4.8+2.5}_{-2.6-1.7}$	11
24	350–600	350–600	2–3	≥2	$362 \pm 27 \pm 14$	$810 \pm 2 \pm 250$	$13 \pm 8^{+13}_{-5}$	$1190 \pm 30 \pm 250$	1159
25	350–600	600–1200	2–3	≥2	$166 \pm 18 \pm 5$	$201 \pm 1 \pm 61$	$5.1 \pm 3.3^{+5.1}_{-1.8}$	$373 \pm 18 \pm 62$	322
26	350–600	≥1200	2–3	≥2	$6.0^{+4.8}_{-2.9} \pm 0.1$	$9.9 \pm 0.2 \pm 3.1$	$1.5 \pm 0.9^{+1.5}_{-0.6}$	$17.5^{+4.9+3.4}_{-3.1-3.1}$	13
27	600–850	600–1200	2–3	≥2	$17.5^{+7.6}_{-5.6} \pm 0.3$	$72 \pm 1 \pm 22$	$0.09 \pm 0.09^{+0.09}_{-0.00}$	$89 \pm 7 \pm 22$	50
28	600–850	≥1200	2–3	≥2	$0.0^{+2.9}_{-0.0} \pm 0.0$	$3.4 \pm 0.1 \pm 1.0$	$0.08 \pm 0.08^{+0.07}_{-0.00}$	$3.4^{+2.9}_{-0.2} \pm 1.0$	4
29	≥850	850–1700	2–3	≥2	$0.0^{+4.4}_{-0.0} \pm 0.0$	$12.5 \pm 0.3 \pm 4.0$	$0.09 \pm 0.07^{+0.09}_{-0.02}$	$12.6^{+4.5}_{-0.3} \pm 4.0$	9
30	≥850	≥1700	2–3	≥2	$0.0^{+3.7}_{-0.0} \pm 0.0$	$0.68 \pm 0.07 \pm 0.22$	$0.04 \pm 0.04^{+0.03}_{-0.00}$	$0.7^{+3.7}_{-0.1} \pm 0.2$	0

Table 3. Observed number of events and pre-fit background predictions in the $2 \leq N_{jet} \leq 3$ search bins. For the background predictions, the first uncertainty is statistical and the second systematic.

JHEP10(2019)244

Bin	$H_{\mathrm{T}}^{\mathrm{miss}}$ [GeV]	H_{T} [GeV]	N_{jet}	$N_{\mathrm{b\text{-}jet}}$	Lost-lepton background	$\mathrm{Z} \to \nu\bar{\nu}$ background	QCD background	Total background	Observed
31	300–350	300–600	4–5	0	$8720 \pm 110 \pm 120$	$13\,930 \pm 70 \pm 590$	$630 \pm 350^{+410}_{-290}$	$23\,280 \pm 370^{+740}_{-660}$	23 241
32	300–350	600–1200	4–5	0	$2990 \pm 48 \pm 54$	$3960 \pm 40 \pm 150$	$490 \pm 260 \pm 230$	$7440 \pm 270 \pm 280$	7277
33	300–350	≥1200	4–5	0	$216 \pm 14 \pm 5$	$317 \pm 12 \pm 18$	$230 \pm 120 \pm 100$	$760 \pm 120 \pm 100$	726
34	350–600	350–600	4–5	0	$5230 \pm 90 \pm 160$	$11\,410 \pm 70 \pm 450$	$180 \pm 100 \pm 80$	$16\,820 \pm 150 \pm 490$	16 720
35	350–600	600–1200	4–5	0	$4654 \pm 59 \pm 68$	$9000 \pm 60 \pm 350$	$210 \pm 110 \pm 100$	$13\,870 \pm 140 \pm 370$	13 837
36	350–600	≥1200	4–5	0	$364 \pm 17 \pm 6$	$680 \pm 17 \pm 37$	$104 \pm 56 \pm 45$	$1148 \pm 61 \pm 59$	1141
37	600–850	600–1200	4–5	0	$428 \pm 19 \pm 9$	$1592 \pm 25 \pm 94$	$5.1 \pm 2.8 \pm 2.3$	$2025 \pm 32 \pm 94$	2028
38	600–850	≥1200	4–5	0	$72.2^{+8.1}_{-7.3} \pm 1.1$	$225 \pm 10 \pm 14$	$1.9 \pm 1.1 \pm 0.8$	$299 \pm 13 \pm 14$	291
39	≥850	850–1700	4–5	0	$42.4 \pm 6.9 \pm 0.8$	$351 \pm 13 \pm 32$	$0.13 \pm 0.09 \pm 0.5$	$393 \pm 15 \pm 32$	360
40	≥850	≥1700	4–5	0	$6.1^{+3.3}_{-2.3} \pm 0.1$	$38.4 \pm 4.2 \pm 4.4$	$0.06 \pm 0.05^{+0.02}_{-0.01}$	$44.6^{+5.5}_{-4.6} \pm 4.4$	51
41	300–350	300–600	4–5	1	$4217 \pm 69 \pm 77$	$2850 \pm 15 \pm 450$	$220 \pm 120^{+200}_{-100}$	$7290 \pm 140 \pm 480$	7157
42	300–350	600–1200	4–5	1	$1389 \pm 35 \pm 23$	$850 \pm 10 \pm 130$	$260 \pm 140^{+210}_{-120}$	$2500 \pm 150^{+250}_{-180}$	2387
43	300–350	≥1200	4–5	1	$93 \pm 10 \pm 3$	$69 \pm 3 \pm 11$	$93 \pm 50^{+71}_{-43}$	$255 \pm 51^{+72}_{-44}$	229
44	350–600	350–600	4–5	1	$2068 \pm 50 \pm 41$	$2330 \pm 10 \pm 370$	$64 \pm 35^{+49}_{-29}$	$4460 \pm 60 \pm 370$	4317
45	350–600	600–1200	4–5	1	$1777 \pm 40 \pm 29$	$1910 \pm 10 \pm 300$	$92 \pm 50^{+73}_{-42}$	$3780 \pm 70 \pm 300$	3822
46	350–600	≥1200	4–5	1	$112 \pm 11 \pm 3$	$148 \pm 4 \pm 24$	$45 \pm 24^{+34}_{-21}$	$305 \pm 27^{+42}_{-32}$	350
47	600–850	600–1200	4–5	1	$107 \pm 11 \pm 3$	$332 \pm 5 \pm 54$	$1.8 \pm 1.1^{+1.5}_{-0.8}$	$441 \pm 12 \pm 54$	388
48	600–850	≥1200	4–5	1	$23.1^{+5.5}_{-4.6} \pm 0.4$	$48.6 \pm 2.2 \pm 8.0$	$0.78 \pm 0.51^{+0.59}_{-0.27}$	$72.5 \pm 5.5 \pm 8.1$	74
49	≥850	850–1700	4–5	1	$9.4^{+4.0}_{-3.0} \pm 0.3$	$73 \pm 3 \pm 13$	$0.12 \pm 0.09^{+0.09}_{-0.03}$	$82 \pm 5 \pm 13$	73
50	≥850	≥1700	4–5	1	$1.0^{+2.3}_{-0.8} \pm 0.0$	$8.3 \pm 1.0 \pm 1.6$	$0.03^{+0.04+0.02}_{-0.03-0.00}$	$9.4^{+2.5}_{-1.2} \pm 1.6$	14
51	300–350	300–600	4–5	2	$1806 \pm 49 \pm 30$	$468 \pm 2 \pm 79$	$68 \pm 45^{+74}_{-24}$	$2340 \pm 70^{+110}_{-90}$	2505
52	300–350	600–1200	4–5	2	$687 \pm 26 \pm 10$	$144 \pm 1 \pm 24$	$71 \pm 39^{+70}_{-32}$	$902 \pm 47^{+75}_{-41}$	864
53	300–350	≥1200	4–5	2	$34.0^{+7.4}_{-6.2} \pm 0.7$	$12.0 \pm 0.4 \pm 2.1$	$24 \pm 13^{+23}_{-11}$	$70 \pm 14^{+23}_{-11}$	72
54	350–600	350–600	4–5	2	$820 \pm 35 \pm 20$	$381 \pm 2 \pm 64$	$17 \pm 10^{+17}_{-7}$	$1218 \pm 36 \pm 68$	1208
55	350–600	600–1200	4–5	2	$794 \pm 29 \pm 12$	$324 \pm 2 \pm 54$	$23 \pm 13^{+23}_{-10}$	$1141 \pm 32 \pm 58$	1180
56	350–600	≥1200	4–5	2	$47.8^{+8.2+1.1}_{-7.2-1.1}$	$25.6^{+0.6+4.4}_{-0.6-4.4}$	12^{+7+12}_{-7-5}	85^{+11+12}_{-10-7}	78
57	600–850	600–1200	4–5	2	$37.1^{+8.0}_{-6.7} \pm 0.7$	$55.5 \pm 0.9 \pm 9.6$	$0.45 \pm 0.30^{+0.45}_{-0.16}$	$93.1^{+8.0}_{-6.8} \pm 9.7$	98
58	600–850	≥1200	4–5	2	$8.8^{+5.3}_{-3.5} \pm 0.1$	$8.4 \pm 0.4 \pm 1.5$	$0.20 \pm 0.18^{+0.19}_{-0.02}$	$17.4^{+5.3}_{-3.6} \pm 1.5$	15
59	≥850	850–1700	4–5	2	$1.2^{+2.8}_{-1.0} \pm 0.0$	$12.0 \pm 0.4 \pm 2.2$	$0.09 \pm 0.07^{+0.09}_{-0.02}$	$13.3^{+2.8}_{-1.1} \pm 2.2$	15
60	≥850	≥1700	4–5	2	$0.0^{+2.6}_{-0.0} \pm 0.0$	$1.44 \pm 0.16 \pm 0.28$	$0.04 \pm 0.04^{+0.03}_{-0.00}$	$1.5^{+2.6}_{-0.1} \pm 0.3$	1
61	300–350	300–600	4–5	≥3	$147 \pm 15 \pm 2$	$40 \pm 0 \pm 14$	$4.4 \pm 4.2^{+6.1}_{-0.2}$	$192 \pm 15 \pm 15$	222
62	300–350	600–1200	4–5	≥3	$76.7 \pm 9.0 \pm 1.3$	$13.5 \pm 0.1 \pm 4.8$	$9 \pm 6^{+12}_{-3}$	$99 \pm 10^{+13}_{-6}$	92
63	300–350	≥1200	4–5	≥3	$5.8^{+3.9}_{-2.5} \pm 0.1$	$1.14 \pm 0.04 \pm 0.41$	$3.7 \pm 2.2^{+4.7}_{-1.5}$	$10.6^{+4.5+4.7}_{-3.3-1.5}$	5
64	350–600	350–600	4–5	≥3	$73 \pm 11 \pm 1$	$33 \pm 0 \pm 12$	$1.2 \pm 1.1^{+1.6}_{-0.1}$	$107 \pm 11 \pm 12$	111
65	350–600	600–1200	4–5	≥3	92^{+11+2}_{-10-2}	30^{+0+11}_{-0-11}	$3.2^{+2.0+4.2}_{-2.0-1.2}$	125^{+11+12}_{-10-11}	138
66	350–600	≥1200	4–5	≥3	$5.0^{+3.4}_{-2.2} \pm 0.1$	$2.45 \pm 0.06 \pm 0.87$	$1.8 \pm 1.2^{+2.3}_{-0.6}$	$9.3^{+3.6+2.5}_{-2.5-1.1}$	5
67	600–850	600–1200	4–5	≥3	$1.3^{+2.9}_{-1.1} \pm 0.0$	$4.9 \pm 0.1 \pm 1.8$	$0.10^{+0.12+0.13}_{-0.10-0.00}$	$6.3^{+2.9}_{-1.1} \pm 1.8$	5
68	600–850	≥1200	4–5	≥3	$0.0^{+2.6}_{-0.0} \pm 0.0$	$0.79 \pm 0.04 \pm 0.28$	$0.10^{+0.12+0.13}_{-0.10-0.00}$	$0.9^{+2.6}_{-0.1} \pm 0.3$	0
69	≥850	850–1700	4–5	≥3	$0.0^{+3.2}_{-0.0} \pm 0.0$	$1.05 \pm 0.04 \pm 0.38$	$0.10 \pm 0.09^{+0.13}_{-0.02}$	$1.2^{+3.2}_{-0.1} \pm 0.4$	1
70	≥850	≥1700	4–5	≥3	$0.0^{+2.3}_{-0.0} \pm 0.0$	$0.13 \pm 0.01 \pm 0.05$	$0.04^{+0.05+0.05}_{-0.04-0.00}$	$0.2^{+2.3}_{-0.0} \pm 0.1$	0

Table 4. Observed number of events and pre-fit background predictions in the $4 \leq N_{\mathrm{jet}} \leq 5$ search bins. For the background predictions, the first uncertainty is statistical and the second systematic.

JHEP10(2019)244

Bin	$H_{\mathrm{T}}^{\mathrm{miss}}$ [GeV]	H_{T} [GeV]	N_{jet}	$N_{\mathrm{b\text{-}jet}}$	Lost-lepton background	$\mathrm{Z} \to \nu\bar{\nu}$ background	QCD background	Total background	Observed
71	300–350	300–600	6–7	0	$686 \pm 29 \pm 11$	$761 \pm 17 \pm 63$	$144 \pm 83^{+92}_{-61}$	$1590 \pm 90^{+110}_{-90}$	1480
72	300–350	600–1200	6–7	0	$967 \pm 25 \pm 14$	$873 \pm 18 \pm 65$	$280 \pm 140 \pm 130$	$2110 \pm 140 \pm 150$	1993
73	300–350	≥1200	6–7	0	$121.5 \pm 8.8 \pm 2.8$	$116.8 \pm 7.3 \pm 9.2$	$172 \pm 86 \pm 74$	$410 \pm 87 \pm 75$	362
74	350–600	350–600	6–7	0	$353 \pm 21 \pm 8$	$514 \pm 14 \pm 40$	$33 \pm 20 \pm 14$	$901 \pm 32 \pm 44$	847
75	350–600	600–1200	6–7	0	$1219 \pm 28 \pm 28$	$1540 \pm 20 \pm 110$	$130 \pm 65 \pm 63$	$2890 \pm 80 \pm 130$	2842
76	350–600	≥1200	6–7	0	$208 \pm 11 \pm 4$	$258 \pm 11 \pm 18$	$81 \pm 40 \pm 35$	$547 \pm 43 \pm 39$	553
77	600–850	600–1200	6–7	0	$76.1^{+1.0}_{-1.0} \pm 1.0$	$182 \pm 8 \pm 15$	$1.70 \pm 0.88 \pm 0.81$	$259 \pm 11 \pm 15$	245
78	600–850	≥1200	6–7	0	$29.7 \pm 4.2 \pm 0.5$	$72.8 \pm 5.6 \pm 5.7$	$2.3 \pm 1.2 \pm 1.0$	$104.8^{+7.4}_{-6.7} \pm 5.8$	122
79	≥850	850–1700	6–7	0	$18.5 \pm 3.5 \pm 0.3$	$35.2 \pm 3.6 \pm 3.8$	$0.10 \pm 0.07^{+0.04}_{-0.02}$	$53.8^{+5.4}_{-4.7} \pm 3.9$	55
80	≥850	≥1700	6–7	0	$4.3^{+2.0}_{-1.4} \pm 0.2$	$12.7 \pm 2.3 \pm 1.9$	$0.05 \pm 0.04^{+0.02}_{-0.01}$	$17.0^{+3.2}_{-2.6} \pm 1.9$	20
81	300–350	300–600	6–7	1	$675 \pm 25 \pm 12$	$248 \pm 6 \pm 45$	$42 \pm 22^{+27}_{-20}$	$965 \pm 34 \pm 53$	946
82	300–350	600–1200	6–7	1	$950 \pm 26 \pm 15$	$289 \pm 6 \pm 52$	$115 \pm 58 \pm 55$	$1355 \pm 63 \pm 77$	1282
83	300–350	≥1200	6–7	1	$105.6^{+9.1}_{-8.4} \pm 2.7$	$39.3 \pm 2.5 \pm 7.1$	$57 \pm 28 \pm 24$	$201 \pm 30 \pm 26$	197
84	350–600	350–600	6–7	1	$252 \pm 16 \pm 5$	$168 \pm 5 \pm 30$	$9.5 \pm 5.0 \pm 4.3$	$429 \pm 18 \pm 31$	425
85	350–600	600–1200	6–7	1	$1050 \pm 28 \pm 19$	$510 \pm 8 \pm 91$	$53 \pm 27 \pm 26$	$1614 \pm 39 \pm 96$	1521
86	350–600	≥1200	6–7	1	$155 \pm 11 \pm 4$	$86 \pm 4 \pm 15$	$26 \pm 13 \pm 11$	$268 \pm 17 \pm 20$	269
87	600–850	600–1200	6–7	1	$34.7^{+5.4}_{-4.8} \pm 0.6$	$60 \pm 3 \pm 11$	$0.69 \pm 0.41^{+0.33}_{-0.28}$	$95 \pm 6 \pm 11$	90
88	600–850	≥1200	6–7	1	$25.9 \pm 4.3 \pm 0.4$	$24.4 \pm 1.9 \pm 4.4$	$0.59 \pm 0.34 \pm 0.25$	$50.9^{+5.1}_{-4.4} \pm 4.4$	49
89	≥850	850–1700	6–7	1	$7.9^{+2.9}_{-2.2} \pm 0.1$	$11.5 \pm 1.1 \pm 2.3$	$0.05 \pm 0.04^{+0.02}_{-0.00}$	$19.4^{+3.2}_{-2.5} \pm 2.3$	17
90	≥850	≥1700	6–7	1	$1.5^{+2.0}_{-1.0} \pm 0.0$	$4.29^{+0.85}_{-0.72} \pm 0.95$	$0.04^{+0.05+0.02}_{-0.04-0.00}$	$5.9^{+2.2}_{-1.2} \pm 0.9$	7
91	300–350	300–600	6–7	2	$376 \pm 19 \pm 8$	$64 \pm 2 \pm 13$	$9.8 \pm 5.5^{+6.3}_{-4.2}$	$450 \pm 20 \pm 16$	450
92	300–350	600–1200	6–7	2	$693 \pm 23 \pm 10$	$76 \pm 2 \pm 15$	$34 \pm 17 \pm 16$	$803 \pm 28 \pm 25$	797
93	300–350	≥1200	6–7	2	$46.7^{+6.4}_{-5.7} \pm 0.7$	$10.5 \pm 0.7 \pm 2.1$	$18.7 \pm 9.4 \pm 8.1$	$76 \pm 11 \pm 8$	84
94	350–600	350–600	6–7	2	$120 \pm 12 \pm 2$	$43.6 \pm 1.2 \pm 8.9$	$2.1 \pm 1.2 \pm 0.9$	$165 \pm 12 \pm 9$	188
95	350–600	600–1200	6–7	2	$661 \pm 23 \pm 11$	$134 \pm 2 \pm 27$	$14.6 \pm 7.5 \pm 7.0$	$809 \pm 24 \pm 30$	762
96	350–600	≥1200	6–7	2	$66.6 \pm 7.3 \pm 2.2$	$22.8 \pm 0.9 \pm 4.6$	$7.5 \pm 3.8 \pm 3.2$	$96.9 \pm 8.3 \pm 6.0$	106
97	600–850	600–1200	6–7	2	$19.3^{+4.7}_{-3.9} \pm 0.3$	$15.7 \pm 0.7 \pm 3.2$	$0.15 \pm 0.10 \pm 0.06$	$35.2 \pm 4.3 \pm 3.2$	32
98	600–850	≥1200	6–7	2	$8.0^{+3.2}_{-2.4} \pm 0.2$	$6.5 \pm 0.5 \pm 1.3$	$0.09 \pm 0.07^{+0.04}_{-0.01}$	$14.5^{+3.3}_{-2.4} \pm 1.3$	14
99	≥850	850–1700	6–7	2	$1.8^{+1.7}_{-1.0} \pm 0.0$	$2.98 \pm 0.30 \pm 0.65$	$0.05 \pm 0.04^{+0.02}_{-0.01}$	$4.8^{+1.8}_{-1.0} \pm 0.7$	9
100	≥850	≥1700	6–7	2	$0.5^{+1.2}_{-0.4} \pm 0.0$	$1.15^{+0.23}_{-0.19} \pm 0.28$	$0.02 \pm 0.02^{+0.01}_{-0.00}$	$1.7^{+1.2}_{-0.5} \pm 0.3$	1
101	300–350	300–600	6–7	≥3	$67.8^{+8.8}_{-7.9} \pm 1.6$	$8.8 \pm 0.2 \pm 3.7$	$1.4 \pm 1.0^{+0.9}_{-0.4}$	$78.0 \pm 8.5 \pm 4.0$	86
102	300–350	600–1200	6–7	≥3	$136 \pm 11 \pm 2$	$10.5 \pm 0.2 \pm 4.3$	$7.4 \pm 4.2^{+3.6}_{-3.2}$	$154 \pm 11 \pm 6$	167
103	300–350	≥1200	6–7	≥3	$15.7^{+4.1}_{-3.4} \pm 0.2$	$1.44 \pm 0.09 \pm 0.59$	$3.9 \pm 2.2 \pm 1.7$	$21.1 \pm 4.3 \pm 1.8$	16
104	350–600	350–600	6–7	≥3	$20.6^{+5.3}_{-4.3} \pm 0.5$	$6.0 \pm 0.2 \pm 2.5$	$0.68 \pm 0.62^{+0.31}_{-0.07}$	$27.2^{+5.4}_{-4.4} \pm 2.5$	28
105	350–600	600–1200	6–7	≥3	$137 \pm 11 \pm 4$	$18.5 \pm 0.3 \pm 7.6$	$2.8 \pm 1.6 \pm 1.3$	$158 \pm 11 \pm 9$	115
106	350–600	≥1200	6–7	≥3	$15.4^{+4.4}_{-3.5} \pm 0.6$	$3.1 \pm 0.1 \pm 1.3$	$1.7 \pm 1.0^{+0.8}_{-0.7}$	$20.2^{+4.5}_{-3.7} \pm 1.6$	23
107	600–850	600–1200	6–7	≥3	$4.1^{+2.5}_{-1.7} \pm 0.0$	$2.16 \pm 0.10 \pm 0.89$	$0.05^{+0.06+0.02}_{-0.05-0.00}$	$6.3^{+2.5}_{-1.7} \pm 0.9$	6
108	600–850	≥1200	6–7	≥3	$2.1^{+2.0}_{-1.1} \pm 0.0$	$0.89 \pm 0.07 \pm 0.37$	$0.07 \pm 0.06^{+0.03}_{-0.01}$	$3.0^{+2.0}_{-1.1} \pm 0.4$	2
109	≥850	850–1700	6–7	≥3	$0.0^{+1.2}_{-0.0} \pm 0.0$	$0.41 \pm 0.04 \pm 0.17$	$0.05 \pm 0.04^{+0.02}_{-0.01}$	$0.5^{+1.2}_{-0.1} \pm 0.2$	1
110	≥850	≥1700	6–7	≥3	$0.0^{+1.9}_{-0.0} \pm 0.0$	$0.16 \pm 0.03 \pm 0.07$	$0.02 \pm 0.02^{+0.01}_{-0.00}$	$0.2^{+1.9}_{-0.0} \pm 0.1$	1

Table 5. Observed number of events and pre-fit background predictions in the $6 \leq N_{\mathrm{jet}} \leq 7$ search bins. For the background predictions, the first uncertainty is statistical and the second systematic.

JHEP10(2019)244

Bin	H_T^{miss} [GeV]	H_T [GeV]	N_{jet}	$N_{b\text{-jet}}$	Lost-lepton background	$Z \to \nu\bar{\nu}$ background	QCD background	Total background	Observed
111	300–350	600–1200	8–9	0	$139.5 \pm 9.5 \pm 1.9$	$60.0 \pm 4.6 \pm 9.7$	$58 \pm 29 \pm 28$	$258 \pm 31 \pm 30$	245
112	300–350	≥1200	8–9	0	$31.0 \pm 4.3 \pm 1.1$	$25.1 \pm 3.5 \pm 2.7$	$57 \pm 28 \pm 24$	$113 \pm 29 \pm 25$	88
113	350–600	600–1200	8–9	0	$136.1 \pm 9.3 \pm 1.7$	$123 \pm 7 \pm 14$	$30 \pm 15 \pm 14$	$289 \pm 19 \pm 20$	280
114	350–600	≥1200	8–9	0	$49.9 \pm 5.3 \pm 0.9$	$52.2 \pm 4.8 \pm 5.4$	$27 \pm 14 \pm 12$	$129 \pm 16 \pm 13$	104
115	600–850	600–1200	8–9	0	$6.6^{+2.3}_{-1.8} \pm 0.2$	$13.9 \pm 2.4 \pm 1.5$	$0.37 \pm 0.21 \pm 0.17$	$20.9^{+3.5}_{-2.9} \pm 1.5$	28
116	600–850	≥1200	8–9	0	$6.1^{+2.1}_{-1.6} \pm 0.1$	$12.9 \pm 2.4 \pm 1.6$	$0.79 \pm 0.44 \pm 0.34$	$19.7 \pm 3.0 \pm 1.6$	22
117	≥850	850–1700	8–9	0	$1.1^{+1.1}_{-0.6} \pm 0.0$	$4.1^{+1.5}_{-1.2} \pm 0.6$	$0.06 \pm 0.04^{+0.03}_{-0.02}$	$5.3^{+1.9}_{-1.3} \pm 0.6$	2
118	≥850	≥1700	8–9	0	$1.5^{+1.2}_{-0.7} \pm 0.1$	$2.2^{+1.3}_{-0.9} \pm 0.3$	$0.02 \pm 0.02^{+0.01}_{-0.00}$	$3.7^{+1.8}_{-1.1} \pm 0.3$	1
119	300–350	600–1200	8–9	1	$183 \pm 11 \pm 3$	$37 \pm 3 \pm 11$	$27 \pm 13 \pm 13$	$247 \pm 18 \pm 17$	229
120	300–350	≥1200	8–9	1	$43.8 \pm 5.3 \pm 0.7$	$13.8 \pm 1.9 \pm 3.8$	$24 \pm 12 \pm 10$	$82 \pm 13 \pm 11$	68
121	350–600	600–1200	8–9	1	$176 \pm 11 \pm 3$	$75 \pm 4 \pm 21$	$10.9 \pm 5.5 \pm 5.3$	$262 \pm 13 \pm 22$	224
122	350–600	≥1200	8–9	1	$68.4 \pm 6.5 \pm 1.2$	$29.5 \pm 2.7 \pm 8.1$	$9.8 \pm 5.0 \pm 4.2$	$107.8 \pm 8.5 \pm 9.3$	90
123	600–850	600–1200	8–9	1	$3.4^{+2.0}_{-1.4} \pm 0.2$	$8.7 \pm 1.5 \pm 2.4$	$0.10 \pm 0.08^{+0.05}_{-0.02}$	$12.2 \pm 2.3 \pm 2.4$	7
124	600–850	≥1200	8–9	1	$8.3^{+2.8}_{-2.1} \pm 0.1$	$8.1 \pm 1.5 \pm 2.3$	$0.31 \pm 0.18 \pm 0.12$	$16.7^{+3.2}_{-2.6} \pm 2.3$	15
125	≥850	850–1700	8–9	1	$0.0^{+1.2}_{-0.0} \pm 0.0$	$2.08^{+0.79}_{-0.59} \pm 0.61$	$0.05 \pm 0.04^{+0.02}_{-0.01}$	$2.1^{+1.5}_{-0.6} \pm 0.6$	2
126	≥850	≥1700	8–9	1	$1.0^{+1.3}_{-0.7} \pm 0.0$	$1.35^{+0.81}_{-0.54} \pm 0.40$	$0.02 \pm 0.02^{+0.01}_{-0.00}$	$2.4^{+1.5}_{-0.8} \pm 0.4$	2
127	300–350	600–1200	8–9	2	$169 \pm 11 \pm 4$	$11.0 \pm 0.9 \pm 4.1$	$9.5 \pm 4.9 \pm 4.6$	$190 \pm 12 \pm 7$	193
128	300–350	≥1200	8–9	2	$28.9 \pm 4.4 \pm 0.5$	$5.5 \pm 0.8 \pm 1.9$	$10.1 \pm 5.1 \pm 4.4$	$44.6 \pm 6.8 \pm 4.8$	53
129	350–600	600–1200	8–9	2	$146 \pm 10 \pm 2$	$23.1 \pm 1.3 \pm 8.1$	$4.5 \pm 2.4 \pm 2.1$	$174 \pm 11 \pm 9$	158
130	350–600	≥1200	8–9	2	$42.9 \pm 5.3 \pm 0.9$	$11.0 \pm 1.1 \pm 3.9$	$4.1 \pm 2.1 \pm 1.8$	$58.0^{+6.1}_{-5.5} \pm 4.4$	74
131	600–850	600–1200	8–9	2	$3.6^{+2.4}_{-1.6} \pm 0.2$	$2.52 \pm 0.44 \pm 0.89$	$0.09 \pm 0.08^{+0.04}_{-0.01}$	$6.2^{+2.5}_{-1.6} \pm 0.9$	7
132	600–850	≥1200	8–9	2	$8.0^{+2.9}_{-2.2} \pm 0.3$	$2.30 \pm 0.42 \pm 0.82$	$0.08^{+0.09+0.04}_{-0.08-0.00}$	$10.4^{+3.0}_{-2.3} \pm 0.9$	9
133	≥850	850–1700	8–9	2	$0.7^{+1.6}_{-0.6} \pm 0.0$	$0.96^{+0.37}_{-0.27} \pm 0.35$	$0.05 \pm 0.04^{+0.02}_{-0.01}$	$1.7^{+1.6}_{-0.7} \pm 0.3$	0
134	≥850	≥1700	8–9	2	$2.5^{+3.3}_{-1.7} \pm 0.1$	$0.40^{+0.24}_{-0.16} \pm 0.15$	$0.02 \pm 0.02^{+0.01}_{-0.00}$	$2.9^{+3.4}_{-1.7} \pm 0.2$	2
135	300–350	600–1200	8–9	≥3	$46.8^{+6.1}_{-5.5} \pm 0.7$	$3.8 \pm 0.3 \pm 2.3$	$3.7 \pm 2.6^{+1.8}_{-1.2}$	$54.3 \pm 6.3 \pm 2.9$	57
136	300–350	≥1200	8–9	≥3	$17.3^{+4.0}_{-3.3} \pm 0.5$	$1.26 \pm 0.17 \pm 0.76$	$3.6 \pm 2.0 \pm 1.5$	$22.2^{+4.4}_{-3.8} \pm 1.8$	17
137	350–600	600–1200	8–9	≥3	$44.4 \pm 5.6 \pm 1.0$	$7.5 \pm 0.4 \pm 4.6$	$1.31 \pm 0.81^{+0.63}_{-0.51}$	$53.2 \pm 5.7 \pm 4.7$	36
138	350–600	≥1200	8–9	≥3	$15.2^{+3.6}_{-2.9} \pm 0.3$	$2.8 \pm 0.3 \pm 1.7$	$1.17 \pm 0.68 \pm 0.50$	$19.2 \pm 3.3 \pm 1.8$	23
139	600–850	600–1200	8–9	≥3	$0.0^{+1.7+0.0}_{-0.0-0.0}$	$0.88^{+0.16+0.54}_{-0.14-0.53}$	$0.04^{+0.04+0.02}_{-0.04-0.00}$	$0.9^{+1.7+0.5}_{-0.1-0.5}$	2
140	600–850	≥1200	8–9	≥3	$2.7^{+2.2}_{-1.3} \pm 0.1$	$0.83 \pm 0.15 \pm 0.51$	$0.05 \pm 0.05^{+0.02}_{-0.00}$	$3.6^{+2.2}_{-1.3} \pm 0.5$	2
141	≥850	850–1700	8–9	≥3	$0.8^{+2.0}_{-0.7} \pm 0.0$	$0.18^{+0.07}_{-0.05} \pm 0.11$	$0.05 \pm 0.04^{+0.02}_{-0.01}$	$1.1^{+2.0}_{-0.7} \pm 0.1$	0
142	≥850	≥1700	8–9	≥3	$0.0^{+1.8}_{-0.0} \pm 0.0$	$0.14^{+0.08}_{-0.05} \pm 0.08$	$0.02 \pm 0.02^{+0.01}_{-0.00}$	$0.2^{+1.8}_{-0.1} \pm 0.1$	0

Table 6. Observed number of events and pre-fit background predictions in the $8 \leq N_{jet} \leq 9$ search bins. For the background predictions, the first uncertainty is statistical and the second systematic.

JHEP10(2019)244

Bin	H_T^{miss} [GeV]	H_T [GeV]	N_{jet}	$N_{b\text{-jet}}$	Lost-lepton background	$Z \to \nu\bar{\nu}$ background	QCD background	Total background	Observed
143	300–350	600–1200	≥10	0	$5.7^{+2.2}_{-1.7} \pm 0.3$	$2.9^{+1.3+0.6}_{-1.0-0.5}$	$7.8 \pm 4.5^{+3.7}_{-3.3}$	$16.4 \pm 5.0^{+3.8}_{-3.3}$	17
144	300–350	≥1200	≥10	0	$5.7^{+2.5}_{-1.8} \pm 0.2$	$2.5^{+1.5}_{-1.0} \pm 0.3$	$12.6 \pm 6.3 \pm 5.4$	$20.8^{+7.0}_{-6.7} \pm 5.4$	20
145	350–600	600–1200	≥10	0	$6.0^{+2.4}_{-1.8} \pm 0.1$	$4.2^{+1.6}_{-1.2} \pm 0.6$	$3.3 \pm 1.8 \pm 1.5$	$13.6^{+3.4}_{-2.8} \pm 1.6$	12
146	350–600	≥1200	≥10	0	$10.7^{+2.9}_{-2.3} \pm 0.2$	$6.5^{+2.1}_{-1.6} \pm 0.9$	$6.0 \pm 3.1 \pm 2.6$	$23.2^{+4.7}_{-4.2} \pm 2.8$	21
147	600–850	600–1200	≥10	0	$0.19^{+0.44}_{-0.17} \pm 0.00$	$0.36^{+0.84}_{-0.30} \pm 0.05$	$0.07 \pm 0.07^{+0.03}_{-0.00}$	$0.63^{+0.95}_{-0.35} \pm 0.05$	2
148	600–850	≥1200	≥10	0	$2.0^{+1.6}_{-1.0} \pm 0.0$	$1.5^{+1.2}_{-0.7} \pm 0.2$	$0.15 \pm 0.13^{+0.06}_{-0.02}$	$3.6^{+2.0}_{-1.2} \pm 0.2$	6
149	≥850	850–1700	≥10	0	$0.0^{+2.3}_{-0.0} \pm 0.0$	$0.00^{+0.64}_{-0.00} \pm 0.00$	$0.05 \pm 0.04^{+0.02}_{-0.01}$	$0.0^{+2.4}_{-0.0} \pm 0.0$	0
150	≥850	≥1700	≥10	0	$0.00^{+0.91}_{-0.00} \pm 0.00$	$0.42^{+0.96}_{-0.35} \pm 0.07$	$0.02 \pm 0.02^{+0.01}_{-0.00}$	$0.4^{+1.3}_{-0.3} \pm 0.1$	2
151	300–350	600–1200	≥10	1	$15.2^{+3.3}_{-2.8} \pm 0.2$	$1.24^{+0.56}_{-0.40} \pm 0.90$	$4.0 \pm 2.1 \pm 1.9$	$20.4^{+4.0}_{-3.5} \pm 2.1$	22
152	300–350	≥1200	≥10	1	$11.2^{+3.2}_{-2.6} \pm 0.4$	$1.05^{+0.63}_{-0.42} \pm 0.76$	$6.9 \pm 3.5 \pm 3.0$	$19.2^{+4.8}_{-4.4} \pm 3.1$	18
153	350–600	600–1200	≥10	1	$13.8^{+3.3}_{-2.7} \pm 0.3$	$1.8^{+0.7}_{-0.5} \pm 1.3$	$1.53 \pm 0.85^{+0.74}_{-0.68}$	$17.1^{+3.5}_{-2.9} \pm 1.5$	9
154	350–600	≥1200	≥10	1	$16.2^{+3.4}_{-2.9} \pm 0.4$	$2.7^{+0.9}_{-0.7} \pm 2.0$	$2.6 \pm 1.3 \pm 1.1$	$21.5^{+3.8}_{-3.2} \pm 2.3$	32
155	600–850	600–1200	≥10	1	$0.0^{+3.6}_{-0.0} \pm 0.0$	$0.15^{+0.35+0.11}_{-0.13-0.09}$	$0.04 \pm 0.04^{+0.02}_{-0.00}$	$0.2^{+3.6}_{-0.1} \pm 0.1$	0
156	600–850	≥1200	≥10	1	$1.3^{+1.3}_{-0.7} \pm 0.0$	$0.61^{+0.49}_{-0.29} \pm 0.44$	$0.06 \pm 0.05^{+0.03}_{-0.01}$	$2.0^{+1.4+0.5}_{-0.8-0.4}$	3
157	≥850	850–1700	≥10	1	$0.0^{+3.2}_{-0.0} \pm 0.0$	$0.00^{+0.27}_{-0.00} \pm 0.00$	$0.05 \pm 0.04^{+0.02}_{-0.01}$	$0.0^{+3.2}_{-0.0} \pm 0.0$	0
158	≥850	≥1700	≥10	1	$0.7^{+1.5}_{-0.6} \pm 0.0$	$0.18^{+0.41+0.13}_{-0.15-0.10}$	$0.03^{+0.04+0.01}_{-0.03-0.00}$	$0.9^{+1.6}_{-0.6} \pm 0.1$	1
159	300–350	600–1200	≥10	2	$13.1^{+3.2}_{-2.6} \pm 0.3$	$0.38^{+0.18+0.42}_{-0.13-0.36}$	$2.1 \pm 1.5^{+1.0}_{-0.6}$	$15.5^{+3.5+1.1}_{-3.0-0.8}$	15
160	300–350	≥1200	≥10	2	$10.8^{+3.0}_{-2.4} \pm 0.4$	$0.33^{+0.19+0.36}_{-0.13-0.30}$	$3.3 \pm 1.7 \pm 1.4$	$14.4^{+3.5}_{-3.0} \pm 1.5$	11
161	350–600	600–1200	≥10	2	$18.2^{+3.8}_{-3.2} \pm 0.3$	$0.55^{+0.21+0.60}_{-0.16-0.53}$	$0.77 \pm 0.52^{+0.37}_{-0.26}$	$19.5 \pm 3.5 \pm 0.7$	11
162	350–600	≥1200	≥10	2	$13.7^{+3.2}_{-2.6} \pm 0.3$	$0.85^{+0.27+0.92}_{-0.21-0.82}$	$1.15 \pm 0.66 \pm 0.50$	$15.7^{+3.3}_{-2.7} \pm 1.0$	12
163	600–850	600–1200	≥10	2	$1.6^{+2.2}_{-1.2} \pm 0.0$	$0.05^{+0.11+0.05}_{-0.04-0.03}$	$0.04 \pm 0.04^{+0.02}_{-0.00}$	$1.7^{+2.2+0.1}_{-1.2-0.0}$	0
164	600–850	≥1200	≥10	2	$0.9^{+1.2}_{-0.6} \pm 0.0$	$0.19^{+0.15+0.21}_{-0.09-0.17}$	$0.06 \pm 0.05^{+0.03}_{-0.01}$	$1.2^{+1.2}_{-0.6} \pm 0.2$	0
165	≥850	850–1700	≥10	2	$0.0^{+2.4}_{-0.0} \pm 0.0$	$0.00^{+0.08}_{-0.00} \pm 0.00$	$0.05 \pm 0.04^{+0.02}_{-0.01}$	$0.0^{+2.4}_{-0.0} \pm 0.0$	0
166	≥850	≥1700	≥10	2	$0.0^{+1.5}_{-0.0} \pm 0.0$	$0.05^{+0.13+0.06}_{-0.04-0.03}$	$0.02 \pm 0.02^{+0.01}_{-0.00}$	$0.1^{+1.5+0.1}_{-0.0-0.0}$	0
167	300–350	600–1200	≥10	≥3	$6.4^{+2.4}_{-1.8} \pm 0.1$	$0.36^{+0.17+0.41}_{-0.12-0.34}$	$0.46 \pm 0.32^{+0.22}_{-0.14}$	$7.2^{+2.4}_{-1.8} \pm 0.4$	13
168	300–350	≥1200	≥10	≥3	$3.8^{+2.1}_{-1.4} \pm 0.1$	$0.31^{+0.19+0.35}_{-0.12-0.28}$	$1.50 \pm 0.87 \pm 0.64$	$5.6^{+2.3}_{-1.7} \pm 0.7$	5
169	350–600	600–1200	≥10	≥3	$1.6^{+1.5}_{-0.9} \pm 0.0$	$0.52^{+0.20+0.59}_{-0.15-0.50}$	$0.11^{+0.12+0.05}_{-0.11-0.00}$	$2.2^{+1.6+0.6}_{-0.9-0.5}$	3
170	350–600	≥1200	≥10	≥3	$4.2^{+2.1}_{-1.4} \pm 0.1$	$0.81^{+0.26+0.90}_{-0.20-0.78}$	$0.71 \pm 0.44^{+0.31}_{-0.27}$	$5.7^{+2.1+0.9}_{-1.5-0.8}$	9
171	600–850	600–1200	≥10	≥3	$0.0^{+3.0}_{-0.0} \pm 0.0$	$0.05^{+0.10+0.05}_{-0.04-0.03}$	$0.04 \pm 0.04^{+0.02}_{-0.00}$	$0.1^{+3.0+0.1}_{-0.1-0.0}$	0
172	600–850	≥1200	≥10	≥3	$0.0^{+1.4}_{-0.0} \pm 0.0$	$0.18^{+0.14+0.20}_{-0.09-0.16}$	$0.04 \pm 0.04^{+0.02}_{-0.00}$	$0.2^{+1.4}_{-0.1} \pm 0.2$	1
173	≥850	850–1700	≥10	≥3	$0.0^{+2.0}_{-0.0} \pm 0.0$	$0.00^{+0.08}_{-0.00} \pm 0.00$	$0.05 \pm 0.04^{+0.02}_{-0.01}$	$0.0^{+2.0}_{-0.0} \pm 0.0$	0
174	≥850	≥1700	≥10	≥3	$0.0^{+1.3}_{-0.0} \pm 0.0$	$0.05^{+0.12+0.06}_{-0.04-0.03}$	$0.02 \pm 0.02^{+0.01}_{-0.00}$	$0.1^{+1.3+0.1}_{-0.0-0.0}$	0

Table 7. Observed number of events and pre-fit background predictions in the $N_{jet} \geq 10$ search bins. For the background predictions, the first uncertainty is statistical and the second systematic.

JHEP10(2019)244

Bin	Parton multiplicity	Heavy flavor	Δm
1	Low	No	Small
2	Low	No	Large
3	Medium	No	Small
4	Medium	No	Large
5	High	No	All
6	Low	Yes	Small
7	Low	Yes	Large
8	Medium	Yes	Small
9	Medium	Yes	Large
10	High	Yes	Small
11	High	Yes	Large
12	High	Yes	All

Table 8. Targeted event topologies for the 12 aggregate search bins. The variable Δm states the difference between the gluino or squark mass and the sum of the masses of the particles into which the gluino or squark decays.

Bin	$H_{\mathrm{T}}^{\mathrm{miss}}$ [GeV]	H_{T} [GeV]	N_{jet}	$N_{\mathrm{b\text{-}jet}}$	Lost-lepton background	$\mathrm{Z} \to \nu\overline{\nu}$ background	QCD background	Total background	Observed
1	$\geq$600	$\geq$600	$\geq$2	0	$2087 \pm 51 \pm 28$	$10\,210 \pm 70 \pm 440$	$25.0 \pm 7.0 \pm 9.8$	$12\,320 \pm 80 \pm 450$	11 281
2	$\geq$850	$\geq$1700	$\geq$4	0	$11.9^{+4.1}_{-2.8} \pm 0.2$	$53.7 \pm 5.0 \pm 4.8$	$0.15 \pm 0.07 \pm 0.04$	$65.8^{+6.7}_{-5.4} \pm 4.9$	74
3	$\geq$600	$\geq$600	$\geq$6	0	$146 \pm 10 \pm 2$	$338 \pm 12 \pm 18$	$5.7 \pm 1.6 \pm 2.1$	$489 \pm 15 \pm 18$	505
4	$\geq$600	$\geq$600	$\geq$8	0–1	$17.6^{+4.6}_{-2.8} \pm 0.2$	$35.2^{+4.6}_{-3.5} \pm 2.5$	$1.51 \pm 0.51 \pm 0.56$	$54.3^{+6.5}_{-4.5} \pm 2.5$	63
5	$\geq$850	$\geq$1700	$\geq$10	0–1	$17.9^{+7.8}_{-3.5} \pm 0.2$	$122.7^{+9.1}_{-7.9} \pm 8.8$	$0.33 \pm 0.11 \pm 0.10$	$141^{+12}_{-9} \pm 9$	153
6	$\geq$300	$\geq$300	$\geq$4	$\geq$2	$7630 \pm 90 \pm 99$	$2070 \pm 10 \pm 160$	$390 \pm 70 \pm 270$	$10\,090 \pm 120 \pm 330$	10 216
7	$\geq$600	$\geq$600	$\geq$2	$\geq$2	$122^{+19}_{-12} \pm 2$	$211 \pm 2 \pm 26$	$2.6 \pm 0.5 \pm 1.6$	$336^{+19}_{-12} \pm 26$	287
8	$\geq$350	$\geq$350	$\geq$6	$\geq$2	$1362 \pm 33 \pm 17$	$314 \pm 4 \pm 41$	$45 \pm 9 \pm 16$	$1720 \pm 35 \pm 47$	1637
9	$\geq$600	$\geq$600	$\geq$4	$\geq$2	$105^{+16}_{-10} \pm 1$	$123 \pm 2 \pm 12$	$2.3 \pm 0.5 \pm 1.4$	$230^{+16}_{-10} \pm 12$	224
10	$\geq$300	$\geq$300	$\geq$8	$\geq$3	$143^{+12}_{-9} \pm 2$	$19.6 \pm 0.7 \pm 9.8$	$12.8 \pm 3.5 \pm 4.7$	$176^{+13}_{-10} \pm 11$	168
11	$\geq$600	$\geq$600	$\geq$6	$\geq$1	$141^{+15}_{-10} \pm 2$	$160 \pm 6 \pm 16$	$3.2 \pm 0.6 \pm 1.1$	$304^{+16}_{-11} \pm 16$	282
12	$\geq$850	$\geq$850	$\geq$10	$\geq$3	$0.0^{+2.4}_{-0.0} \pm 0.0$	$0.05^{+0.14+0.06}_{-0.04-0.01}$	$0.07 \pm 0.04^{+0.03}_{-0.02}$	$0.1^{+2.4+0.1}_{-0.1-0.0}$	0

Table 9. Selection criteria, pre-fit background predictions, and observed number of events for the 12 aggregate search bins. For the background predictions, the first uncertainty is statistical and the second systematic.

B Aggregate search bins

To simplify the results from the full set of search bins, we present in this appendix the observed number of events and corresponding SM background prediction in 12 aggregate search bins, obtained by summing the results from the nominal search bins while taking correlations into account. The aggregate bins are intended to represent 12 general topologies of interest, as indicated in table 8. The intervals used to define the aggregate bins are optimized using the signal models described in this paper. The definitions of the aggregate bins, along with the corresponding background predictions and observed event counts, are given in table 9. The corresponding data are presented in figure 15.

JHEP10(2019)244

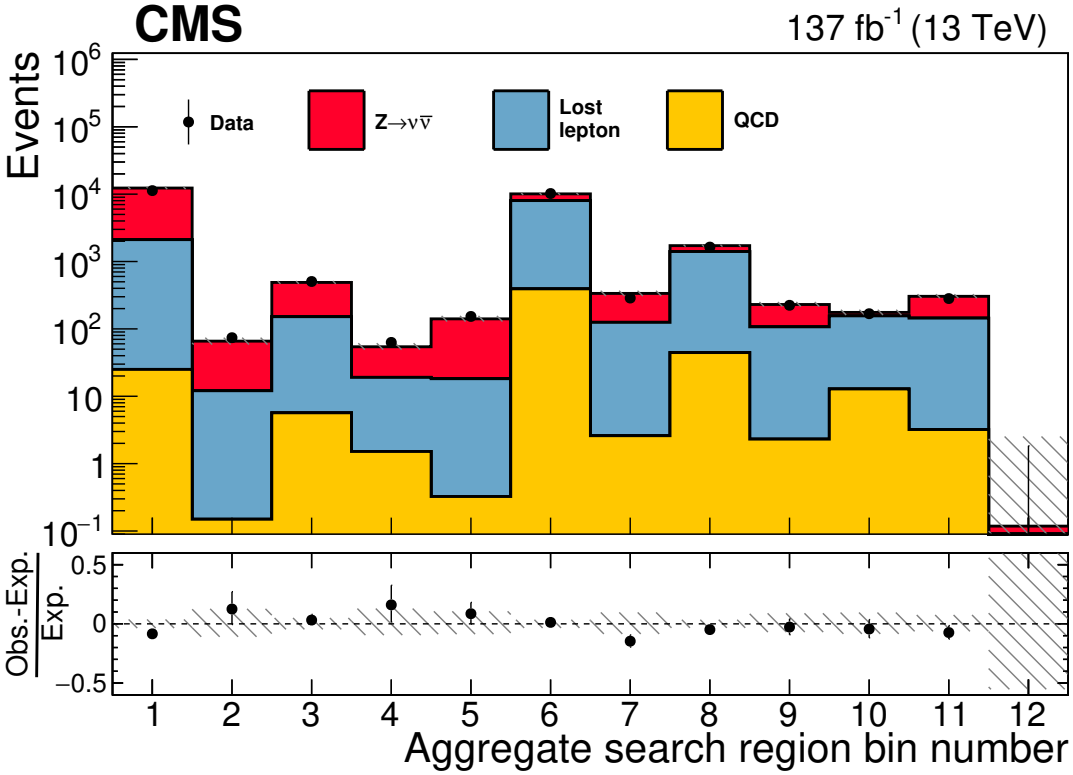

Figure 15. The observed numbers of events and pre-fit SM background predictions in the aggregate search bins. The total background uncertainty is shown by the hatched regions. The lower panel displays the fractional differences between the data and the SM predictions.

References

[1] ATLAS collaboration, *Search for pair production of gluinos decaying via stop and sbottom in events with b-jets and large missing transverse momentum in pp collisions at* $\sqrt{s} = 13$ *TeV with the ATLAS detector*, *Phys. Rev.* **D 94** (2016) 032003 [arXiv:1605.09318] [INSPIRE].

[2] ATLAS collaboration, *Search for squarks and gluinos in final states with jets and missing transverse momentum using* 36 fb^{-1} *of* $\sqrt{s} = 13$ *TeV pp collision data with the ATLAS detector*, *Phys. Rev.* **D 97** (2018) 112001 [arXiv:1712.02332] [INSPIRE].

[3] ATLAS collaboration, *Search for bottom-squark pair production with the ATLAS detector in final states containing Higgs bosons, b-jets and missing transverse momentum*, arXiv:1908.03122 [INSPIRE].

[4] CMS collaboration, *Search for supersymmetry in the multijet and missing transverse momentum final state in pp collisions at* 13 *TeV*, *Phys. Lett.* **B 758** (2016) 152 [arXiv:1602.06581] [INSPIRE].

JHEP10(2019)244

[5] CMS collaboration, *Search for new physics with the M_{T2} variable in all-jets final states produced in pp collisions at $\sqrt{s} = 13$ TeV*, *JHEP* **10** (2016) 006 [arXiv:1603.04053] [INSPIRE].

[6] CMS collaboration, *Inclusive search for supersymmetry using razor variables in pp collisions at $\sqrt{s} = 13$ TeV*, *Phys. Rev.* **D 95** (2017) 012003 [arXiv:1609.07658] [INSPIRE].

[7] CMS collaboration, *A search for new phenomena in pp collisions at $\sqrt{s} = 13$ TeV in final states with missing transverse momentum and at least one jet using the α_T variable*, *Eur. Phys. J.* **C 77** (2017) 294 [arXiv:1611.00338] [INSPIRE].

[8] CMS collaboration, *Search for supersymmetry in multijet events with missing transverse momentum in proton-proton collisions at 13 TeV*, *Phys. Rev.* **D 96** (2017) 032003 [arXiv:1704.07781] [INSPIRE].

[9] P. Ramond, *Dual theory for free fermions*, *Phys. Rev.* **D 3** (1971) 2415 [INSPIRE].

[10] Y.A. Golfand and E.P. Likhtman, *Extension of the algebra of Poincaré group generators and violation of p invariance*, *JETP Lett.* **13** (1971) 323 [INSPIRE].

[11] A. Neveu and J.H. Schwarz, *Factorizable dual model of pions*, *Nucl. Phys.* **B 31** (1971) 86 [INSPIRE].

[12] D.V. Volkov and V.P. Akulov, *Possible universal neutrino interaction*, *JETP Lett.* **16** (1972) 438 [INSPIRE].

[13] J. Wess and B. Zumino, *A Lagrangian model invariant under supergauge transformations*, *Phys. Lett.* **49B** (1974) 52 [INSPIRE].

[14] J. Wess and B. Zumino, *Supergauge transformations in four-dimensions*, *Nucl. Phys.* **B 70** (1974) 39 [INSPIRE].

[15] P. Fayet, *Supergauge invariant extension of the Higgs mechanism and a model for the electron and its neutrino*, *Nucl. Phys.* **B 90** (1975) 104 [INSPIRE].

[16] P. Fayet and S. Ferrara, *Supersymmetry*, *Phys. Rept.* **32** (1977) 249 [INSPIRE].

[17] H.P. Nilles, *Supersymmetry, supergravity and particle physics*, *Phys. Rept.* **110** (1984) 1 [INSPIRE].

[18] S.P. Martin, *A Supersymmetry primer*, *Adv. Ser. Direct. High Energy Phys.* **21** (2010) 1 [hep-ph/9709356] [INSPIRE].

[19] B. Gripaios, *Composite leptoquarks at the LHC*, *JHEP* **02** (2010) 045 [arXiv:0910.1789] [INSPIRE].

[20] S. Dimopoulos, *Technicolored signatures*, *Nucl. Phys.* **B 168** (1980) 69 [INSPIRE].

[21] M. Perelstein, *Little Higgs models and their phenomenology*, *Prog. Part. Nucl. Phys.* **58** (2007) 247 [hep-ph/0512128] [INSPIRE].

[22] C. Grojean, E. Salvioni and R. Torre, *A weakly constrained W' at the early LHC*, *JHEP* **07** (2011) 002 [arXiv:1103.2761] [INSPIRE].

[23] L. Lopez-Honorez, T. Schwetz and J. Zupan, *Higgs portal, fermionic dark matter and a Standard Model like Higgs at 125 GeV*, *Phys. Lett.* **B 716** (2012) 179 [arXiv:1203.2064] [INSPIRE].

[24] J.M. No, *Looking through the pseudoscalar portal into dark matter: Novel mono-Higgs and mono-Z signatures at the LHC*, *Phys. Rev.* **D 93** (2016) 031701 [arXiv:1509.01110] [INSPIRE].

[25] R. Barbieri and G.F. Giudice, *Upper bounds on supersymmetric particle masses*, *Nucl. Phys.* **B 306** (1988) 63 [INSPIRE].

JHEP10(2019)244

[26] S. Dimopoulos and G.F. Giudice, *Naturalness constraints in supersymmetric theories with nonuniversal soft terms*, *Phys. Lett.* **B 357** (1995) 573 [hep-ph/9507282] [INSPIRE].

[27] R. Barbieri and D. Pappadopulo, *S-particles at their naturalness limits*, *JHEP* **10** (2009) 061 [arXiv:0906.4546] [INSPIRE].

[28] M. Papucci, J.T. Ruderman and A. Weiler, *Natural SUSY endures*, *JHEP* **09** (2012) 035 [arXiv:1110.6926] [INSPIRE].

[29] G.R. Farrar and P. Fayet, *Phenomenology of the production, decay and detection of new hadronic states associated with supersymmetry*, *Phys. Lett.* **76B** (1978) 575 [INSPIRE].

[30] ATLAS collaboration, *Search for squarks and gluinos in final states with jets and missing transverse momentum at* $\sqrt{s} = 13$ *TeV with the ATLAS detector*, *Eur. Phys. J.* **C 76** (2016) 392 [arXiv:1605.03814] [INSPIRE].

[31] CMS collaboration, *Search for new physics with jets and missing transverse momentum in pp collisions at* $\sqrt{s} = 7$ *TeV*, *JHEP* **08** (2011) 155 [arXiv:1106.4503] [INSPIRE].

[32] CMS collaboration, *Search for new physics in the multijet and missing transverse momentum final state in proton-proton collisions at* $\sqrt{s} = 8$ *TeV*, *JHEP* **06** (2014) 055 [arXiv:1402.4770] [INSPIRE].

[33] N. Arkani-Hamed et al., *MARMOSET: the path from LHC data to the new standard model via on-shell effective theories*, hep-ph/0703088 [INSPIRE].

[34] J. Alwall, M.-P. Le, M. Lisanti and J.G. Wacker, *Model-independent jets plus missing energy searches*, *Phys. Rev.* **D 79** (2009) 015005 [arXiv:0809.3264] [INSPIRE].

[35] J. Alwall, P. Schuster and N. Toro, *Simplified models for a first characterization of new physics at the LHC*, *Phys. Rev.* **D 79** (2009) 075020 [arXiv:0810.3921] [INSPIRE].

[36] LHC New Physics Working Group collaboration, *Simplified models for LHC new physics searches*, *J. Phys.* **G 39** (2012) 105005 [arXiv:1105.2838] [INSPIRE].

[37] CMS collaboration, *Interpretation of searches for supersymmetry with simplified models*, *Phys. Rev.* **D 88** (2013) 052017 [arXiv:1301.2175] [INSPIRE].

[38] CMS collaboration, *The CMS experiment at the CERN LHC*, 2008 *JINST* **3** S08004 [INSPIRE].

[39] CMS collaboration, *The CMS trigger system*, 2017 *JINST* **12** P01020 [arXiv:1609.02366] [INSPIRE].

[40] CMS collaboration, *Particle-flow reconstruction and global event description with the CMS detector*, 2017 *JINST* **12** P10003 [arXiv:1706.04965] [INSPIRE].

[41] CMS collaboration, *Performance of photon reconstruction and identification with the CMS detector in proton-proton collisions at* $\sqrt{s} = 8$ *TeV*, 2015 *JINST* **10** P08010 [arXiv:1502.02702] [INSPIRE].

[42] CMS collaboration, *Performance of electron reconstruction and selection with the CMS detector in proton-proton collisions at* $\sqrt{s} = 8$ *TeV*, 2015 *JINST* **10** P06005 [arXiv:1502.02701] [INSPIRE].

[43] CMS collaboration, *Performance of the CMS muon detector and muon reconstruction with proton-proton collisions at* $\sqrt{s} = 13$ *TeV*, 2018 *JINST* **13** P06015 [arXiv:1804.04528] [INSPIRE].

[44] M. Cacciari, G.P. Salam and G. Soyez, *The anti-*k_t *jet clustering algorithm*, *JHEP* **04** (2008) 063 [arXiv:0802.1189] [INSPIRE].

JHEP10(2019)244

[45] M. Cacciari, G.P. Salam and G. Soyez, *FastJet user manual*, *Eur. Phys. J.* **C 72** (2012) 1896 [arXiv:1111.6097] [INSPIRE].

[46] M. Cacciari and G.P. Salam, *Pileup subtraction using jet areas*, *Phys. Lett.* **B 659** (2008) 119 [arXiv:0707.1378] [INSPIRE].

[47] K. Rehermann and B. Tweedie, *Efficient identification of boosted semileptonic top quarks at the LHC*, *JHEP* **03** (2011) 059 [arXiv:1007.2221] [INSPIRE].

[48] CMS Collaboration, *Jet Performance in pp Collisions at 7 TeV*, CMS-PAS-JME-10-003 (Jet Performance in pp Collisions at 7 TeV).

[49] CMS collaboration, *Jet algorithms performance in* 13 *TeV data*, CMS-PAS-JME-16-003 (2016).

[50] CMS collaboration, *Jet energy scale and resolution in the CMS experiment in pp collisions at* 8 *TeV*, 2017 *JINST* **12** P02014 [arXiv:1607.03663] [INSPIRE].

[51] CMS collaboration, *Identification of heavy-flavour jets with the CMS detector in pp collisions at* 13 *TeV*, 2018 *JINST* **13** P05011 [arXiv:1712.07158] [INSPIRE].

[52] UA1 collaboration, *Experimental observation of isolated large transverse energy electrons with associated missing energy at* $\sqrt{s} = 540$ *GeV*, *Phys. Lett.* **122B** (1983) 103 [INSPIRE].

[53] CMS collaboration, *Performance of missing transverse momentum reconstruction in proton-proton collisions at* $\sqrt{s} = 13$ *TeV using the CMS detector*, 2019 *JINST* **14** P07004 [arXiv:1903.06078] [INSPIRE].

[54] CMS collaboration, *Search for supersymmetry in events with a photon, jets, b-jets and missing transverse momentum in proton–proton collisions at* 13 *TeV*, *Eur. Phys. J.* **C 79** (2019) 444 [arXiv:1901.06726] [INSPIRE].

[55] J. Alwall et al., *The automated computation of tree-level and next-to-leading order differential cross sections and their matching to parton shower simulations*, *JHEP* **07** (2014) 079 [arXiv:1405.0301] [INSPIRE].

[56] J. Alwall et al., *Comparative study of various algorithms for the merging of parton showers and matrix elements in hadronic collisions*, *Eur. Phys. J.* **C 53** (2008) 473 [arXiv:0706.2569] [INSPIRE].

[57] R. Frederix and S. Frixione, *Merging meets matching in MC@NLO*, *JHEP* **12** (2012) 061 [arXiv:1209.6215] [INSPIRE].

[58] P. Nason, *A new method for combining NLO QCD with shower Monte Carlo algorithms*, *JHEP* **11** (2004) 040 [hep-ph/0409146] [INSPIRE].

[59] S. Frixione, P. Nason and C. Oleari, *Matching NLO QCD computations with Parton Shower simulations: the POWHEG method*, *JHEP* **11** (2007) 070 [arXiv:0709.2092] [INSPIRE].

[60] S. Alioli, P. Nason, C. Oleari and E. Re, *A general framework for implementing NLO calculations in shower Monte Carlo programs: the POWHEG BOX*, *JHEP* **06** (2010) 043 [arXiv:1002.2581] [INSPIRE].

[61] S. Alioli, P. Nason, C. Oleari and E. Re, *NLO single-top production matched with shower in POWHEG: s- and t-channel contributions*, *JHEP* **09** (2009) 111 [*Erratum ibid.* **1002** (2010) 011] [arXiv:0907.4076] [INSPIRE].

[62] E. Re, *Single-top Wt-channel production matched with parton showers using the POWHEG method*, *Eur. Phys. J.* **C 71** (2011) 1547 [arXiv:1009.2450] [INSPIRE].

[63] GEANT4 collaboration, *GEANT4 — a simulation toolkit*, *Nucl. Instrum. Meth.* **A 506** (2003) 250 [INSPIRE].

JHEP10(2019)244

[64] T. Melia, P. Nason, R. Rontsch and G. Zanderighi, W^+W^-, WZ and ZZ production in the POWHEG BOX, JHEP **11** (2011) 078 [arXiv:1107.5051] [INSPIRE].

[65] M. Beneke, P. Falgari, S. Klein and C. Schwinn, *Hadronic top-quark pair production with NNLL threshold resummation*, Nucl. Phys. **B 855** (2012) 695 [arXiv:1109.1536] [INSPIRE].

[66] M. Cacciari et al., *Top-pair production at hadron colliders with next-to-next-to-leading logarithmic soft-gluon resummation*, Phys. Lett. **B 710** (2012) 612 [arXiv:1111.5869] [INSPIRE].

[67] P. Bärnreuther, M. Czakon and A. Mitov, *Percent level precision physics at the tevatron: first genuine NNLO QCD corrections to $q\bar{q} \to t\bar{t} + X$*, Phys. Rev. Lett. **109** (2012) 132001 [arXiv:1204.5201] [INSPIRE].

[68] M. Czakon and A. Mitov, *NNLO corrections to top-pair production at hadron colliders: the all-fermionic scattering channels*, JHEP **12** (2012) 054 [arXiv:1207.0236] [INSPIRE].

[69] M. Czakon and A. Mitov, *NNLO corrections to top pair production at hadron colliders: the quark-gluon reaction*, JHEP **01** (2013) 080 [arXiv:1210.6832] [INSPIRE].

[70] M. Czakon, P. Fiedler and A. Mitov, *Total top-quark pair-production cross section at hadron colliders through $O(\alpha_S^4)$*, Phys. Rev. Lett. **110** (2013) 252004 [arXiv:1303.6254] [INSPIRE].

[71] R. Gavin, Y. Li, F. Petriello and S. Quackenbush, *W physics at the LHC with FEWZ 2.1*, Comput. Phys. Commun. **184** (2013) 208 [arXiv:1201.5896] [INSPIRE].

[72] R. Gavin, Y. Li, F. Petriello and S. Quackenbush, *FEWZ 2.0: a code for hadronic Z production at next-to-next-to-leading order*, Comput. Phys. Commun. **182** (2011) 2388 [arXiv:1011.3540] [INSPIRE].

[73] W. Beenakker, R. Höpker, M. Spira and P.M. Zerwas, *Squark and gluino production at hadron colliders*, Nucl. Phys. **B 492** (1997) 51 [hep-ph/9610490] [INSPIRE].

[74] A. Kulesza and L. Motyka, *Threshold resummation for squark-antisquark and gluino-pair production at the LHC*, Phys. Rev. Lett. **102** (2009) 111802 [arXiv:0807.2405] [INSPIRE].

[75] A. Kulesza and L. Motyka, *Soft gluon resummation for the production of gluino-gluino and squark-antisquark pairs at the LHC*, Phys. Rev. **D 80** (2009) 095004 [arXiv:0905.4749] [INSPIRE].

[76] W. Beenakker et al., *Soft-gluon resummation for squark and gluino hadroproduction*, JHEP **12** (2009) 041 [arXiv:0909.4418] [INSPIRE].

[77] W. Beenakker et al., *Squark and gluino hadroproduction*, Int. J. Mod. Phys. **A 26** (2011) 2637 [arXiv:1105.1110] [INSPIRE].

[78] W. Beenakker et al., *NNLL-fast: predictions for coloured supersymmetric particle production at the LHC with threshold and Coulomb resummation*, JHEP **12** (2016) 133 [arXiv:1607.07741] [INSPIRE].

[79] W. Beenakker et al., *NNLL resummation for squark-antisquark pair production at the LHC*, JHEP **01** (2012) 076 [arXiv:1110.2446] [INSPIRE].

[80] W. Beenakker et al., *Towards NNLL resummation: hard matching coefficients for squark and gluino hadroproduction*, JHEP **10** (2013) 120 [arXiv:1304.6354] [INSPIRE].

[81] W. Beenakker et al., *NNLL resummation for squark and gluino production at the LHC*, JHEP **12** (2014) 023 [arXiv:1404.3134] [INSPIRE].

[82] W. Beenakker et al., *Stop production at hadron colliders*, Nucl. Phys. B **515** (1998) 3 [hep-ph/9710451] [INSPIRE].

JHEP10(2019)244

[83] W. Beenakker et al., *Supersymmetric top and bottom squark production at hadron colliders*, *JHEP* **08** (2010) 098 [arXiv:1006.4771] [INSPIRE].

[84] W. Beenakker et al., *NNLL resummation for stop pair-production at the LHC*, *JHEP* **05** (2016) 153 [arXiv:1601.02954] [INSPIRE].

[85] T. Sjöstrand et al., *An introduction to PYTHIA 8.2*, *Comput. Phys. Commun.* **191** (2015) 159 [arXiv:1410.3012] [INSPIRE].

[86] S. Abdullin et al., *The fast simulation of the CMS detector at LHC*, *J. Phys. Conf. Ser.* **331** (2011) 032049 [INSPIRE].

[87] A. Giammanco, *The fast simulation of the CMS experiment*, *J. Phys. Conf. Ser.* **513** (2014) 022012 [INSPIRE].

[88] CMS collaboration, *Event generator tunes obtained from underlying event and multiparton scattering measurements*, *Eur. Phys. J.* **C 76** (2016) 155 [arXiv:1512.00815] [INSPIRE].

[89] CMS collaboration, *Extraction and validation of a new set of CMS PYTHIA8 tunes from underlying-event measurements*, arXiv:1903.12179 [INSPIRE].

[90] NNPDF collaboration, *Parton distributions with QED corrections*, *Nucl. Phys.* **B 877** (2013) 290 [arXiv:1308.0598] [INSPIRE].

[91] NNPDF collaboration, *Parton distributions from high-precision collider data*, *Eur. Phys. J.* **C 77** (2017) 663 [arXiv:1706.00428] [INSPIRE].

[92] A. Kalogeropoulos and J. Alwall, *The SysCalc code: a tool to derive theoretical systematic uncertainties*, arXiv:1801.08401 [INSPIRE].

[93] S. Catani, D. de Florian, M. Grazzini and P. Nason, *Soft gluon resummation for Higgs boson production at hadron colliders*, *JHEP* **07** (2003) 028 [hep-ph/0306211] [INSPIRE].

[94] M. Cacciari, S. Frixione, M.L. Mangano, P. Nason and G. Ridolfi, *The $t\bar{t}$ cross-section at 1.8 TeV and 1.96 TeV: a study of the systematics due to parton densities and scale dependence*, *JHEP* **04** (2004) 068 [hep-ph/0303085] [INSPIRE].

[95] CMS collaboration, *Measurement of the inelastic proton-proton cross section at $\sqrt{s} = 13$ TeV*, *JHEP* **07** (2018) 161 [arXiv:1802.02613] [INSPIRE].

[96] CMS collaboration, *CMS luminosity measurements for the 2016 data taking period*, CMS-PAS-LUM-17-001 (2017).

[97] CMS collaboration, *CMS luminosity measurement for the 2017 data-taking period at $\sqrt{s} = 13$ TeV*, CMS-PAS-LUM-17-004 (2018).

[98] CMS collaboration, *CMS luminosity measurement for the 2018 data-taking period at $\sqrt{s} = 13$ TeV*, CMS-PAS-LUM-18-002 (2019).

[99] G. Cowan, K. Cranmer, E. Gross and O. Vitells, *Asymptotic formulae for likelihood-based tests of new physics*, *Eur. Phys. J.* **C 71** (2011) 1554 [*Erratum ibid.* **C 73** (2013) 2501] [arXiv:1007.1727] [INSPIRE].

[100] T. Junk, *Confidence level computation for combining searches with small statistics*, *Nucl. Instrum. Meth.* **A 434** (1999) 435 [hep-ex/9902006] [INSPIRE].

[101] A.L. Read, *Presentation of search results: the CL_s technique*, *J. Phys.* **G 28** (2002) 2693 [INSPIRE].

[102] C. Borschensky et al., *Squark and gluino production cross sections in pp collisions at $\sqrt{s} = 13$, 14, 33 and 100 TeV*, *Eur. Phys. J.* **C 74** (2014) 3174 [arXiv:1407.5066] [INSPIRE].

JHEP10(2019)244

The CMS collaboration

Yerevan Physics Institute, Yerevan, Armenia

A.M. Sirunyan[†], A. Tumasyan

Institut für Hochenergiephysik, Wien, Austria

W. Adam, F. Ambrogi, T. Bergauer, J. Brandstetter, M. Dragicevic, J. Erö, A. Escalante Del Valle, M. Flechl, R. Frühwirth[1], M. Jeitler[1], N. Krammer, I. Krätschmer, D. Liko, T. Madlener, I. Mikulec, N. Rad, J. Schieck[1], R. Schöfbeck, M. Spanring, D. Spitzbart, W. Waltenberger, C.-E. Wulz[1], M. Zarucki

Institute for Nuclear Problems, Minsk, Belarus

V. Drugakov, V. Mossolov, J. Suarez Gonzalez

Universiteit Antwerpen, Antwerpen, Belgium

M.R. Darwish, E.A. De Wolf, D. Di Croce, X. Janssen, A. Lelek, M. Pieters, H. Rejeb Sfar, H. Van Haevermaet, P. Van Mechelen, S. Van Putte, N. Van Remortel

Vrije Universiteit Brussel, Brussel, Belgium

F. Blekman, E.S. Bols, S.S. Chhibra, J. D'Hondt, J. De Clercq, D. Lontkovskyi, S. Lowette, I. Marchesini, S. Moortgat, Q. Python, K. Skovpen, S. Tavernier, W. Van Doninck, P. Van Mulders

Université Libre de Bruxelles, Bruxelles, Belgium

D. Beghin, B. Bilin, H. Brun, B. Clerbaux, G. De Lentdecker, H. Delannoy, B. Dorney, L. Favart, A. Grebenyuk, A.K. Kalsi, A. Popov, N. Postiau, E. Starling, L. Thomas, C. Vander Velde, P. Vanlaer, D. Vannerom

Ghent University, Ghent, Belgium

T. Cornelis, D. Dobur, I. Khvastunov[2], M. Niedziela, C. Roskas, D. Trocino, M. Tytgat, W. Verbeke, B. Vermassen, M. Vit, N. Zaganidis

Université Catholique de Louvain, Louvain-la-Neuve, Belgium

O. Bondu, G. Bruno, C. Caputo, P. David, C. Delaere, M. Delcourt, A. Giammanco, V. Lemaitre, A. Magitteri, J. Prisciandaro, A. Saggio, M. Vidal Marono, P. Vischia, J. Zobec

Centro Brasileiro de Pesquisas Fisicas, Rio de Janeiro, Brazil

F.L. Alves, G.A. Alves, G. Correia Silva, C. Hensel, A. Moraes, P. Rebello Teles

Universidade do Estado do Rio de Janeiro, Rio de Janeiro, Brazil

E. Belchior Batista Das Chagas, W. Carvalho, J. Chinellato[3], E. Coelho, E.M. Da Costa, G.G. Da Silveira[4], D. De Jesus Damiao, C. De Oliveira Martins, S. Fonseca De Souza, L.M. Huertas Guativa, H. Malbouisson, J. Martins[5], D. Matos Figueiredo, M. Medina Jaime[6], M. Melo De Almeida, C. Mora Herrera, L. Mundim, H. Nogima, W.L. Prado Da Silva, L.J. Sanchez Rosas, A. Santoro, A. Sznajder, M. Thiel, E.J. Tonelli Manganote[3], F. Torres Da Silva De Araujo, A. Vilela Pereira

JHEP10(2019)244

Universidade Estadual Paulista[a], Universidade Federal do ABC[b], São Paulo, Brazil

C.A. Bernardes[a], L. Calligaris[a], T.R. Fernandez Perez Tomei[a], E.M. Gregores[b], D.S. Lemos, P.G. Mercadante[b], S.F. Novaes[a], SandraS. Padula[a]

Institute for Nuclear Research and Nuclear Energy, Bulgarian Academy of Sciences, Sofia, Bulgaria

A. Aleksandrov, G. Antchev, R. Hadjiiska, P. Iaydjiev, M. Misheva, M. Rodozov, M. Shopova, G. Sultanov

University of Sofia, Sofia, Bulgaria

M. Bonchev, A. Dimitrov, T. Ivanov, L. Litov, B. Pavlov, P. Petkov

Beihang University, Beijing, China

W. Fang[7], X. Gao[7], L. Yuan

Institute of High Energy Physics, Beijing, China

G.M. Chen, H.S. Chen, M. Chen, C.H. Jiang, D. Leggat, H. Liao, Z. Liu, A. Spiezia, J. Tao, E. Yazgan, H. Zhang, S. Zhang[8], J. Zhao

State Key Laboratory of Nuclear Physics and Technology, Peking University, Beijing, China

A. Agapitos, Y. Ban, G. Chen, A. Levin, J. Li, L. Li, Q. Li, Y. Mao, S.J. Qian, D. Wang, Q. Wang

Tsinghua University, Beijing, China

M. Ahmad, Z. Hu, Y. Wang

Zhejiang University — Department of Physics

M. Xiao

Universidad de Los Andes, Bogota, Colombia

C. Avila, A. Cabrera, C. Florez, C.F. González Hernández, M.A. Segura Delgado

Universidad de Antioquia, Medellin, Colombia

J. Mejia Guisao, J.D. Ruiz Alvarez, C.A. Salazar González, N. Vanegas Arbelaez

University of Split, Faculty of Electrical Engineering, Mechanical Engineering and Naval Architecture, Split, Croatia

D. Giljanović, N. Godinovic, D. Lelas, I. Puljak, T. Sculac

University of Split, Faculty of Science, Split, Croatia

Z. Antunovic, M. Kovac

Institute Rudjer Boskovic, Zagreb, Croatia

V. Brigljevic, S. Ceci, D. Ferencek, K. Kadija, B. Mesic, M. Roguljic, A. Starodumov[9], T. Susa

JHEP10(2019)244

University of Cyprus, Nicosia, Cyprus

M.W. Ather, A. Attikis, E. Erodotou, A. Ioannou, M. Kolosova, S. Konstantinou, G. Mavromanolakis, J. Mousa, C. Nicolaou, F. Ptochos, P.A. Razis, H. Rykaczewski, D. Tsiakkouri

Charles University, Prague, Czech Republic

M. Finger[10], M. Finger Jr.[10], A. Kveton, J. Tomsa

Escuela Politecnica Nacional, Quito, Ecuador

E. Ayala

Universidad San Francisco de Quito, Quito, Ecuador

E. Carrera Jarrin

Academy of Scientific Research and Technology of the Arab Republic of Egypt, Egyptian Network of High Energy Physics, Cairo, Egypt

S. Abu Zeid[11], S. Khalil[12]

National Institute of Chemical Physics and Biophysics, Tallinn, Estonia

S. Bhowmik, A. Carvalho Antunes De Oliveira, R.K. Dewanjee, K. Ehataht, M. Kadastik, M. Raidal, C. Veelken

Department of Physics, University of Helsinki, Helsinki, Finland

P. Eerola, L. Forthomme, H. Kirschenmann, K. Osterberg, M. Voutilainen

Helsinki Institute of Physics, Helsinki, Finland

F. Garcia, J. Havukainen, J.K. Heikkilä, T. Järvinen, V. Karimäki, M.S. Kim, R. Kinnunen, T. Lampén, K. Lassila-Perini, S. Laurila, S. Lehti, T. Lindén, P. Luukka, T. Mäenpää, H. Siikonen, E. Tuominen, J. Tuominiemi

Lappeenranta University of Technology, Lappeenranta, Finland

T. Tuuva

IRFU, CEA, Université Paris-Saclay, Gif-sur-Yvette, France

M. Besancon, F. Couderc, M. Dejardin, D. Denegri, B. Fabbro, J.L. Faure, F. Ferri, S. Ganjour, A. Givernaud, P. Gras, G. Hamel de Monchenault, P. Jarry, C. Leloup, E. Locci, J. Malcles, J. Rander, A. Rosowsky, M.Ö. Sahin, A. Savoy-Navarro[13], M. Titov

Laboratoire Leprince-Ringuet, Ecole polytechnique, CNRS/IN2P3, Université Paris-Saclay, Palaiseau, France

S. Ahuja, C. Amendola, F. Beaudette, P. Busson, C. Charlot, B. Diab, G. Falmagne, R. Granier de Cassagnac, I. Kucher, A. Lobanov, C. Martin Perez, M. Nguyen, C. Ochando, P. Paganini, J. Rembser, R. Salerno, J.B. Sauvan, Y. Sirois, A. Zabi, A. Zghiche

Université de Strasbourg, CNRS, IPHC UMR 7178, Strasbourg, France

J.-L. Agram[14], J. Andrea, D. Bloch, G. Bourgatte, J.-M. Brom, E.C. Chabert, C. Collard, E. Conte[14], J.-C. Fontaine[14], D. Gelé, U. Goerlach, M. Jansová, A.-C. Le Bihan, N. Tonon, P. Van Hove

JHEP10(2019)244

Centre de Calcul de l'Institut National de Physique Nucleaire et de Physique des Particules, CNRS/IN2P3, Villeurbanne, France
S. Gadrat

Université de Lyon, Université Claude Bernard Lyon 1, CNRS-IN2P3, Institut de Physique Nucléaire de Lyon, Villeurbanne, France
S. Beauceron, C. Bernet, G. Boudoul, C. Camen, A. Carle, N. Chanon, R. Chierici, D. Contardo, P. Depasse, H. El Mamouni, J. Fay, S. Gascon, M. Gouzevitch, B. Ille, Sa. Jain, F. Lagarde, I.B. Laktineh, H. Lattaud, A. Lesauvage, M. Lethuillier, L. Mirabito, S. Perries, V. Sordini, L. Torterotot, G. Touquet, M. Vander Donckt, S. Viret

Georgian Technical University, Tbilisi, Georgia
A. Khvedelidze[10]

Tbilisi State University, Tbilisi, Georgia
Z. Tsamalaidze[10]

RWTH Aachen University, I. Physikalisches Institut, Aachen, Germany
C. Autermann, L. Feld, M.K. Kiesel, K. Klein, M. Lipinski, D. Meuser, A. Pauls, M. Preuten, M.P. Rauch, J. Schulz, M. Teroerde, B. Wittmer

RWTH Aachen University, III. Physikalisches Institut A, Aachen, Germany
A. Albert, M. Erdmann, B. Fischer, S. Ghosh, T. Hebbeker, K. Hoepfner, H. Keller, L. Mastrolorenzo, M. Merschmeyer, A. Meyer, P. Millet, G. Mocellin, S. Mondal, S. Mukherjee, D. Noll, A. Novak, T. Pook, A. Pozdnyakov, T. Quast, M. Radziej, Y. Rath, H. Reithler, J. Roemer, A. Schmidt, S.C. Schuler, A. Sharma, S. Wiedenbeck, S. Zaleski

RWTH Aachen University, III. Physikalisches Institut B, Aachen, Germany
G. Flügge, W. Haj Ahmad[15], O. Hlushchenko, T. Kress, T. Müller, A. Nehrkorn, A. Nowack, C. Pistone, O. Pooth, D. Roy, H. Sert, A. Stahl[16]

Deutsches Elektronen-Synchrotron, Hamburg, Germany
M. Aldaya Martin, P. Asmuss, I. Babounikau, H. Bakhshiansohi, K. Beernaert, O. Behnke, A. Bermúdez Martínez, D. Bertsche, A.A. Bin Anuar, K. Borras[17], V. Botta, A. Campbell, A. Cardini, P. Connor, S. Consuegra Rodríguez, C. Contreras-Campana, V. Danilov, A. De Wit, M.M. Defranchis, C. Diez Pardos, D. Domínguez Damiani, G. Eckerlin, D. Eckstein, T. Eichhorn, A. Elwood, E. Eren, E. Gallo[18], A. Geiser, A. Grohsjean, M. Guthoff, M. Haranko, A. Harb, A. Jafari, N.Z. Jomhari, H. Jung, A. Kasem[17], M. Kasemann, H. Kaveh, J. Keaveney, C. Kleinwort, J. Knolle, D. Krücker, W. Lange, T. Lenz, J. Lidrych, K. Lipka, W. Lohmann[19], R. Mankel, I.-A. Melzer-Pellmann, A.B. Meyer, M. Meyer, M. Missiroli, G. Mittag, J. Mnich, A. Mussgiller, V. Myronenko, D. Pérez Adán, S.K. Pflitsch, D. Pitzl, A. Raspereza, A. Saibel, M. Savitskyi, V. Scheurer, P. Schütze, C. Schwanenberger, R. Shevchenko, A. Singh, H. Tholen, O. Turkot, A. Vagnerini, M. Van De Klundert, R. Walsh, Y. Wen, K. Wichmann, C. Wissing, O. Zenaiev, R. Zlebcik

University of Hamburg, Hamburg, Germany
R. Aggleton, S. Bein, L. Benato, A. Benecke, V. Blobel, T. Dreyer, A. Ebrahimi, F. Feindt, A. Fröhlich, C. Garbers, E. Garutti, D. Gonzalez, P. Gunnellini, J. Haller, A. Hinzmann,

JHEP10(2019)244

A. Karavdina, G. Kasieczka, R. Klanner, R. Kogler, N. Kovalchuk, S. Kurz, V. Kutzner, J. Lange, T. Lange, A. Malara, J. Multhaup, C.E.N. Niemeyer, A. Perieanu, A. Reimers, O. Rieger, C. Scharf, P. Schleper, S. Schumann, J. Schwandt, J. Sonneveld, H. Stadie, G. Steinbrück, F.M. Stober, B. Vormwald, I. Zoi

Karlsruher Institut fuer Technologie, Karlsruhe, Germany

M. Akbiyik, C. Barth, M. Baselga, S. Baur, T. Berger, E. Butz, R. Caspart, T. Chwalek, W. De Boer, A. Dierlamm, K. El Morabit, N. Faltermann, M. Giffels, P. Goldenzweig, A. Gottmann, M.A. Harrendorf, F. Hartmann[16], U. Husemann, S. Kudella, S. Mitra, M.U. Mozer, D. Müller, Th. Müller, M. Musich, A. Nürnberg, G. Quast, K. Rabbertz, M. Schröder, I. Shvetsov, H.J. Simonis, R. Ulrich, M. Wassmer, M. Weber, C. Wöhrmann, R. Wolf

Institute of Nuclear and Particle Physics (INPP), NCSR Demokritos, Aghia Paraskevi, Greece

G. Anagnostou, P. Asenov, G. Daskalakis, T. Geralis, A. Kyriakis, D. Loukas, G. Paspalaki

National and Kapodistrian University of Athens, Athens, Greece

M. Diamantopoulou, G. Karathanasis, P. Kontaxakis, A. Manousakis-katsikakis, A. Panagiotou, I. Papavergou, N. Saoulidou, A. Stakia, K. Theofilatos, K. Vellidis, E. Vourliotis

National Technical University of Athens, Athens, Greece

G. Bakas, K. Kousouris, I. Papakrivopoulos, G. Tsipolitis

University of Ioánnina, Ioánnina, Greece

I. Evangelou, C. Foudas, P. Gianneios, P. Katsoulis, P. Kokkas, S. Mallios, K. Manitara, N. Manthos, I. Papadopoulos, J. Strologas, F.A. Triantis, D. Tsitsonis

MTA-ELTE Lendület CMS Particle and Nuclear Physics Group, Eötvös Loránd University, Budapest, Hungary

M. Bartók[20], R. Chudasama, M. Csanad, P. Major, K. Mandal, A. Mehta, M.I. Nagy, G. Pasztor, O. Surányi, G.I. Veres

Wigner Research Centre for Physics, Budapest, Hungary

G. Bencze, C. Hajdu, D. Horvath[21], F. Sikler, T.Á. Vámi, V. Veszpremi, G. Vesztergombi[†]

Institute of Nuclear Research ATOMKI, Debrecen, Hungary

N. Beni, S. Czellar, J. Karancsi[20], A. Makovec, J. Molnar, Z. Szillasi

Institute of Physics, University of Debrecen, Debrecen, Hungary

P. Raics, D. Teyssier, Z.L. Trocsanyi, B. Ujvari

Eszterhazy Karoly University, Karoly Robert Campus, Gyongyos, Hungary

T. Csorgo, W.J. Metzger, F. Nemes, T. Novak

Indian Institute of Science (IISc), Bangalore, India

S. Choudhury, J.R. Komaragiri, P.C. Tiwari

JHEP10(2019)244

National Institute of Science Education and Research, HBNI, Bhubaneswar, India

S. Bahinipati[23], C. Kar, G. Kole, P. Mal, T. Mishra, V.K. Muraleedharan Nair Bindhu, A. Nayak[24], D.K. Sahoo[23], S.K. Swain

Panjab University, Chandigarh, India

S. Bansal, S.B. Beri, V. Bhatnagar, S. Chauhan, R. Chawla, N. Dhingra, R. Gupta, A. Kaur, M. Kaur, S. Kaur, P. Kumari, M. Lohan, M. Meena, K. Sandeep, S. Sharma, J.B. Singh, A.K. Virdi, G. Walia

University of Delhi, Delhi, India

A. Bhardwaj, B.C. Choudhary, R.B. Garg, M. Gola, S. Keshri, Ashok Kumar, M. Naimuddin, P. Priyanka, K. Ranjan, Aashaq Shah, R. Sharma

Saha Institute of Nuclear Physics, HBNI, Kolkata, India

R. Bhardwaj[25], M. Bharti[25], R. Bhattacharya, S. Bhattacharya, U. Bhawandeep[25], D. Bhowmik, S. Dutta, S. Ghosh, M. Maity[26], K. Mondal, S. Nandan, A. Purohit, P.K. Rout, G. Saha, S. Sarkar, T. Sarkar[26], M. Sharan, B. Singh[25], S. Thakur[25]

Indian Institute of Technology Madras, Madras, India

P.K. Behera, P. Kalbhor, A. Muhammad, P.R. Pujahari, A. Sharma, A.K. Sikdar

Bhabha Atomic Research Centre, Mumbai, India

D. Dutta, V. Jha, V. Kumar, D.K. Mishra, P.K. Netrakanti, L.M. Pant, P. Shukla

Tata Institute of Fundamental Research-A, Mumbai, India

T. Aziz, M.A. Bhat, S. Dugad, G.B. Mohanty, N. Sur, RavindraKumar Verma

Tata Institute of Fundamental Research-B, Mumbai, India

S. Banerjee, S. Bhattacharya, S. Chatterjee, P. Das, M. Guchait, S. Karmakar, S. Kumar, G. Majumder, K. Mazumdar, N. Sahoo, S. Sawant

Indian Institute of Science Education and Research (IISER), Pune, India

S. Chauhan, S. Dube, V. Hegde, B. Kansal, A. Kapoor, K. Kothekar, S. Pandey, A. Rane, A. Rastogi, S. Sharma

Institute for Research in Fundamental Sciences (IPM), Tehran, Iran

S. Chenarani[27], E. Eskandari Tadavani, S.M. Etesami[27], M. Khakzad, M. Mohammadi Najafabadi, M. Naseri, F. Rezaei Hosseinabadi

University College Dublin, Dublin, Ireland

M. Felcini, M. Grunewald

INFN Sezione di Bari[a], Università di Bari[b], Politecnico di Bari[c], Bari, Italy

M. Abbrescia[a,b], R. Aly[a,b,28], C. Calabria[a,b], A. Colaleo[a], D. Creanza[a,c], L. Cristella[a,b], N. De Filippis[a,c], M. De Palma[a,b], A. Di Florio[a,b], W. Elmetenawee[a,b], L. Fiore[a], A. Gelmi[a,b], G. Iaselli[a,c], M. Ince[a,b], S. Lezki[a,b], G. Maggi[a,c], M. Maggi[a], G. Miniello[a,b], S. My[a,b], S. Nuzzo[a,b], A. Pompili[a,b], G. Pugliese[a,c], R. Radogna[a], A. Ranieri[a], G. Selvaggi[a,b], L. Silvestris[a], F.M. Simone[a], R. Venditti[a], P. Verwilligen[a]

JHEP10(2019)244

INFN Sezione di Bologna[a], Università di Bologna[b], Bologna, Italy

G. Abbiendi[a], C. Battilana[a,b], D. Bonacorsi[a,b], L. Borgonovi[a,b], S. Braibant-Giacomelli[a,b], R. Campanini[a,b], P. Capiluppi[a,b], A. Castro[a,b], F.R. Cavallo[a], C. Ciocca[a], G. Codispoti[a,b], M. Cuffiani[a,b], G.M. Dallavalle[a], F. Fabbri[a], A. Fanfani[a,b], E. Fontanesi[a,b], P. Giacomelli[a], C. Grandi[a], L. Guiducci[a,b], F. Iemmi[a,b], S. Lo Meo[a,29], S. Marcellini[a], G. Masetti[a], F.L. Navarria[a,b], A. Perrotta[a], F. Primavera[a,b], A.M. Rossi[a,b], T. Rovelli[a,b], G.P. Siroli[a,b], N. Tosi[a]

INFN Sezione di Catania[a], Università di Catania[b], Catania, Italy

S. Albergo[a,b,30], S. Costa[a,b], A. Di Mattia[a], R. Potenza[a,b], A. Tricomi[a,b,30], C. Tuve[a,b]

INFN Sezione di Firenze[a], Università di Firenze[b], Firenze, Italy

G. Barbagli[a], A. Cassese, R. Ceccarelli, V. Ciulli[a,b], C. Civinini[a], R. D'Alessandro[a,b], E. Focardi[a,b], G. Latino[a,b], P. Lenzi[a,b], M. Meschini[a], S. Paoletti[a], G. Sguazzoni[a], L. Viliani[a]

INFN Laboratori Nazionali di Frascati, Frascati, Italy

L. Benussi, S. Bianco, D. Piccolo

INFN Sezione di Genova[a], Università di Genova[b], Genova, Italy

M. Bozzo[a,b], F. Ferro[a], R. Mulargia[a,b], E. Robutti[a], S. Tosi[a,b]

INFN Sezione di Milano-Bicocca[a], Università di Milano-Bicocca[b], Milano, Italy

A. Benaglia[a], A. Beschi[a,b], F. Brivio[a,b], V. Ciriolo[a,b,16], S. Di Guida[a,b,16], M.E. Dinardo[a,b], P. Dini[a], S. Gennai[a], A. Ghezzi[a,b], P. Govoni[a,b], L. Guzzi[a,b], M. Malberti[a], S. Malvezzi[a], D. Menasce[a], F. Monti[a,b], L. Moroni[a], M. Paganoni[a,b], D. Pedrini[a], S. Ragazzi[a,b], T. Tabarelli de Fatis[a,b], D. Zuolo[a,b]

INFN Sezione di Napoli[a], Università di Napoli 'Federico II'[b], Napoli, Italy, Università della Basilicata[c], Potenza, Italy, Università G. Marconi[d], Roma, Italy

S. Buontempo[a], N. Cavallo[a,c], A. De Iorio[a,b], A. Di Crescenzo[a,b], F. Fabozzi[a,c], F. Fienga[a], G. Galati[a], A.O.M. Iorio[a,b], L. Lista[a,b], S. Meola[a,d,16], P. Paolucci[a,16], B. Rossi[a], C. Sciacca[a,b], E. Voevodina[a,b]

INFN Sezione di Padova[a], Università di Padova[b], Padova, Italy, Università di Trento[c], Trento, Italy

P. Azzi[a], N. Bacchetta[a], D. Bisello[a,b], A. Boletti[a,b], A. Bragagnolo[a,b], R. Carlin[a,b], P. Checchia[a], P. De Castro Manzano[a], T. Dorigo[a], U. Dosselli[a], F. Gasparini[a,b], U. Gasparini[a,b], A. Gozzelino[a], S.Y. Hoh[a,b], P. Lujan[a], M. Margoni[a,b], A.T. Meneguzzo[a,b], J. Pazzini[a,b], M. Presilla[b], P. Ronchese[a,b], R. Rossin[a,b], F. Simonetto[a,b], A. Tiko[a], M. Tosi[a,b], M. Zanetti[a,b], P. Zotto[a,b], G. Zumerle[a,b]

INFN Sezione di Pavia[a], Università di Pavia[b], Pavia, Italy

A. Braghieri[a], D. Fiorina[a,b], P. Montagna[a,b], S.P. Ratti[a,b], V. Re[a], M. Ressegotti[a,b], C. Riccardi[a,b], P. Salvini[a], I. Vai[a], P. Vitulo[a,b]

JHEP10(2019)244

INFN Sezione di Perugia[a], Università di Perugia[b], Perugia, Italy
M. Biasini[a,b], G.M. Bilei[a], D. Ciangottini[a,b], L. Fanò[a,b], P. Lariccia[a,b], R. Leonardi[a,b], E. Manoni[a], G. Mantovani[a,b], V. Mariani[a,b], M. Menichelli[a], A. Rossi[a,b], A. Santocchia[a,b], D. Spiga[a]

INFN Sezione di Pisa[a], Università di Pisa[b], Scuola Normale Superiore di Pisa[c], Pisa, Italy
K. Androsov[a], P. Azzurri[a], G. Bagliesi[a], V. Bertacchi[a,c], L. Bianchini[a], T. Boccali[a], R. Castaldi[a], M.A. Ciocci[a,b], R. Dell'Orso[a], G. Fedi[a], L. Giannini[a,c], A. Giassi[a], M.T. Grippo[a], F. Ligabue[a,c], E. Manca[a,c], G. Mandorli[a,c], A. Messineo[a,b], F. Palla[a], A. Rizzi[a,b], G. Rolandi[31], S. Roy Chowdhury, A. Scribano[a], P. Spagnolo[a], R. Tenchini[a], G. Tonelli[a,b], N. Turini, A. Venturi[a], P.G. Verdini[a]

INFN Sezione di Roma[a], Sapienza Università di Roma[b], Rome, Italy
F. Cavallari[a], M. Cipriani[a,b], D. Del Re[a,b], E. Di Marco[a,b], M. Diemoz[a], E. Longo[a,b], P. Meridiani[a], G. Organtini[a,b], F. Pandolfi[a], R. Paramatti[a,b], C. Quaranta[a,b], S. Rahatlou[a,b], C. Rovelli[a], F. Santanastasio[a,b], L. Soffi[a,b]

INFN Sezione di Torino[a], Università di Torino[b], Torino, Italy, Università del Piemonte Orientale[c], Novara, Italy
N. Amapane[a,b], R. Arcidiacono[a,c], S. Argiro[a,b], M. Arneodo[a,c], N. Bartosik[a], R. Bellan[a,b], A. Bellora, C. Biino[a], A. Cappati[a,b], N. Cartiglia[a], S. Cometti[a], M. Costa[a,b], R. Covarelli[a,b], N. Demaria[a], B. Kiani[a,b], C. Mariotti[a], S. Maselli[a], E. Migliore[a,b], V. Monaco[a,b], E. Monteil[a,b], M. Monteno[a], M.M. Obertino[a,b], G. Ortona[a,b], L. Pacher[a,b], N. Pastrone[a], M. Pelliccioni[a], G.L. Pinna Angioni[a,b], A. Romero[a,b], M. Ruspa[a,c], R. Salvatico[a,b], V. Sola[a], A. Solano[a,b], D. Soldi[a,b], A. Staiano[a]

INFN Sezione di Trieste[a], Università di Trieste[b], Trieste, Italy
S. Belforte[a], V. Candelise[a,b], M. Casarsa[a], F. Cossutti[a], A. Da Rold[a,b], G. Della Ricca[a,b], F. Vazzoler[a,b], A. Zanetti[a]

Kyungpook National University, Daegu, Korea
B. Kim, D.H. Kim, G.N. Kim, J. Lee, S.W. Lee, C.S. Moon, Y.D. Oh, S.I. Pak, S. Sekmen, D.C. Son, Y.C. Yang

Chonnam National University, Institute for Universe and Elementary Particles, Kwangju, Korea
H. Kim, D.H. Moon, G. Oh

Hanyang University, Seoul, Korea
B. Francois, T.J. Kim, J. Park

Korea University, Seoul, Korea
S. Cho, S. Choi, Y. Go, D. Gyun, S. Ha, B. Hong, K. Lee, K.S. Lee, J. Lim, J. Park, S.K. Park, Y. Roh, J. Yoo

Kyung Hee University, Department of Physics
J. Goh

JHEP10(2019)244

Sejong University, Seoul, Korea
H.S. Kim

Seoul National University, Seoul, Korea
J. Almond, J.H. Bhyun, J. Choi, S. Jeon, J. Kim, J.S. Kim, H. Lee, K. Lee, S. Lee, K. Nam, M. Oh, S.B. Oh, B.C. Radburn-Smith, U.K. Yang, H.D. Yoo, I. Yoon, G.B. Yu

University of Seoul, Seoul, Korea
D. Jeon, H. Kim, J.H. Kim, J.S.H. Lee, I.C. Park, I.J Watson

Sungkyunkwan University, Suwon, Korea
Y. Choi, C. Hwang, Y. Jeong, J. Lee, Y. Lee, I. Yu

Riga Technical University, Riga, Latvia
V. Veckalns[32]

Vilnius University, Vilnius, Lithuania
V. Dudenas, A. Juodagalvis, G. Tamulaitis, J. Vaitkus

National Centre for Particle Physics, Universiti Malaya, Kuala Lumpur, Malaysia
Z.A. Ibrahim, F. Mohamad Idris[33], W.A.T. Wan Abdullah, M.N. Yusli, Z. Zolkapli

Universidad de Sonora (UNISON), Hermosillo, Mexico
J.F. Benitez, A. Castaneda Hernandez, J.A. Murillo Quijada, L. Valencia Palomo

Centro de Investigacion y de Estudios Avanzados del IPN, Mexico City, Mexico
H. Castilla-Valdez, E. De La Cruz-Burelo, I. Heredia-De La Cruz[34], R. Lopez-Fernandez, A. Sanchez-Hernandez

Universidad Iberoamericana, Mexico City, Mexico
S. Carrillo Moreno, C. Oropeza Barrera, M. Ramirez-Garcia, F. Vazquez Valencia

Benemerita Universidad Autonoma de Puebla, Puebla, Mexico
J. Eysermans, I. Pedraza, H.A. Salazar Ibarguen, C. Uribe Estrada

Universidad Autónoma de San Luis Potosí, San Luis Potosí, Mexico
A. Morelos Pineda

University of Montenegro, Podgorica, Montenegro
J. Mijuskovic, N. Raicevic

University of Auckland, Auckland, New Zealand
D. Krofcheck

University of Canterbury, Christchurch, New Zealand
S. Bheesette, P.H. Butler

National Centre for Physics, Quaid-I-Azam University, Islamabad, Pakistan
A. Ahmad, M. Ahmad, Q. Hassan, H.R. Hoorani, W.A. Khan, M.A. Shah, M. Shoaib, M. Waqas

JHEP10(2019)244

AGH University of Science and Technology Faculty of Computer Science, Electronics and Telecommunications, Krakow, Poland

V. Avati, L. Grzanka, M. Malawski

National Centre for Nuclear Research, Swierk, Poland

H. Bialkowska, M. Bluj, B. Boimska, M. Górski, M. Kazana, M. Szleper, P. Zalewski

Institute of Experimental Physics, Faculty of Physics, University of Warsaw, Warsaw, Poland

K. Bunkowski, A. Byszuk[35], K. Doroba, A. Kalinowski, M. Konecki, J. Krolikowski, M. Misiura, M. Olszewski, M. Walczak

Laboratório de Instrumentação e Física Experimental de Partículas, Lisboa, Portugal

M. Araujo, P. Bargassa, D. Bastos, A. Di Francesco, P. Faccioli, B. Galinhas, M. Gallinaro, J. Hollar, N. Leonardo, T.S. Niknejad, J. Seixas, K. Shchelina, G. Strong, O. Toldaiev, J. Varela

Joint Institute for Nuclear Research, Dubna, Russia

S. Afanasiev, P. Bunin, M. Gavrilenko, I. Golutvin, I. Gorbunov, A. Kamenev, V. Karjavine, A. Lanev, A. Malakhov, V. Matveev[36,37], P. Moisenz, V. Palichik, V. Perelygin, M. Savina, S. Shmatov, S. Shulha, N. Skatchkov, V. Smirnov, N. Voytishin, A. Zarubin

Petersburg Nuclear Physics Institute, Gatchina (St. Petersburg), Russia

L. Chtchipounov, V. Golovtcov, Y. Ivanov, V. Kim[38], E. Kuznetsova[39], P. Levchenko, V. Murzin, V. Oreshkin, I. Smirnov, D. Sosnov, V. Sulimov, L. Uvarov, A. Vorobyev

Institute for Nuclear Research, Moscow, Russia

Yu. Andreev, A. Dermenev, S. Gninenko, N. Golubev, A. Karneyeu, M. Kirsanov, N. Krasnikov, A. Pashenkov, D. Tlisov, A. Toropin

Institute for Theoretical and Experimental Physics named by A.I. Alikhanov of NRC 'Kurchatov Institute', Moscow, Russia

V. Epshteyn, V. Gavrilov, N. Lychkovskaya, A. Nikitenko[40], V. Popov, I. Pozdnyakov, G. Safronov, A. Spiridonov, A. Stepennov, M. Toms, E. Vlasov, A. Zhokin

Moscow Institute of Physics and Technology, Moscow, Russia

T. Aushev

National Research Nuclear University 'Moscow Engineering Physics Institute' (MEPhI), Moscow, Russia

O. Bychkova, R. Chistov[41], M. Danilov[41], S. Polikarpov[41], E. Tarkovskii

P.N. Lebedev Physical Institute, Moscow, Russia

V. Andreev, M. Azarkin, I. Dremin, M. Kirakosyan, A. Terkulov

JHEP10(2019)244

Skobeltsyn Institute of Nuclear Physics, Lomonosov Moscow State University, Moscow, Russia

A. Belyaev, E. Boos, M. Dubinin[42], L. Dudko, A. Ershov, A. Gribushin, V. Klyukhin, O. Kodolova, I. Lokhtin, S. Obraztsov, S. Petrushanko, V. Savrin, A. Snigirev

Novosibirsk State University (NSU), Novosibirsk, Russia

A. Barnyakov[43], V. Blinov[43], T. Dimova[43], L. Kardapoltsev[43], Y. Skovpen[43]

Institute for High Energy Physics of National Research Centre 'Kurchatov Institute', Protvino, Russia

I. Azhgirey, I. Bayshev, S. Bitioukov, V. Kachanov, D. Konstantinov, P. Mandrik, V. Petrov, R. Ryutin, S. Slabospitskii, A. Sobol, S. Troshin, N. Tyurin, A. Uzunian, A. Volkov

National Research Tomsk Polytechnic University, Tomsk, Russia

A. Babaev, A. Iuzhakov, V. Okhotnikov

Tomsk State University, Tomsk, Russia

V. Borchsh, V. Ivanchenko, E. Tcherniaev

University of Belgrade: Faculty of Physics and VINCA Institute of Nuclear Sciences

P. Adzic[44], P. Cirkovic, D. Devetak, M. Dordevic, P. Milenovic, J. Milosevic, M. Stojanovic

Centro de Investigaciones Energéticas Medioambientales y Tecnológicas (CIEMAT), Madrid, Spain

M. Aguilar-Benitez, J. Alcaraz Maestre, A. Álvarez Fernández, I. Bachiller, M. Barrio Luna, J.A. Brochero Cifuentes, C.A. Carrillo Montoya, M. Cepeda, M. Cerrada, N. Colino, B. De La Cruz, A. Delgado Peris, C. Fernandez Bedoya, J.P. Fernández Ramos, J. Flix, M.C. Fouz, O. Gonzalez Lopez, S. Goy Lopez, J.M. Hernandez, M.I. Josa, D. Moran, Á. Navarro Tobar, A. Pérez-Calero Yzquierdo, J. Puerta Pelayo, I. Redondo, L. Romero, S. Sánchez Navas, M.S. Soares, A. Triossi, C. Willmott

Universidad Autónoma de Madrid, Madrid, Spain

C. Albajar, J.F. de Trocóniz, R. Reyes-Almanza

Universidad de Oviedo, Instituto Universitario de Ciencias y Tecnologías Espaciales de Asturias (ICTEA), Oviedo, Spain

B. Alvarez Gonzalez, J. Cuevas, C. Erice, J. Fernandez Menendez, S. Folgueras, I. Gonzalez Caballero, J.R. González Fernández, E. Palencia Cortezon, V. Rodríguez Bouza, S. Sanchez Cruz

Instituto de Física de Cantabria (IFCA), CSIC-Universidad de Cantabria, Santander, Spain

I.J. Cabrillo, A. Calderon, B. Chazin Quero, J. Duarte Campderros, M. Fernandez, P.J. Fernández Manteca, A. García Alonso, G. Gomez, C. Martinez Rivero, P. Martinez Ruiz del Arbol, F. Matorras, J. Piedra Gomez, C. Prieels, T. Rodrigo, A. Ruiz-Jimeno, L. Russo[45], L. Scodellaro, N. Trevisani, I. Vila, J.M. Vizan Garcia

JHEP10(2019)244

University of Colombo, Colombo, Sri Lanka
K. Malagalage

University of Ruhuna, Department of Physics, Matara, Sri Lanka
W.G.D. Dharmaratna, N. Wickramage

CERN, European Organization for Nuclear Research, Geneva, Switzerland
D. Abbaneo, B. Akgun, E. Auffray, G. Auzinger, J. Baechler, P. Baillon, A.H. Ball, D. Barney, J. Bendavid, M. Bianco, A. Bocci, P. Bortignon, E. Bossini, C. Botta, E. Brondolin, T. Camporesi, A. Caratelli, G. Cerminara, E. Chapon, G. Cucciati, D. d'Enterria, A. Dabrowski, N. Daci, V. Daponte, A. David, O. Davignon, A. De Roeck, M. Deile, M. Dobson, M. Dünser, N. Dupont, A. Elliott-Peisert, N. Emriskova, F. Fallavollita[46], D. Fasanella, S. Fiorendi, G. Franzoni, J. Fulcher, W. Funk, S. Giani, D. Gigi, A. Gilbert, K. Gill, F. Glege, M. Gruchala, M. Guilbaud, D. Gulhan, J. Hegeman, C. Heidegger, Y. Iiyama, V. Innocente, P. Janot, O. Karacheban[19], J. Kaspar, J. Kieseler, M. Krammer[1], N. Kratochwil, C. Lange, P. Lecoq, C. Lourenço, L. Malgeri, M. Mannelli, A. Massironi, F. Meijers, J.A. Merlin, S. Mersi, E. Meschi, F. Moortgat, M. Mulders, J. Ngadiuba, J. Niedziela, S. Nourbakhsh, S. Orfanelli, L. Orsini, F. Pantaleo[16], L. Pape, E. Perez, M. Peruzzi, A. Petrilli, G. Petrucciani, A. Pfeiffer, M. Pierini, F.M. Pitters, D. Rabady, A. Racz, M. Rieger, M. Rovere, H. Sakulin, C. Schäfer, C. Schwick, M. Selvaggi, A. Sharma, P. Silva, W. Snoeys, P. Sphicas[47], J. Steggemann, S. Summers, V.R. Tavolaro, D. Treille, A. Tsirou, G.P. Van Onsem, A. Vartak, M. Verzetti, W.D. Zeuner

Paul Scherrer Institut, Villigen, Switzerland
L. Caminada[48], K. Deiters, W. Erdmann, R. Horisberger, Q. Ingram, H.C. Kaestli, D. Kotlinski, U. Langenegger, T. Rohe, S.A. Wiederkehr

ETH Zurich — Institute for Particle Physics and Astrophysics (IPA), Zurich, Switzerland
M. Backhaus, P. Berger, N. Chernyavskaya, G. Dissertori, M. Dittmar, M. Donegà, C. Dorfer, T.A. Gómez Espinosa, C. Grab, D. Hits, T. Klijnsma, W. Lustermann, R.A. Manzoni, M. Marionneau, M.T. Meinhard, F. Micheli, P. Musella, F. Nessi-Tedaldi, F. Pauss, G. Perrin, L. Perrozzi, S. Pigazzini, M.G. Ratti, M. Reichmann, C. Reissel, T. Reitenspiess, D. Ruini, D.A. Sanz Becerra, M. Schönenberger, L. Shchutska, M.L. Vesterbacka Olsson, R. Wallny, D.H. Zhu

Universität Zürich, Zurich, Switzerland
T.K. Aarrestad, C. Amsler[49], D. Brzhechko, M.F. Canelli, A. De Cosa, R. Del Burgo, S. Donato, B. Kilminster, S. Leontsinis, V.M. Mikuni, I. Neutelings, G. Rauco, P. Robmann, D. Salerno, K. Schweiger, C. Seitz, Y. Takahashi, S. Wertz, A. Zucchetta

National Central University, Chung-Li, Taiwan
T.H. Doan, C.M. Kuo, W. Lin, A. Roy, S.S. Yu

National Taiwan University (NTU), Taipei, Taiwan
P. Chang, Y. Chao, K.F. Chen, P.H. Chen, W.-S. Hou, Y.y. Li, R.-S. Lu, E. Paganis, A. Psallidas, A. Steen

JHEP10(2019)244

Chulalongkorn University, Faculty of Science, Department of Physics, Bangkok, Thailand

B. Asavapibhop, C. Asawatangtrakuldee, N. Srimanobhas, N. Suwonjandee

Çukurova University, Physics Department, Science and Art Faculty, Adana, Turkey

A. Bat, F. Boran, A. Celik[50], S. Cerci[51], S. Damarseckin[52], Z.S. Demiroglu, F. Dolek, C. Dozen[53], I. Dumanoglu, G. Gokbulut, EmineGurpinar Guler[54], Y. Guler, I. Hos[55], C. Isik, E.E. Kangal[56], O. Kara, A. Kayis Topaksu, U. Kiminsu, G. Onengut, K. Ozdemir[57], S. Ozturk[58], A.E. Simsek, D. Sunar Cerci[51], U.G. Tok, S. Turkcapar, I.S. Zorbakir, C. Zorbilmez

Middle East Technical University, Physics Department, Ankara, Turkey

B. Isildak[59], G. Karapinar[60], M. Yalvac

Bogazici University, Istanbul, Turkey

I.O. Atakisi, E. Gülmez, M. Kaya[61], O. Kaya[62], Ö. Özçelik, S. Tekten, E.A. Yetkin[63]

Istanbul Technical University, Istanbul, Turkey

A. Cakir, K. Cankocak, Y. Komurcu, S. Sen[64]

Istanbul University, Istanbul, Turkey

B. Kaynak, S. Ozkorucuklu

Institute for Scintillation Materials of National Academy of Science of Ukraine, Kharkov, Ukraine

B. Grynyov

National Scientific Center, Kharkov Institute of Physics and Technology, Kharkov, Ukraine

L. Levchuk

University of Bristol, Bristol, United Kingdom

E. Bhal, S. Bologna, J.J. Brooke, D. Burns[65], E. Clement, D. Cussans, H. Flacher, J. Goldstein, G.P. Heath, H.F. Heath, L. Kreczko, S. Paramesvaran, B. Penning, T. Sakuma, S. Seif El Nasr-Storey, V.J. Smith, J. Taylor, A. Titterton

Rutherford Appleton Laboratory, Didcot, United Kingdom

K.W. Bell, A. Belyaev[66], C. Brew, R.M. Brown, D. Cieri, D.J.A. Cockerill, J.A. Coughlan, K. Harder, S. Harper, J. Linacre, K. Manolopoulos, D.M. Newbold, E. Olaiya, D. Petyt, T. Reis, T. Schuh, C.H. Shepherd-Themistocleous, A. Thea, I.R. Tomalin, T. Williams, W.J. Womersley

Imperial College, London, United Kingdom

R. Bainbridge, P. Bloch, J. Borg, S. Breeze, O. Buchmuller, A. Bundock, GurpreetSingh CHAHAL[67], D. Colling, P. Dauncey, G. Davies, M. Della Negra, R. Di Maria, P. Everaerts, G. Hall, G. Iles, T. James, M. Komm, C. Laner, L. Lyons, A.-M. Magnan, S. Malik, A. Martelli, V. Milosevic, J. Nash[68], V. Palladino, M. Pesaresi, D.M. Raymond,

JHEP10(2019)244

A. Richards, A. Rose, E. Scott, C. Seez, A. Shtipliyski, M. Stoye, T. Strebler, A. Tapper, K. Uchida, T. Virdee[16], N. Wardle, D. Winterbottom, J. Wright, A.G. Zecchinelli, S.C. Zenz

Brunel University, Uxbridge, United Kingdom

J.E. Cole, P.R. Hobson, A. Khan, P. Kyberd, C.K. Mackay, A. Morton, I.D. Reid, L. Teodorescu, S. Zahid

Baylor University, Waco, U.S.A.

K. Call, B. Caraway, J. Dittmann, K. Hatakeyama, C. Madrid, B. McMaster, N. Pastika, C. Smith

Catholic University of America, Washington, DC, U.S.A.

R. Bartek, A. Dominguez, R. Uniyal, A.M. Vargas Hernandez

The University of Alabama, Tuscaloosa, U.S.A.

A. Buccilli, S.I. Cooper, C. Henderson, P. Rumerio, C. West

Boston University, Boston, U.S.A.

D. Arcaro, Z. Demiragli, D. Gastler, C. Richardson, J. Rohlf, D. Sperka, I. Suarez, L. Sulak, D. Zou

Brown University, Providence, U.S.A.

G. Benelli, B. Burkle, X. Coubez[17], D. Cutts, Y.t. Duh, M. Hadley, J. Hakala, U. Heintz, J.M. Hogan[69], K.H.M. Kwok, E. Laird, G. Landsberg, J. Lee, Z. Mao, M. Narain, S. Sagir[70], R. Syarif, E. Usai, D. Yu, W. Zhang

University of California, Davis, Davis, U.S.A.

R. Band, C. Brainerd, R. Breedon, M. Calderon De La Barca Sanchez, M. Chertok, J. Conway, R. Conway, P.T. Cox, R. Erbacher, C. Flores, G. Funk, F. Jensen, W. Ko, O. Kukral, R. Lander, M. Mulhearn, D. Pellett, J. Pilot, M. Shi, D. Taylor, K. Tos, M. Tripathi, Z. Wang, F. Zhang

University of California, Los Angeles, U.S.A.

M. Bachtis, C. Bravo, R. Cousins, A. Dasgupta, A. Florent, J. Hauser, M. Ignatenko, N. Mccoll, W.A. Nash, S. Regnard, D. Saltzberg, C. Schnaible, B. Stone, V. Valuev

University of California, Riverside, Riverside, U.S.A.

K. Burt, Y. Chen, R. Clare, J.W. Gary, S.M.A. Ghiasi Shirazi, G. Hanson, G. Karapostoli, E. Kennedy, O.R. Long, M. Olmedo Negrete, M.I. Paneva, W. Si, L. Wang, S. Wimpenny, B.R. Yates, Y. Zhang

University of California, San Diego, La Jolla, U.S.A.

J.G. Branson, P. Chang, S. Cittolin, S. Cooperstein, N. Deelen, M. Derdzinski, R. Gerosa, D. Gilbert, B. Hashemi, D. Klein, V. Krutelyov, J. Letts, M. Masciovecchio, S. May, S. Padhi, M. Pieri, V. Sharma, M. Tadel, F. Würthwein, A. Yagil, G. Zevi Della Porta

JHEP10(2019)244

University of California, Santa Barbara — Department of Physics, Santa Barbara, U.S.A.

N. Amin, R. Bhandari, C. Campagnari, M. Citron, V. Dutta, M. Franco Sevilla, L. Gouskos, J. Incandela, B. Marsh, H. Mei, A. Ovcharova, H. Qu, J. Richman, U. Sarica, D. Stuart, S. Wang

California Institute of Technology, Pasadena, U.S.A.

D. Anderson, A. Bornheim, O. Cerri, I. Dutta, J.M. Lawhorn, N. Lu, J. Mao, H.B. Newman, T.Q. Nguyen, J. Pata, M. Spiropulu, J.R. Vlimant, S. Xie, Z. Zhang, R.Y. Zhu

Carnegie Mellon University, Pittsburgh, U.S.A.

M.B. Andrews, T. Ferguson, T. Mudholkar, M. Paulini, M. Sun, I. Vorobiev, M. Weinberg

University of Colorado Boulder, Boulder, U.S.A.

J.P. Cumalat, W.T. Ford, A. Johnson, E. MacDonald, T. Mulholland, R. Patel, A. Perloff, K. Stenson, K.A. Ulmer, S.R. Wagner

Cornell University, Ithaca, U.S.A.

J. Alexander, J. Chaves, Y. Cheng, J. Chu, A. Datta, A. Frankenthal, K. Mcdermott, J.R. Patterson, D. Quach, A. Rinkevicius[71], A. Ryd, S.M. Tan, Z. Tao, J. Thom, P. Wittich, M. Zientek

Fermi National Accelerator Laboratory, Batavia, U.S.A.

S. Abdullin, M. Albrow, M. Alyari, G. Apollinari, A. Apresyan, A. Apyan, S. Banerjee, L.A.T. Bauerdick, A. Beretvas, D. Berry, J. Berryhill, P.C. Bhat, K. Burkett, J.N. Butler, A. Canepa, G.B. Cerati, H.W.K. Cheung, F. Chlebana, M. Cremonesi, J. Duarte, V.D. Elvira, J. Freeman, Z. Gecse, E. Gottschalk, L. Gray, D. Green, S. Grünendahl, O. Gutsche, AllisonReinsvold Hall, J. Hanlon, R.M. Harris, S. Hasegawa, R. Heller, J. Hirschauer, B. Jayatilaka, S. Jindariani, M. Johnson, U. Joshi, B. Klima, M.J. Kortelainen, B. Kreis, S. Lammel, J. Lewis, D. Lincoln, R. Lipton, M. Liu, T. Liu, J. Lykken, K. Maeshima, J.M. Marraffino, D. Mason, P. McBride, P. Merkel, S. Mrenna, S. Nahn, V. O'Dell, V. Papadimitriou, K. Pedro, C. Pena, G. Rakness, F. Ravera, L. Ristori, B. Schneider, E. Sexton-Kennedy, N. Smith, A. Soha, W.J. Spalding, L. Spiegel, S. Stoynev, J. Strait, N. Strobbe, L. Taylor, S. Tkaczyk, N.V. Tran, L. Uplegger, E.W. Vaandering, C. Vernieri, R. Vidal, M. Wang, H.A. Weber

University of Florida, Gainesville, U.S.A.

D. Acosta, P. Avery, D. Bourilkov, A. Brinkerhoff, L. Cadamuro, A. Carnes, V. Cherepanov, F. Errico, R.D. Field, S.V. Gleyzer, B.M. Joshi, M. Kim, J. Konigsberg, A. Korytov, K.H. Lo, P. Ma, K. Matchev, N. Menendez, G. Mitselmakher, D. Rosenzweig, K. Shi, J. Wang, S. Wang, X. Zuo

Florida International University, Miami, U.S.A.

Y.R. Joshi

Florida State University, Tallahassee, U.S.A.

T. Adams, A. Askew, S. Hagopian, V. Hagopian, K.F. Johnson, R. Khurana, T. Kolberg, G. Martinez, T. Perry, H. Prosper, C. Schiber, R. Yohay, J. Zhang

JHEP10(2019)244

Florida Institute of Technology, Melbourne, U.S.A.

M.M. Baarmand, M. Hohlmann, D. Noonan, M. Rahmani, M. Saunders, F. Yumiceva

University of Illinois at Chicago (UIC), Chicago, U.S.A.

M.R. Adams, L. Apanasevich, R.R. Betts, R. Cavanaugh, X. Chen, S. Dittmer, O. Evdokimov, C.E. Gerber, D.A. Hangal, D.J. Hofman, K. Jung, C. Mills, T. Roy, M.B. Tonjes, N. Varelas, J. Viinikainen, H. Wang, X. Wang, Z. Wu

The University of Iowa, Iowa City, U.S.A.

M. Alhusseini, B. Bilki[54], W. Clarida, K. Dilsiz[72], S. Durgut, R.P. Gandrajula, M. Haytmyradov, V. Khristenko, O.K. Köseyan, J.-P. Merlo, A. Mestvirishvili[73], A. Moeller, J. Nachtman, H. Ogul[74], Y. Onel, F. Ozok[75], A. Penzo, C. Snyder, E. Tiras, J. Wetzel

Johns Hopkins University, Baltimore, U.S.A.

B. Blumenfeld, A. Cocoros, N. Eminizer, A.V. Gritsan, W.T. Hung, S. Kyriacou, P. Maksimovic, J. Roskes, M. Swartz

The University of Kansas, Lawrence, U.S.A.

C. Baldenegro Barrera, P. Baringer, A. Bean, S. Boren, J. Bowen, A. Bylinkin, T. Isidori, S. Khalil, J. King, G. Krintiras, A. Kropivnitskaya, C. Lindsey, D. Majumder, W. Mcbrayer, N. Minafra, M. Murray, C. Rogan, C. Royon, S. Sanders, E. Schmitz, J.D. Tapia Takaki, Q. Wang, J. Williams, G. Wilson

Kansas State University, Manhattan, U.S.A.

S. Duric, A. Ivanov, K. Kaadze, D. Kim, Y. Maravin, D.R. Mendis, T. Mitchell, A. Modak, A. Mohammadi

Lawrence Livermore National Laboratory, Livermore, U.S.A.

F. Rebassoo, D. Wright

University of Maryland, College Park, U.S.A.

A. Baden, O. Baron, A. Belloni, S.C. Eno, Y. Feng, N.J. Hadley, S. Jabeen, G.Y. Jeng, R.G. Kellogg, J. Kunkle, A.C. Mignerey, S. Nabili, F. Ricci-Tam, M. Seidel, Y.H. Shin, A. Skuja, S.C. Tonwar, K. Wong

Massachusetts Institute of Technology, Cambridge, U.S.A.

D. Abercrombie, B. Allen, A. Baty, R. Bi, S. Brandt, W. Busza, I.A. Cali, M. D'Alfonso, G. Gomez Ceballos, M. Goncharov, P. Harris, D. Hsu, M. Hu, M. Klute, D. Kovalskyi, Y.-J. Lee, P.D. Luckey, B. Maier, A.C. Marini, C. Mcginn, C. Mironov, S. Narayanan, X. Niu, C. Paus, D. Rankin, C. Roland, G. Roland, Z. Shi, G.S.F. Stephans, K. Sumorok, K. Tatar, D. Velicanu, J. Wang, T.W. Wang, B. Wyslouch

University of Minnesota, Minneapolis, U.S.A.

R.M. Chatterjee, A. Evans, S. Guts, P. Hansen, J. Hiltbrand, Y. Kubota, Z. Lesko, J. Mans, R. Rusack, M.A. Wadud

University of Mississippi, Oxford, U.S.A.

J.G. Acosta, S. Oliveros

JHEP10(2019)244

University of Nebraska-Lincoln, Lincoln, U.S.A.

K. Bloom, D.R. Claes, C. Fangmeier, L. Finco, F. Golf, R. Kamalieddin, I. Kravchenko, J.E. Siado, G.R. Snow[†], B. Stieger, W. Tabb

State University of New York at Buffalo, Buffalo, U.S.A.

G. Agarwal, C. Harrington, I. Iashvili, A. Kharchilava, C. McLean, D. Nguyen, A. Parker, J. Pekkanen, S. Rappoccio, B. Roozbahani

Northeastern University, Boston, U.S.A.

G. Alverson, E. Barberis, C. Freer, Y. Haddad, A. Hortiangtham, G. Madigan, B. Marzocchi, D.M. Morse, T. Orimoto, L. Skinnari, A. Tishelman-Charny, T. Wamorkar, B. Wang, A. Wisecarver, D. Wood

Northwestern University, Evanston, U.S.A.

S. Bhattacharya, J. Bueghly, T. Gunter, K.A. Hahn, N. Odell, M.H. Schmitt, K. Sung, M. Trovato, M. Velasco

University of Notre Dame, Notre Dame, U.S.A.

R. Bucci, N. Dev, R. Goldouzian, M. Hildreth, K. Hurtado Anampa, C. Jessop, D.J. Karmgard, K. Lannon, W. Li, N. Loukas, N. Marinelli, I. Mcalister, F. Meng, C. Mueller, Y. Musienko[36], M. Planer, R. Ruchti, P. Siddireddy, G. Smith, S. Taroni, M. Wayne, A. Wightman, M. Wolf, A. Woodard

The Ohio State University, Columbus, U.S.A.

J. Alimena, B. Bylsma, L.S. Durkin, S. Flowers, B. Francis, C. Hill, W. Ji, A. Lefeld, T.Y. Ling, B.L. Winer

Princeton University, Princeton, U.S.A.

G. Dezoort, P. Elmer, J. Hardenbrook, N. Haubrich, S. Higginbotham, A. Kalogeropoulos, S. Kwan, D. Lange, M.T. Lucchini, J. Luo, D. Marlow, K. Mei, I. Ojalvo, J. Olsen, C. Palmer, P. Piroué, J. Salfeld-Nebgen, D. Stickland, C. Tully, Z. Wang

University of Puerto Rico, Mayaguez, U.S.A.

S. Malik, S. Norberg

Purdue University, West Lafayette, U.S.A.

A. Barker, V.E. Barnes, S. Das, L. Gutay, M. Jones, A.W. Jung, A. Khatiwada, B. Mahakud, D.H. Miller, G. Negro, N. Neumeister, C.C. Peng, S. Piperov, H. Qiu, J.F. Schulte, J. Sun, F. Wang, R. Xiao, W. Xie

Purdue University Northwest, Hammond, U.S.A.

T. Cheng, J. Dolen, N. Parashar

Rice University, Houston, U.S.A.

U. Behrens, K.M. Ecklund, S. Freed, F.J.M. Geurts, M. Kilpatrick, Arun Kumar, W. Li, B.P. Padley, R. Redjimi, J. Roberts, J. Rorie, W. Shi, A.G. Stahl Leiton, Z. Tu, A. Zhang

JHEP10(2019)244

University of Rochester, Rochester, U.S.A.

A. Bodek, P. de Barbaro, R. Demina, J.L. Dulemba, C. Fallon, T. Ferbel, M. Galanti, A. Garcia-Bellido, O. Hindrichs, A. Khukhunaishvili, E. Ranken, R. Taus

Rutgers, The State University of New Jersey, Piscataway, U.S.A.

B. Chiarito, J.P. Chou, A. Gandrakota, Y. Gershtein, E. Halkiadakis, A. Hart, M. Heindl, E. Hughes, S. Kaplan, I. Laflotte, A. Lath, R. Montalvo, K. Nash, M. Osherson, H. Saka, S. Salur, S. Schnetzer, S. Somalwar, R. Stone, S. Thomas

University of Tennessee, Knoxville, U.S.A.

H. Acharya, A.G. Delannoy, G. Riley, S. Spanier

Texas A&M University, College Station, U.S.A.

O. Bouhali[76], M. Dalchenko, M. De Mattia, A. Delgado, S. Dildick, R. Eusebi, J. Gilmore, T. Huang, T. Kamon[77], S. Luo, S. Malhotra, D. Marley, R. Mueller, D. Overton, L. Perniè, D. Rathjens, A. Safonov

Texas Tech University, Lubbock, U.S.A.

N. Akchurin, J. Damgov, F. De Guio, S. Kunori, K. Lamichhane, S.W. Lee, T. Mengke, S. Muthumuni, T. Peltola, S. Undleeb, I. Volobouev, Z. Wang, A. Whitbeck

Vanderbilt University, Nashville, U.S.A.

S. Greene, A. Gurrola, R. Janjam, W. Johns, C. Maguire, A. Melo, H. Ni, K. Padeken, F. Romeo, P. Sheldon, S. Tuo, J. Velkovska, M. Verweij

University of Virginia, Charlottesville, U.S.A.

M.W. Arenton, P. Barria, B. Cox, G. Cummings, R. Hirosky, M. Joyce, A. Ledovskoy, C. Neu, B. Tannenwald, Y. Wang, E. Wolfe, F. Xia

Wayne State University, Detroit, U.S.A.

R. Harr, P.E. Karchin, N. Poudyal, J. Sturdy, P. Thapa

University of Wisconsin — Madison, Madison, WI, U.S.A.

T. Bose, J. Buchanan, C. Caillol, D. Carlsmith, S. Dasu, I. De Bruyn, L. Dodd, F. Fiori, C. Galloni, B. Gomber[78], H. He, M. Herndon, A. Hervé, U. Hussain, P. Klabbers, A. Lanaro, A. Loeliger, K. Long, R. Loveless, J. Madhusudanan Sreekala, D. Pinna, T. Ruggles, A. Savin, V. Sharma, W.H. Smith, D. Teague, S. Trembath-reichert, N. Woods

†: Deceased
1: Also at Vienna University of Technology, Vienna, Austria
2: Also at IRFU, CEA, Université Paris-Saclay, Gif-sur-Yvette, France
3: Also at Universidade Estadual de Campinas, Campinas, Brazil
4: Also at Federal University of Rio Grande do Sul, Porto Alegre, Brazil
5: Also at UFMS, Nova Andradina, Brazil
6: Also at Universidade Federal de Pelotas, Pelotas, Brazil
7: Also at Université Libre de Bruxelles, Bruxelles, Belgium
8: Also at University of Chinese Academy of Sciences, Beijing, China

JHEP10(2019)244

9: Also at Institute for Theoretical and Experimental Physics named by A.I. Alikhanov of NRC 'Kurchatov Institute', Moscow, Russia
10: Also at Joint Institute for Nuclear Research, Dubna, Russia
11: Also at Ain Shams University, Cairo, Egypt
12: Also at Zewail City of Science and Technology, Zewail, Egypt
13: Also at Purdue University, West Lafayette, U.S.A.
14: Also at Université de Haute Alsace, Mulhouse, France
15: Also at Erzincan Binali Yildirim University, Erzincan, Turkey
16: Also at CERN, European Organization for Nuclear Research, Geneva, Switzerland
17: Also at RWTH Aachen University, III. Physikalisches Institut A, Aachen, Germany
18: Also at University of Hamburg, Hamburg, Germany
19: Also at Brandenburg University of Technology, Cottbus, Germany
20: Also at Institute of Physics, University of Debrecen, Debrecen, Hungary, Debrecen, Hungary
21: Also at Institute of Nuclear Research ATOMKI, Debrecen, Hungary
22: Also at MTA-ELTE Lendület CMS Particle and Nuclear Physics Group, Eötvös Loránd University, Budapest, Hungary, Budapest, Hungary
23: Also at IIT Bhubaneswar, Bhubaneswar, India, Bhubaneswar, India
24: Also at Institute of Physics, Bhubaneswar, India
25: Also at Shoolini University, Solan, India
26: Also at University of Visva-Bharati, Santiniketan, India
27: Also at Isfahan University of Technology, Isfahan, Iran
28: Now at INFN Sezione di Bari[a], Università di Bari[b], Politecnico di Bari[c], Bari, Italy
29: Also at Italian National Agency for New Technologies, Energy and Sustainable Economic Development, Bologna, Italy
30: Also at Centro Siciliano di Fisica Nucleare e di Struttura Della Materia, Catania, Italy
31: Also at Scuola Normale e Sezione dell'INFN, Pisa, Italy
32: Also at Riga Technical University, Riga, Latvia, Riga, Latvia
33: Also at Malaysian Nuclear Agency, MOSTI, Kajang, Malaysia
34: Also at Consejo Nacional de Ciencia y Tecnología, Mexico City, Mexico
35: Also at Warsaw University of Technology, Institute of Electronic Systems, Warsaw, Poland
36: Also at Institute for Nuclear Research, Moscow, Russia
37: Now at National Research Nuclear University 'Moscow Engineering Physics Institute' (MEPhI), Moscow, Russia
38: Also at St. Petersburg State Polytechnical University, St. Petersburg, Russia
39: Also at University of Florida, Gainesville, U.S.A.
40: Also at Imperial College, London, United Kingdom
41: Also at P.N. Lebedev Physical Institute, Moscow, Russia
42: Also at California Institute of Technology, Pasadena, U.S.A.
43: Also at Budker Institute of Nuclear Physics, Novosibirsk, Russia
44: Also at Faculty of Physics, University of Belgrade, Belgrade, Serbia
45: Also at Università degli Studi di Siena, Siena, Italy
46: Also at INFN Sezione di Pavia[a], Università di Pavia[b], Pavia, Italy, Pavia, Italy
47: Also at National and Kapodistrian University of Athens, Athens, Greece
48: Also at Universität Zürich, Zurich, Switzerland
49: Also at Stefan Meyer Institute for Subatomic Physics, Vienna, Austria, Vienna, Austria
50: Also at Burdur Mehmet Akif Ersoy University, BURDUR, Turkey
51: Also at Adiyaman University, Adiyaman, Turkey
52: Also at Şırnak University, Sirnak, Turkey

JHEP10(2019)244

53: Also at Tsinghua University, Beijing, China
54: Also at Beykent University, Istanbul, Turkey, Istanbul, Turkey
55: Also at Istanbul Aydin University, Istanbul, Turkey
56: Also at Mersin University, Mersin, Turkey
57: Also at Piri Reis University, Istanbul, Turkey
58: Also at Gaziosmanpasa University, Tokat, Turkey
59: Also at Ozyegin University, Istanbul, Turkey
60: Also at Izmir Institute of Technology, Izmir, Turkey
61: Also at Marmara University, Istanbul, Turkey
62: Also at Kafkas University, Kars, Turkey
63: Also at Istanbul Bilgi University, Istanbul, Turkey
64: Also at Hacettepe University, Ankara, Turkey
65: Also at Vrije Universiteit Brussel, Brussel, Belgium
66: Also at School of Physics and Astronomy, University of Southampton, Southampton, United Kingdom
67: Also at IPPP Durham University, Durham, United Kingdom
68: Also at Monash University, Faculty of Science, Clayton, Australia
69: Also at Bethel University, St. Paul, Minneapolis, U.S.A., St. Paul, U.S.A.
70: Also at Karamanoğlu Mehmetbey University, Karaman, Turkey
71: Also at Vilnius University, Vilnius, Lithuania
72: Also at Bingol University, Bingol, Turkey
73: Also at Georgian Technical University, Tbilisi, Georgia
74: Also at Sinop University, Sinop, Turkey
75: Also at Mimar Sinan University, Istanbul, Istanbul, Turkey
76: Also at Texas A&M University at Qatar, Doha, Qatar
77: Also at Kyungpook National University, Daegu, Korea, Daegu, Korea
78: Also at University of Hyderabad, Hyderabad, India

JHEP10(2019)244